Delft University of Technology

MASTER IN SUSTAINABLE ENERGY TECHNOLOGY (SET)
FACULTY OF ELECTRICAL ENGINEERING, MATHEMATICS AND COMPUTER SCIENCE (EEMCS)

GRADUATION THESIS

Reducing the effects of co-ion transportation in the Acid-Base Flow Battery

Author
A. Th. van Weezel
(1360647)

Supervisor
Prof.dr.ir. M. Wagemaker

July 28, 2020

Disclaimer

This graduation thesis is part of the Master Sustainable Energy Technology at the Electrical Engineering, Mathematics and Computer Science (EEMCS) faculty on the University of Technology Delft in The Netherlands.

This text is confidential and cannot be made public.

July 2, 2020

Graduation thesis written by
A. Th. van Weezel (Alexander)
Kloosterkade 10
2628 JB Delft
mail@alexandervanweezel.nl

Thesis supervisor
Prof.dr.ir. M. Wagemaker (Marnix)

Company supervisor
Dr.ir. W.J. van Egmond (Jan-Willem)

Profile leader
Prof.dr.ir. F.M. Mulder (Fokko)

Graduation committee
Prof.dr.ir. M. Wagemaker (Marnix)
Prof.dr.ir. F.M. Mulder (Fokko)
Dr.ir. D.A. Vermaas (David)

Company
AquaBattery B.V.
Contact: Emil Goossen
Lijnbaan 3C
2352 CK Leiderdorp

In loving memory of my father
Arnoldus Theodorus van Weezel
March 5, 1937 - October 12, 2019
Don't worry, be happy

Abstract

With the advent of the sustainable energy transition, the deployment of renewable energy sources is rapidly growing. One of the main problems for sustainable systems like wind and polar power is the fluctuating and intermittent behaviour of these sources. In order to make these systems more reliable energy storage is needed to compliment these systems. A multitude of different systems are now in development at different institutions and companies in order to fulfill this need, one of which being the Greenbattery under development at AquaBattery. The Greenbattery is an Acid Base Flow Battery (AB-FB), which is a further iteration of their original Concentration Gradient Flow Battery (CGFB or Bluebattery). The AB-FB shows promising market potential due to its low impact on the environment, relatively low cost and being easily scalable. Currently the AB-FB is on par in energy densities with systems such as Pumped Hydro Storage and Compressed Air Storage, while not being dependent on geological features or scale of size. However, the AB-FB still needs improvement as co-ion transportation degrades its potential energy density over time. In order to make this technology more viable parameters must be found in order to limit the co-ion transportation. During this thesis research is performed to identify any other potential losses, as well as testing the operational limits and behaviour of the membranes. After this the battery is subjugated to conditions simulating real life operation. During these tests the charge/discharge density, as well as depth of charge, is incrementally changed. By doing this insight is gained in the amount of co-ion transportation that is occurring and whether or not this improves the battery lifetime. The results show the battery can last up to twice as long before falling below 80 % of its original energy density. This is done by reducing the upper and lower limits of the state of charge. However, as a trade off, there is reduction in the energy density of the battery. Following this, research has been performed into the viability of resetting the system, which led to promising results. With this knowledge the operator gains insight whether he wants to put priority in higher energy density or longer lifetime, as well as when he should reset the system to keep it at maximum potential energy density. This gives flexibility to the AB-FB and hopefully help AquaBattery sell its product in the coming years.

Acknowledgements

The past year has been one of the most challenging and valuable learning moments in my life, both in terms of personal as well as professional growth. My master thesis was actually the first time in my life that I did such a theoretical research project on my own, but by doing this I was able to grow in my abilities and gain confidence in my own knowledge. The funny thing is, I started my thesis as a mechanical engineer, with no chemical engineering background at all. This meant that this entire thesis become a leap of faith for me and my trust in my abilities. A large part of this is thanks to AquaBattery. From the moment I stepped through the door on my first work day I felt at home. The passionate drive and friendly work environment actually helped me go to work every day with a smile. Of course, there was also a lot of hard work involved. I have long lost count of the amount of times my stack was leaking. A few times the setbacks, the stress and the pressure actually wanted me to punch a hole in the wall. But the thing is, that this is all part of doing research, and every next day I woke up and said to myself 'Today I will succeed.' I think this drive to keep going forward, because you believe in your research, is something that is ingrained in the DNA of AquaBattery. That in itself is immensely valuable for a company.

I would there like to thank all employees at AquaBattery. Most notably first, my company supervisor Jan-Willem van Egmond. His positive energy on the office floor is amazing and he always takes the time to listen to your problems and answer your questions. I highly doubt I'll ever find somebody so enthusiastic and inspirational about science. I'm also still not sure if I've ever heard of the silver fleet of Spain. I would also like to thank Jelle Zeilstra, for being a fellow motorcycle nerd. I would like to thank Juan Sebastián Álvarez for showing me the ropes of the lab and guiding me through my first experiments. I'm also thankful for Emil Goossen and Isaac Nandgavkar for making me feel welcome at the company and also being great discussion partners at the lunch table. Lastly, I would like to give a shout out to my fellow interns: Grigorios Antoniadis and Luca Bertoni for being amazing research partners and great people to spar thoughts with. As well as Chaturika Kota and Alexandros Papapanos for all the fun we had in 'The Dungeon' (aka the lab).

I would like to thank my TU Delft supervisor Marnix Wagemaker. Despite being an extremely busy person, he was still willing to become my supervisor. We weren't able to meet as much as originally planned, but the conversations we had gave me a lot of inspiration and drive to continue. It was extremely insightful to be able to discuss my results with somebody that wasn't in the so involved with my research subject.

Of course I also want to thank my best friends: Abel Heinsbroek, Alexander Valstar, Seb Harrevelt, Jippe de Groot and Florian Vandepoel. Even though we don't live as close to each other as in the past, all the weekends spent hanging out with each other really helped give me fresh energy. Especially when the corona pandemic started it was great to have a group to talk to while being locked up at home with mostly only your computer. That, and a game of Age of Empires 2 multiplayer is the perfect distraction after a long day focusing on your thesis.

To save the best for last, I would like to mention how grateful I am for my girlfriend Mandy Kok. I tend to get anxious and nervous when stressed, but she always had the patience to deal with it and supported me through it. The past year has be extremely trying for us with the passing away of her mother, Ria Kok, and my father, Ar van Weezel, during my thesis, but we've been able to find strength in each other and always be there to support each other without even asking. Especially in the final stages of my thesis I noticed how much it saddens me they weren't able to see the fruition of my work. Therefor, as a final note, I would like to dedicate this work to my father. He was the person that first inspired me to become an engineer and created the foundation for the man I am now.

Contents

List of Abbreviations and Symbols

Abbreviations

AB AquaBattery B.V.

$AB-FB$ Acid Base Flow Battery

AEM Anion Exchange Membrane

BPM Bipolar Membrane

$BPM-ED$ Bipolar Membrane Electrodialysis

$BPM-RED$ Bipolar Membrane Reverse Electrodialysis

$CAES$ Compressed Air Energy Storage

CEM Cation Exchange Membrane

$CGFB$ Concentration Gradient Flow Battery

DBL Diffusion Boundary Layer

DoC Depth of Charge

EBL Electric Boundary Layer

$ECHA$ European Chemicals Agency

EES Electrical Energy Storage

FB Flow Battery

IEM Ion Exchange Membrane

OCV Open Circuit Voltage

PHS Pumped Hydro Storage

PV Photovoltaic

RES Renewable Energy System

RFB Redox Flow Battery

SGB Small Green Battery

SoC State of Charge

UPS Uninterruptible Power Supply

VRB Vanadium Redox Flow Battery

$ZnBr$ Zinc Bromide Flow Battery

Symbols

α Permselectivity (-)

ΔG Total energy content in (JL^{-1})

$\Delta\phi$ Potential difference over membrane (V)

η_{CE} Coulombic efficiency (-)

η_{RTE} Roundtrip efficiency (-)

η_{VE} Voltage efficiency (-)

γ Porosity of the spacer (-)

A Active surface area of the membrane (m^2)

E_{co-ion} Total amount of energy lost by co-ion transport (Wh)

E_{lost} Total amount of energy lost (Wh)

E_{Ri} Total amount of energy lost by internal resistance (Wh)

ED Energy Density (kWh/m^3)

F Faraday's constant (96485.2 $sAmol^{-1}$)

I Current (A)

I_d Discharge current (A)

I_{charge} Charge current (A)

M Amount of membranes in the stack (-)

M Molarity in (mol/L)

m_x^i Concentrations in the solutions ($molL^{-1}$)

N Number of cells (-)

PD Power Density (W/m^2)

R Universal gas constant in $Jmol^{-1}K^{-1}$

R_{acid} Resistance of the acid solutions compartment (Ω)

R_{AEM} Resistance over the AEM (Ω)

R_{base} Resistance of the base solutions compartment (Ω)

R_{BPM} Resistance over the BPM (Ω)

R_{CEM} Resistance over the CEM (Ω)

$R_{electrodes}$ Resistance over the electrodes (Ω)

$R_{electrolyte}$ Resistance of the electrolyte compartment (Ω)

R_i Internal resistance of the cell (Ω)

$R_{non-Ohmic}$ The non-Ohmic resistance of the cell (Ω)

R_{Ohmic} The Ohmic resistance of the cell (Ω)

R_{salt} Resistance of the salt solutions compartment (Ω)

RTE	Round Trip Efficiency (%)
T	Temperature (K)
t	Time (s)
U	Voltage (V)
U_0	Cell potential of the cell (V)
U_c	Charge voltage (V)
U_d	Discharge voltage (V)
U_{AEM}	Cell potential over the AEM (V)
$U_{BPM-AEM}$	Cell potential over the AEM side of the BPM (V)
$U_{BPM-CEM}$	Cell potential over the CEM side of the BPM (V)
U_{CEM}	Cell potential over the CEM (V)
$U_{d,mean}$	Average voltage during discharge (V)
V_{acid}	Volume acid compartment filled with solutions (m^3)
V_{base}	Volume base compartment filled with solutions (m^3)
V_{ideal}	Ideal voltage over the membrane (V)
V_{real}	Real voltage measured over the membrane (V)
V_{salt}	Volume salt compartment filled with solutions (m^3)
V_{total}	Total available volume filled with solutions (m^3)
X	Fixed charge density (-)
z	Electrochemical valence (-)

1 Introduction

1.1 Problem Introduction

As of 2020 the energy market is undergoing rapid change. Innovations in Renewable Energy Sources (RES) have rapidly decreased the kWh cost for energy and has finally made these forms of energy generation a viable alternative to non-renewable energy sources. Across Europe countries are investing heavily in RES in order to meet the Paris Agreement before 2050[1] . Implementing RES does come with problems as both wind and solar energy have output fluctuations in both daily and seasonal time frames. The resulting intermittency means that demand and production curves often do not align as seen in Figure 1[2]. This means that RES will either output above or below the demand curve, decreasing the reliability needed for a dependable energy system. With the growth of RES and the movement to more decentralized energy grids increasing worldwide, the aforementioned issue will only increase with time [3].

One of the main ways to counteract this growing problem is with the use of Electrical Energy Storage (EES)[4]. In EES is the ability to store the excess energy produced by RES during periods with production exceeding demand. The stored energy can then be used during periods when demand exceeds production as seen in Figure 1. The usefulness of EES does go beyond that. First of all it reduces the need for peak shaving of energy production facilities. This allows the facility to operate more consistently at optimal performance throughout operation, thus increasing its overall efficiency. Furthermore, storing energy for shorter periods of time allows for smoothing out of fluctuations in the frequency of the energy grid, which stabilizes it as a whole [5]. Each system is suited for different applications as can be seen in Figure 2.

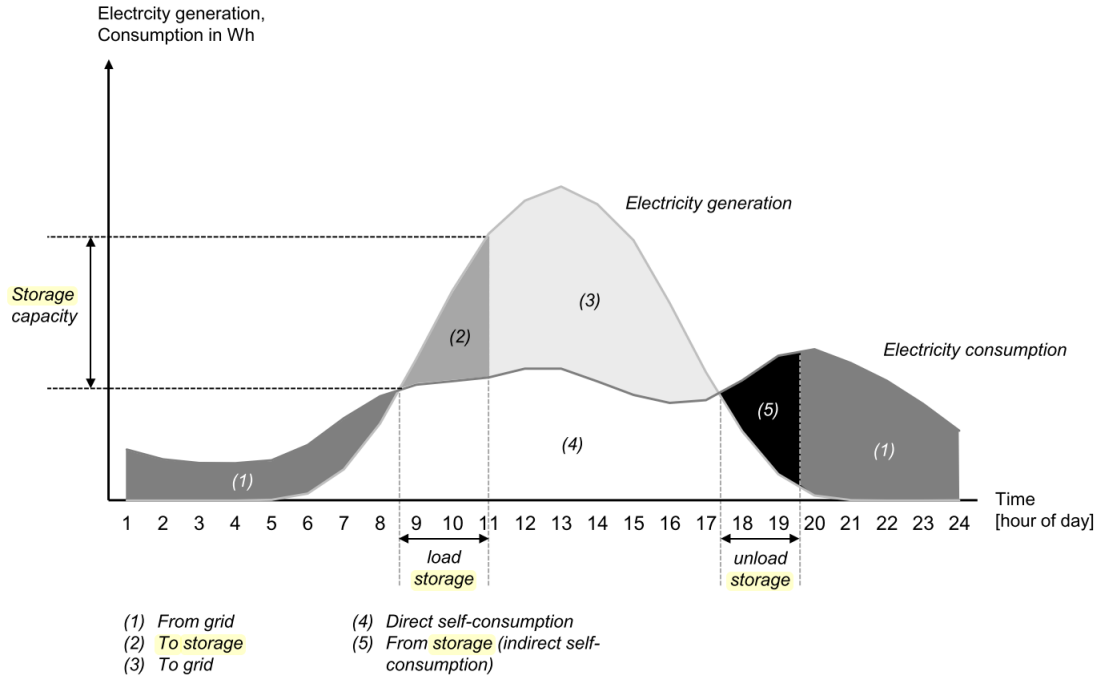

Figure 1: An example of how energy storage can be used in combination with a Photovoltaic (PV) system. EES can be used to capture excess power generation so it can be used later when PV power production drops, while demand increases. It is also possible to make a system completely independent from the electricity grid by scaling up the storage system [2].

One method of storing energy is the use of Flow Batteries [6][7][8]. The most common known version of this is the vanadium redox flow battery (VRB), which works with vanadium salt solutions, although alternatives are being researched. One such alternative is the Acid-Base Flow Battery (AB-FB) currently under development by AquaBattery (AB). With the use of a bipolar membrane it becomes possible to store energy by splitting salt water into an acid and a base, in this case HCl and NaOH. These chemicals are a cheap and abundant resource and converting NaCl into HCl and NaOH by electrodialysis is a well known and common practice. The main focus of development currently applies for the reverse part of the process during which the battery is discharged and HCl and NaOH is converted back to NaCl.
The following literature review will focus on three parts:

1. Exploring the different types of flow batteries currently under development
2. Explaining the workings of the Acid-Base Flow Battery
3. Identifying the largest loss factor.

From there the literature review will be used to define the research question and approach for this master thesis.

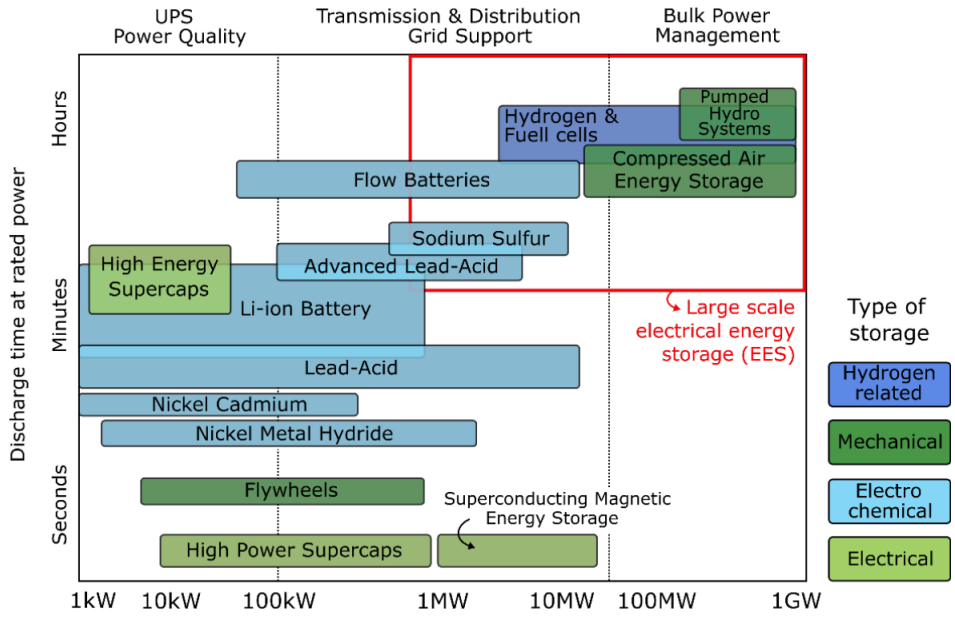

Figure 2: Comparison of different Electrical Energy Storage Systems. UPS stands for Uninterruptible Power Supply. The red square indicates the required discharge time and power rating for a storage system to fall into the large scale storage category. This figure is reprinted from Egmond et al [9], which in turn is a further iteration of the works of Taylor et al [10] and Akhil et al [11].

1.2 Literature Review

1.2.1 Current Technologies in Flow Batteries

With the development of the first redox flow battery in 1971 by Ashimura and Miyake in Japan; the flow battery system has undergone many stages of development throughout the 1970's and 80's. During this period many different types and combinations of membranes, redox couples and electrodes were tested, which led to the development of the first VRB in 1978, the most well known flow battery, and the first

AB-FB around that same time period[8]. A study published in the 1980's by Emrén used a similar system layout as used in this thesis, but wasn't able to reach efficiencies above 0.1%[12].

In essence the flow battery represents a rechargeable battery in which redox active chemicals are dissolved into liquids contained within the system and separated by Ion Exchange Membranes (IEM). When discussing a flow battery it is often only referenced as the electrodes, chemicals and the membranes; but the complete system is much larger than that and can be divided into storage tanks, the stack itself, tubes, pumps and any other electrical components needed.
In many ways the flow battery looks very similar to a fuel cell, but where they stand out the most is their ability to decouple the rated power from rated capacity; being able to recharge; and their nearly unlimited lifespan when comparing them to more conventional batteries. This is because of the flow batteries ability to refresh its solutions and because any parts that impede its performance can be easily replaced, compared to more conventional batteries in which the entire system needs to be replaced [7][13].

Theoretically the AB-FB can reach an energy density of 11.1 kWh/m^3 when using 1 M of acid and base. Actually using 1 M is when operating under stable conditions. The system could go higher and reach values of for example 44 kWh/m^3 when using 4 M of acid and base[14], but leads to other issues as IEMs start to gradually destabilize over the long term when using concentrations above the 1 M acid or base [15]. In practice only a maximum energy density of 3.2-3.3 kWh/m^3 has been measured in this study, which is a significant difference. This is mainly explained by the effects of co-ion transport, the focus of this study, and the state of charge. It should be noted that the energy density is related to the volume of the acid and base solutions inside the cell. In practice this energy density will be lower when one also takes into account the salt/redox solutions, pumps, housing, membranes, etc. When comparing to other typical RFBs, the AB-FB does display significantly lower ED. A VRB or ZnBr redox flow system typically display around 35 kWh/m^3 and 20 to 65 kWh/m^3 respectively[16][17][18]. Currently the AB-FB compares more favourably to systems like Pumped Hydro Storage (PHS) and Compressed Air Systems (CAES), which both range at 0.5-2 kWh/m^3 and 2-6 kWh/m^3 respectively[6].

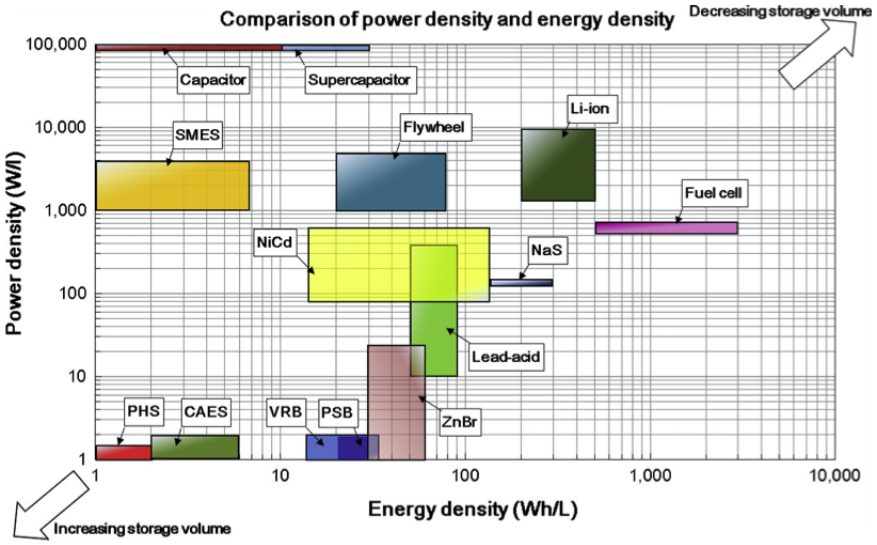

Figure 3: Comparing the Energy Density versus the Power Density of different systems. The highly compact technologies suitable for volume limited applications can be found in the top right corner. Large volume consuming systems more suited for energy management can be found in the bottom left corner [6].

When comparing EES options, this can generally be placed in two different types of categories: Power quality and reliability or Energy Management. Power quality represents systems with high power ratings, but low energy capacity; while energy management represents systems with low power ratings, but are capable of high energy capacity[14]. As it stands now flow batteries, and more specifically the AB-FB, fall into the energy management category. In fact, as can been seen in Figure3, redox flow batteries is the most suited of all batteries for large scale grid operation on a stationairy level. Although not yet represented in Figure 3. the AB-FB falls in between the CAES and VRB systems.

By using the AB-FB for grid scale operation, this would mean that it could be used to store solar and wind energy on a daily to weekly scale just like CAES and PHS. The main disadvantage of PHS and CAES is the fact that these systems need specific geological formations in order to operate and are only employable in large capacities of 50 MW and above[4]. The AB-FB on the other hand can be deployed anywhere with no constraints to geography and is scalable.

1.2.2 The Acid-Base Flow Battery

As discussed in Section 1.2.1, the AB-FB is a further iteration of older flow battery designs such as the Vanadium Redox Flow Battery (VRB) and the Concentration Gradient Flow Battery (CGFB) . Where the system mainly differs, next to the used solutions, is the buildup of its Ion Exchange Membranes (IEM). IEMs are polymeric materials containing charged ion groups. Cation Exchange Membranes (CEM) are able to let mobile cations pass as it contains fixed anionic groups, thus blocking anions. Anion Exchange Membranes (AEM) work in the same way only vice versa, so it lets mobile anions through while blocking cations. Both these types of membranes are called mono-polar membranes. The VRB and CGFB only make use of monopolar membranes[19][16].

The AB-FB takes it a step futher and makes use of not only monopolar membranes, but also a bipolar

membrane (BPM). As the name suggests, the BPM contains two IEM layers, one of which is the AEM and the other the CEM. One could notice that this does change the functionality of the membrane, as in theory the BPM would block all ions in passing through. This is why CEM and AEM are strictly used for separation purposes, while BPMs are generally used for splitting H_2O [20][17][21]. In Figure 4 one can see a schematic of the AB-FB. The system consists out of multiple triplets, with each triplet consisting a acid, base and salt compartment, as seen in Figure 4B and C. In a real life AB-FB a system can consist out of dozens of triplets connected in series and sandwiched between two electrodes, which mounts the system as a whole, this is called a 'Stack'. There are limitations to the amount triplets that can be set in series, as this can cause short circuit current. This will be discussed in Section 2.4. The space between the membranes are the compartments in which the solutions flow through. These compartments are created by spacers which also separate the membranes from each other. The spacer does have more influence on the system beyond membrane separation. During operation a boundary layer is formed across the membrane, which in turn has an influence on the ion flux across this membrane. The thickness of this boundary layer is a function of the velocity and flow geometry of the spacer, and can be minimized by promoting turbulent flow. This is done by placing a mesh in the flow area. How boundary layers are formed and their effects will be discussed more in depth in Section 2.3.

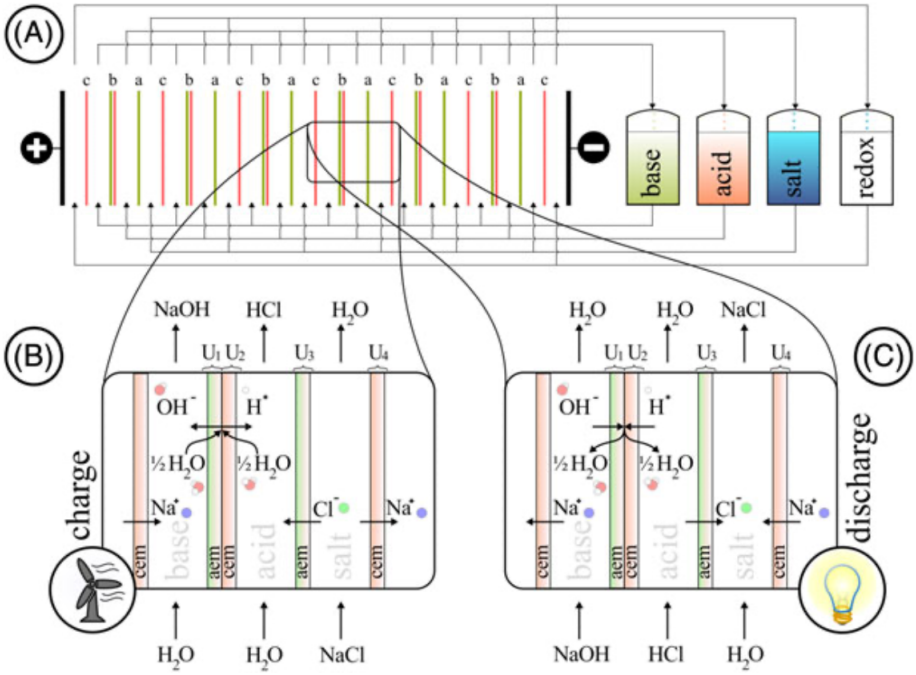

Figure 4: Concept drawing of AB-FB. Each triplet consists out of a AEM, CEM and BPM. Multiple triplets can be placed next to each other in series to create a 'stack'. The triplets are placed between two electrodes to create a cell. The figure is reprinted from Egmond et al [17].

There are four different types of solutions that are stored in external tanks: acid, base, salt and electrolyte. The redox tank shown in Figure 4 contains the electrolyte and is pumped through two external compartments that is in contact with the electrodes. The electrolyte enables the system to convert the ionic current that occurs at the membranes to an electric current. The system in this study uses 0.25M

$FeCl_2/FeCl_3$ and has the following redox reaction at the electrodes:

$$\begin{aligned} \textbf{Cathode:} Fe^{3+} + e^- &\rightarrow Fe^{2+} \\ \textbf{Anode:} Fe^{2+} &\rightarrow Fe^{3+} + e^- \end{aligned} \tag{1}$$

This redox reaction is reversible and occurs both during charging and discharging. Furthermore it must be noted that the type of electrolyte used determines the type of IEM used bordering the electrolyte compartment. As the electrolyte used for this study dissociates into Cl^-, a AEM should be used for anions to move through the membrane. This differs from the IEM sequence shown in figure 4.
$FeCl_2/FeCl_3$ is chosen because it is cheap, non toxic for the environment (as classified by the ECHA) and has a low overpotential. The downside is that when the current is too high or the flow of the electrolyte is too low. In this case side reactions can occur as there is no fresh electrolyte. The available iron will run out and therefor the electrons are forced onto or from other available ion species as shown in Eq. 2.

$$\begin{aligned} &\textbf{On the cathode side:} \\ &2H^+ + 2e^- \rightarrow H_2(g) \\ &H_2O + 2e^- \rightarrow OH^- + H_2(g) \\ &\textbf{On the anode side:} \\ &Cl^- \rightarrow Cl_2(g) + e^- \end{aligned} \tag{2}$$

H_2 is a well known, highly flammable compound and Cl_2 is a highly poisonous gas. There is also the potential of $Na(s)$ forming, which is highly explosive, due to trace amounts of Na^+ being present in the solution from co-ion transport. The risk of $Na(s)$ forming can be considered negligible though, as in order for this reaction to take place all other possible reactions have to take place first. Furthermore, when using $FeCl_2/FeCl_3$ concentrations above 0.25 M there is the possibility of $FeCl_4^-$ forming. This chance increases at higher molarities as the concentration gradient is larger. Because $FeCl_4^-$ is a anion, it is able to move through the AEM and form Fe^{2+}/Fe^{3+} again. This will poison the CEM as $Fe^(2+)/Fe^(3+)$ is not a highly mobile ion and becomes embedded in the CEM. In order to mitigate these risks it is important to make sure sufficient fresh electrolyte is pumped through the system. Generally speaking, the higher the charge/discharge current density, the faster the pumps must operate in order to make sure no side reactions happen.

During charge, as seen in Figure 4B, H_2O is pumped into the acid and base compartments, while $NaCl$ is pumped through the salt compartment. Through application of an electric field water is split into H^+ and OH^- ions at the BPM interface. In the salt compartment $NaCl$ is split into Na^+ and Cl^- ions. With the application of an electric field and use of IEM's these ions are separated and $NaOH$, HCl and H_2O are formed in the base, acid and salt compartment respectively. Charging the battery resembles BPM electrodialysis (BPM-ED). Theoretically the splitting of H_2O into H^+ and OH^- occurs at 0.83V, but in practice the required voltage falls above that. The presence of a catalyst in the BPM lowers this back to 0.83V as far as possible [22][23].

The discharge process, as seen in Figure 4C, is also known as Bipolar Membrane Reverse Electrodialysis (BPM-RED), in which the energy is recovered through neutralization of the acid and base solution in the BPM interface. This neutralization reaction is a spontaneous reaction as the Gibbs free energy for H^+ and OH^- is $-80kJ/mol$ at $25°C$. If the conversion from chemical to electrical energy was 100%, then this would mean the system could reach an energy density of 22 Wh/mol. The H^+ and OH^- ions recombine at the BPM interface, thus neutralizing the acid and base solutions. Both the Na^+ and Cl^- ions reverse in direction and move back into the salt compartment and form $NaCl$, this for is largely

driven by both diffusion and electroneutrality forces [24][7]. The corresponding potentials generated for both BPM-ED and BPM-RED will be discussed further in Section 2.2.

In order for membranes to be selective of which ions pass through they make use of a so called fixed charge. A schematic version of this can be seen in Figure 5. The fixed charge is entwined in a polymer, thus creating a charge over the membrane as a whole. This charge creates a selectivity for ions to pass through, named counter ions. Ions with the same charge as the membrane are called co-ions. With a permselectivity of 1 would mean that no co-ions would enter the membrane. This is a perfect membrane, which is never the case. The IEMs of this thesis have a permselectivity of 0.96-0.99, but this may differ between manufactures [25] and even between production runs. The permselectivity of the membrane can even further be lowered by the swelling of the membrane [26]. How the fixed charge density, permselectivity and swelling relate to each other can be found in Section 2.2.

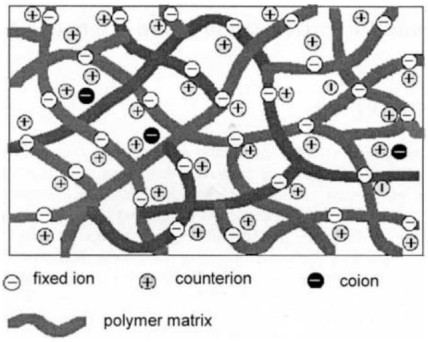

Figure 5: An illustration of a CEM monopolar membrane. Figure reprinted from Strathmann [27].

This non ideal selectivity of the membranes does create an issue for the systems utilizing this technology and co-ions are regarded as a major loss mechanism for AB-FB. In a publication by Xia et al [7] it can be found that co-ions in the membrane can have significant effect on the resistance over the membranes as well as being the leading cause for self discharge. The paper of van Egmond et al [17] shows that co-ions in the acid base solutions can lead to significant voltage drop during discharge and can form up to 60% of the observed losses.

To finalize there are two different types pumping operations for the battery to choose from: Continuous flow or start stop method. During continuous operation the influent and effluent flow from the same container and is pumped continuously during charge and discharge operation. With start stop operation the pumps are turned off during charge and discharge. Up till recently the continuous flow method was the default mode for the AB-FB at AquaBattery B.V., but does have several downsides. Firstly there is an issue with concentration distribution within the stack as ions are gradually transported across the membrane as it flows through the system, this also has an effect on the round trip efficiency as the charge voltage slowly increases as the ion concentration drops. This will be discussed in Section 2.3. Secondly, is the system quickly suffers from leakage issue as local pressure issues start to form within the stack. This problem goes beyond the scope of this thesis as this is a common issue in larger sized stacks containing multiple cells. As noted in Section 3 this thesis will use two triplets at best. More information about the phenomena can be read in the works of D.A. Vermaas [28]. Finally is the co-ion build up during operation has a much more direct effect on the system as the in and output streams share the same container. This means that any co-ions gained in the solutions is pumped right back into the system. It is possible to use separate tanks for the influent and effluent streams, but this will greatly increase the size of the battery. The start stop method negates all problems except the last issue, but as a trade-off

the boundary layer in the stack increases which in turn increases the overall resistance. During this study both methods will be utilized for the purpose of streamlining and optimizing the experiments. Generally the start stop method is used when co-ion transport effect have to be minimized, such as in the 50 Cycle test in Section 3.2.2. In the Characterization experiment co-ion minimization isn't a priority, therefore continuous flow is chosen as this method is significantly faster than start stop operation. Which method is actually more efficient goes beyond the scope of this thesis.

1.3 Main Research Question

As mentioned earlier in this section, the effects of co-ion transport is one of the main loss mechanisms of the AB-FB and encompasses several subjects that influence it. It is therefore important to know how this loss mechanism has an effect on the lifespan and efficiency of the battery [17]. One of the most common reasons cited reason for co-ion transport is a low permselectivity in the IEMs [29][21], this is sadly entirely dependent on the quality of the membranes used in the system, but it is still possible to investigate how much the factor weighs amongst the other losses. Is it possible to find parameters to reduce co-ion transportation through reduction of the depth of charge or current densities? In the works of Xia [7] for example it is stated that the formed potential difference that is established over the BPMs changes depending on positive, negative or no current at all. By finding these parameters and tweaking them it will hopefully become possible to extend the lifespan of the AB-FB before its energy drops below 80% of its original value.
This leads to the following the main research question: *What is the influence of co-ion transport on the lifespan and efficiency of the AB-FB and what are the variables that can minimize or neutralize this phenomenon?*

In order to answer this question several sub-questions have to be formulated:

- What are the other losses that occur during operation?
- How does co-ion transport occur and is it different between the charge and the discharge cycle?
- To what degree does co-ion transport effect the lifetime of the AB-FB?
- Is it possible to 'reset' the system after the accumulation of co-ions hit a certain level?

1.4 Thesis outline

To answer the questions asked in section 1.3 an outline for the research has to be established. In section 2.1 the basic formula's will be laid out in how the performance of a battery can be evaluated. From there the co-ion transport phenomena will be investigated with the corresponding electroneutrality forces and concentration gradients in section 2.2. Section 2.3 and 2.4 will give a brief explanation of boundary layer formation and short circuit currents. Both are losses that occur in the AB-FB to a certain extent. In order to get more insight in the performance of the used membranes a set of characterization experiments has been set up in section 3.2.1. This helps establish a baseline for a scaled down version of real life operation in section 3.2.2. In this section parameters with be slightly adjusted in an attempt to reduce the energy density degradation of the battery and improve overall efficiency. Finally as method of resetting the battery in an attempt to regain its original energy density is performed in section 3.2.3. How these experiments are setup is outlined in section 3. To sum it up, a short conclusion of all the results and recommendations for future research can be found in section 5. In addition to the main body of text appendices can be found after the conclusion. This contains a curated sample of results that explain small possible differences in the results, as well as supporting pictures/tables to gain more insight about the experiments. Many repeat experiments were run during this thesis, and only the differences deemed important enough were added to the appendix.

2 Theoretical Background

While Section 1.2.2 a more general overview has been given in the workings and performance parameters of the AB-FB, in this section a more theoretical in depth look will be taken. Section 2.1 and 2.2 shall form the bulk the bulk of this chapter as it will give us the tools to evaluate the systems performance as well as giving insight in how to influence co-ion transport in the system. After this Section 2.3 and 2.4 shall give a brief explanation of the Boundary Layer Formation and Short Circuit Currents respectively. While both are not the main focus of this study it is still important to a least get a better understanding of these loss mechanisms as these still occur during operation.

2.1 Evaluating the system

In order to understand how the system performs it is important to know how energy is extracted out of the system and the establishment of membrane potentials. As mentioned in Section 1.2.2 the BPM is made by fusing an AEM and CEM together with a catalyst processed in the AEM and/or CEM. Between the AEM and CEM there is an area what is typically called the BPM interface or junction. In this area the H^+ and OH^- concentration is very low (10^{-7}). When the battery is in a charged state the concentration of H^+ and OH^- is much higher inside the acid and base solutions (0.5 M for both solutions in this example), due to the Donnan exclusion a membrane potential is established over each layer of the BPM (Equation 3 and 4) [17]. Consequently in a charged flow battery the concentration of NaCl in the salt reservoir is low (0.25 M in this example). As the concentrations of the Cl^- (0.5 M) in the acid compartment and the Na^+ (0.5 M) in the base compartment are higher a membrane potential over the AEM and CEM develops as well (Equation 6 and 5). By using the Nernst equation the ideal membrane potential is calculated, assuming the solutions are ideal and water transport can be neglected [17][24]. The overall cell potential U_{cell}, or Open Circuit Voltage (OCV), is then calculated by summing up Equations 3-6 as each membrane can be seen as in series of each other.

$$U_{BPM-AEM} = \frac{RT}{zF} ln \frac{[OH^-]_{BPM}}{[OH^-]_{BASE}} \approx \frac{8.314 \cdot 298}{-1 \cdot 96485} ln \frac{10^{-7}}{0.5} = 0.396V \tag{3}$$

$$U_{BPM-CEM} = \frac{RT}{zF} ln \frac{[H^+]_{ACID}}{[H^+]_{BPM}} \approx \frac{8.314 \cdot 298}{1 \cdot 96485} ln \frac{0.5}{10^{-7}} = 0.396V \tag{4}$$

$$U_{AEM} = \frac{RT}{zF} ln \frac{[Cl^-]_{SALT}}{[Cl^-]_{ACID}} \approx \frac{8.314 \cdot 298}{-1 \cdot 96485} ln \frac{0.25}{0.5} = 0.018V \tag{5}$$

$$U_{CEM} = \frac{RT}{zF} ln \frac{[Na^+]_{BASE}}{[Na^+]_{SALT}} \approx \frac{8.314 \cdot 298}{1 \cdot 96485} ln \frac{0.5}{0.25} = 0.018V \tag{6}$$

$$U_0 = U_{BPM-AEM} + U_{BPM-CEM} + U_{AEM} + U_{CEM} = 0.83V \tag{7}$$

where U (V) is the membrane potential, R (J mol^{-1} K^{-1}) is the universal gas constant, T (K) is the temperature, z(-) is the electrochemical valence and F (C mol^{-1}) is the Faraday constant. In theory, when stacking many cells in series, the voltage over the electrodes can reach up to tens of volts.
Eq. 7 only describes the cell potential during OCV state, so when no current is applied. During operation U_0 will actually change over time, as the concentrations in the compartments change. As the concentration changes during discharge the cell potential will decrease. This decrease in cell potential also means a decrease of the remaining energy potential of the solutions. When the system is treated as an ideal flow battery, the remaining energy content can be calculated as a function of the H^+ concentration as seen in Eq. 8:

$$\Delta G = \int_{10^{-7}}^{[H^+]} F U_{cell} d[H^+] \tag{8}$$

where ΔG(J L^{-1}) is the total energy content, $[H^+]$ is the concentration of protons in the solution (mol L^{-1}), and F is the Faraday's constant (C $mol^{-}1$).
The internal resistance of the battery, R_i, is the sum of the Ohmic and the non-Ohmic resistance, as show in Eq. 9:

$$R_i = \overbrace{R_{BPM} + R_{AEM} + R_{CEM} + R_{base} + R_{acid} + R_{salt} + R_{electrodes}}^{\Omega} + \overbrace{R_{non-\Omega}}^{non-\Omega} \tag{9}$$

where R_{BPM} is the resistance of the bipolar membranes, R_{AEM} and R_{CEM} the resistance of the anion and cation exchange membranes, respectively, R_{acid}, R_{base}, and R_{salt} the resistance of the solutions compartments, and $R_{electrodes}$ is the combined resistance of the electrodes, the electrolyte solution in the electrode compartment and the extra AEM that is used to complete the the stack. While in practice many cells will be put in series, thus making $R_{electrodes}$ negligible, this is not the case during this thesis. As will be explained further in Section 3, the experimental setup will only operate with up to two cells. In order to evaluate the performance of the battery $R_{electrodes}$ must be determined and substracted from the results, this is done with the Blank Test as explained in Section A. All these combined form the Ohmic resistance, as denoted by Ω in Eq. 9, of the flow battery. When current is applied a boundary layer, or otherwise know as concentration polarisation, will form at the membrane interface. This boundary layer is referred as an non-ohmic resistance ($R_{non-\Omega}$) in Eq.9 and will further be explained in Section 2.3.
Now that the internal resistance (R_i) is know, the total measured cell potential U can be calculated with Eq. 10:

$$U = U_{cell} + IR_i \tag{10}$$

where U (V) is the total battery voltage across the terminals and I (A) is the applied current. Note that during operation the concentrations in the compartments will change, thus U_{cell} will change over time during (dis)charge.

Eq. 11 - 19 represent the equations needed in order to evaluate the performance of the battery, i.e.: the round-trip efficiency, coulombic efficiency, voltage efficiency, energy density and power density [19][30]. The round-trip efficiency, η_{RTE}, is defined by the ratio of energy released during discharge of the battery and the energy used during charge of the battery. For this thesis all experiments are operated with constant current, therefor η_{RTE} van be expressed as the product of the coulombic efficiency (η_{CE}) and the voltage efficiency (η_{VE}):

$$\eta_{RTE} = \frac{\int_0^{t_d} I_d U_d dt}{\int_0^{t_c} I_c U_c dt} = \eta_{CE}\eta_{VE} \tag{11}$$

where t (s) is the process time, I (A) the measured current, U (V) the measured potential and the subscripts c and d indicate whether the system is charging or discharging. The coulombic efficiency is the ration of the total amount of charge released during the discharge process over the amount of charge transferred during the charge process:

$$\eta_{CE} = \frac{\int_0^{t_d} I_d dt}{\int_0^{t_c} I_c dt} \tag{12}$$

The voltage efficiency is calculated by taking the ratio of η_{RTE} and η_{CE}:

$$\eta_{VE} = \frac{\eta_{RTE}}{\eta_{CE}} \tag{13}$$

The voltage efficiency is a useful tool to determine the magnitude of internal losses due to internal resistance. The total amount of energy lost can be calculated by:

$$E_{lost} = \int_0^{t_c} I_c U_c dt - \int_0^{t_d} I_d U_d dt \tag{14}$$

The total amount of energy lost by internal resistance is calculated as follows:

$$E_{Ri} = \int_0^{t_c} R_i I_c dt + \int_0^{t_d} R_i I_d dt \tag{15}$$

By subtracting E_{Ri} from E_{lost} it becomes possible to calculate the losses in the system besides internal resistance losses. In the ABFB this is predominately co-ion losses as water transport is not an issue in the ABFB [17]:

$$E_{co-ion} = E_{lost} - E_{Ri} \tag{16}$$

The energy density, ED (kWh m^{-3}), represents the amount of available energy for a certain volume of solutions:

$$ED = \frac{\int_0^{t_d} I_d U_d dt}{V_{total}} \tag{17}$$

$$V_{total} = N(V_{acid} + V_{base} + V_{salt})\gamma_{spacer} \tag{18}$$

where N is the number of cells in the battery, V(m^3) is the volume in each solution compartment and γ (-) is the porosity of the spacer. Lastly there is the power density, PD (W m^{-3}), of the battery which represents the amount of power available from a certain membrane surface area:

$$PD = \frac{I_d U_{d,mean}}{MA} \tag{19}$$

where $U_{d,mean}$ (V) is the average voltage during discharge, M is the amount of membranes in the stack and A(m^2) is the active surface area of the membrane.

2.2 The Donnan Equilibrium and the Co-Ion Transport Phenomena

In this section a deeper look will be taken at the exact processes occurring in and around the membrane. Up till now it is assumed that the system behaves as an ideal battery, but this is of course not the case. In order to better understand how co-ion transport occurs it is important to first explain the Donnan Equilibrium, which on a more practical level is the parameter linked to the permselectivity of the IEM [26].

In order to only let anions or cations through, IEM are in fact ions which are formed into a polymer. The ions (e.g. COO^-) form together a fixed charge. The higher charge, the better the permselectivity of the membrane. This fixed charge density is denoted by X. In order to better visualize this phenomenon an example will be made with a CEM seen in Figure 6 [9].

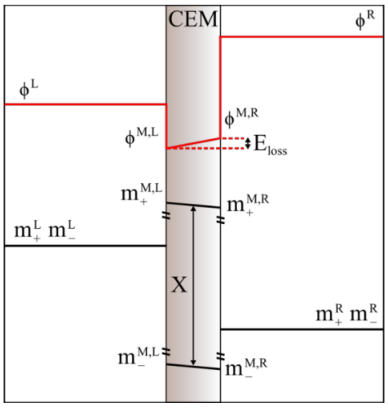

Figure 6: A schematic representation of a CEM with two different concentrations on either side. On the left hand the solution has a high concentration and on the right hand a lower concentration. The black lines represents the molarities and the red lines the potentials. This figure is reprinted from J.W. van Egmond [9].

The concentrations in the solutions is expressed as m_i^x, where the super script shows the location (L, left, R, right, M, membrane) and the subscript the charge. In this case m_+^x represents the counterion and m_-^x represents the co-ion. Eventually an equilibrium will develop between the ions in the solution and the ions in the membrane, this equilibrium is called the Donnan equilibrium. When considering the left side of the membrane it can be expressed as [9][28][7]:

$$m_+^L m_-^L = m_+^{M,L} m_-^{M,L} \tag{20}$$

As electroneutrality has to be observed in the membrane this leads to:

$$m_+^{M,L} = X + m_-^{M,L} \quad i.e. \quad \bar{c}_{counterion} = X + \bar{c}_{co-ion} \tag{21}$$

Assuming $m_+^L = m_-^L$, Eq. 21 can be inserted into Eq. 20 which leads to the following:

$$(m_-^{M,L})^2 + X m_-^{M,L} - (m_+^L)^2 \tag{22}$$

By solving Eq. 22 for $m_-^{M,L}$ it is possible to get a formula which calculates the co-ion concentration in the left side of the CEM in Figure 6 as a function of the counterion concentration in the solution. This equation is also repeatable for the right hand side of the membrane:

$$m_-^{M,L} = \frac{-X + \sqrt{X^2 + 4(m_+^L)^2}}{2} \tag{23}$$

Now that the ion concentrations both within the membrane and within the solution are known it becomes possible to calculate the potential difference ($\Delta\phi$) , i.e. the Donnan potential, between the solution and the membrane[29][31]:

$$\Delta\phi^L = \phi^{M,L} - \phi^L = E_{Donnan,left} = \frac{RT}{zF} ln\left(\frac{m_+^L}{m_+^{M,L}}\right) \tag{24}$$

This can be repeated for the right hand side of the membrane as well:

$$\Delta\phi^R = \phi^R - \phi^{M,R} = E_{Donnan,right} = \frac{RT}{zF} ln\left(\frac{m_+^{M,R}}{m_+^R}\right) \tag{25}$$

Adding Eq. 24 and 25 together, as well as adding Eq. 20 and Eq., will give the total membrane potential based on the Donnan potential[9]:

$$E_0 = E_{Donnan,left} + E_{Donnan,right} = \frac{RT}{zF} ln\left(\frac{m_+^L}{m_+^R}\frac{X + m_-^{M,R}}{X + m_-^{M,L}}\right) = \frac{RT}{zF} ln\left(\frac{m_+^L}{m_+^R}\frac{X + \sqrt{X^2 + 4(m_+^R)^2}}{X + \sqrt{X^2 + 4(m_+^L)^2}}\right) \tag{26}$$

This equation gives a more accurate representation of the potential over a membrane by taking into account the fixed charge density and the non-ideal behaviour of the solutions. It is also possible to replace the molarity values with activity [9][29].

Eq. 21 implicates that at a set $\bar{c}_{counterion}$, the larger value X, the more the membrane is shielded from co-ions entering. For ideal membranes only counterion flux will occur in the membrane, but in reality this is not the case and co-ion transport has significant effect on efficiency. In fact the fixed charge value X also has a significant effect on the boundary layer, which in turn increases the non-ohmic resistance in the system as will be discussed in Section 2.3 [29]. Furthermore X is not a constant value as it is effected by swelling. Cross-links in the membrane polymer reduce the swelling and because high swelling reduces the fixed charge density, low swelling is desired. Unfortunately, polymers containing charge groups (active polymers) have a high swelling degree and thus have a low area resistance. Therefor a balance must be found between reinforcing polymers and active polymers in order to obtain a high charge density. This is a complex study and goes beyond the scope of this thesis [28][26][32].
Due to the fact that real IEM never block all co-ions the actual potential over a membrane is in fact less than what is initially calculated with the Nernst equation in Eq. 7. For this the permselectivity (α) is introduced. Manufacturers use this value to characterize their membranes and give an indication of the actual potential difference over a membrane. One way to determine is to measure the actual potential difference and divide it with the theoretical value[24]:

$$\alpha = \frac{V_{real}}{V_{ideal}} \tag{27}$$

The average permselectivity of the membranes used in this thesis is around 0.96-0.99 [25]. The calculated permselectivity value can then be used in the Nernst equation to calculate the actual potential difference over the membrane [28]. For example in the case of the anionic side of the BPM in Eq. 3 the acutal value will become:

$$U_{BPM-AEM} = \alpha\frac{RT}{zF} ln\frac{[OH^-]_{BPM}}{[OH^-]_{BASE}} \approx 0.96\frac{8.314 \cdot 298}{-1 \cdot 96485} ln\frac{10^{-7}}{0.5} = 0.38V \tag{28}$$

Since permselectivity effects all membranes, one can rewrite Eq. 7 by multiplying each membrane potential with its respective permselectivity:

$$U_{cell} = \alpha_{BPM-AEM}U_{BPM-AEM} + \alpha_{BPM-CEM}U_{BPM-CEM} + \alpha_{AEM}U_{AEM} + \alpha_{CEM}U_{CEM} \tag{29}$$

Now that the basis for how the Donnan equilibrium and permselectivity is established a deeper look can be taken in how this translates to the BPM and co-ion transport in the system, as up till now these effects have only been discussed with the use of Monopolar membranes. In Figure 7 a sketch is made with a BPM in three separate situations with no current applied. All three BPM's have a fixed charge density of X=1, with the CEM (left) in contact with HCl and the AEM (right) in contact with NaOH. The CEM and AEM in Figure 7a are completely separated. From here a Donnan equilibrium will form and a small potential difference ($\Delta\phi$) between the membrane and the solution is formed. This potential difference makes sure the counterions stay in the membrane and prevents co-ions from entering, thus only a small concentration of co-ions is present in the membrane.

Figure 7b depicts what happens when the CEM and AEM come in contact with each other, i.e. both IEM's form a bipolar membrane. The concentrations of $[H^+]$and $[OH^-]$ on the outside of the membranes stays the same, but at the interface between the CEM and AEM H^+ and OH^- start to rapidly recombine into H_2O. This sudden decrease in concentration creates a shift in the potential $\Delta\phi$. On the CEM side a strong negative potential develops, which blocks OH^- from entering. While on the AEM side a strong positive potential develops and blocks H^+ from entering. Therefor the concentrations of H^+ and OH^- rapidly decrease to 0 at the interface. This potential difference also has a strong attracting effect on the co-ions (Cl^- in CEM and Na^+ in AEM). This creates a co-ion flux over the respective membranes. The dotted line in Figure 7 shows the concentration of co-ions slowely decreasing over the membrane after which it suddenly increases again at the adjacent membrane. Since the potential gradient between both membranes, the co-ions are quickly sucked across the interface towards the adjacent membrane [31]. Therefor the concentration of co-ions is very low at the interface and increases once more at the accepting membrane. This creates a high concentration gradient at the accepting membrane after which co-ions start to diffuse into the corresponding solution (Cl^- into the base and Na^+ into the acid). Due to the fact there is co-ion crossover through the BPM does mean that another unwanted side effect occurs: The self discharge of the battery. In order to maintain electroneutrality the ionic flux of Cl^- and Na^- has to be compensated with an equivalent flux of H^+ and OH^- ions. This leads to a neutralization reaction at zero current, i.e. the battery is self discharging.
This same process is repeated in Figure 7, but with higher concentrations. The increased concentrations also increase the potential difference, which in turn increases the amount of co-ions at the accepting membrane.

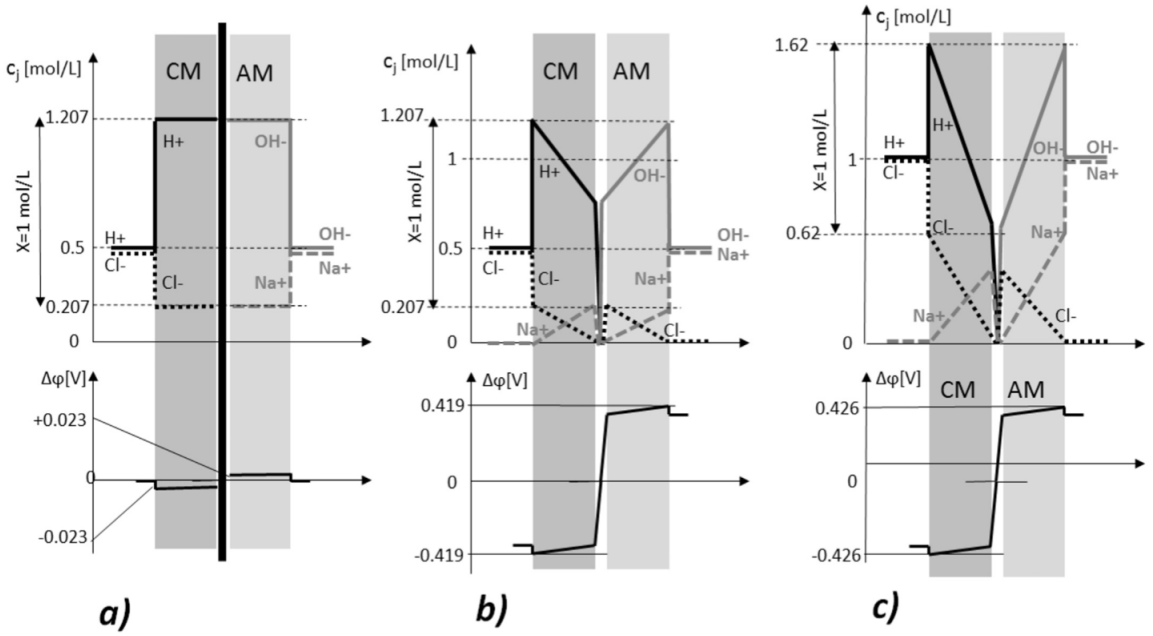

Figure 7: A schematic representation of the ionic concentrations (c_j) and potential difference ($\Delta\phi$) across the bipolar membrane. a) Depicts the cation (CM) and anion (AM) membrane completely separate from each other. In b) and c) the CM and AM are in contact with each other, forming a bipolar membrane with an interface in between the two membranes. In a) and b) the concentrations in the acid/base solution is 0.5 M HCl/NaOH. In c) the solution is 1 M HCl/NaOH in the acid/base compartments. This figure is reprinted from Jiabing Xia [31].

Co-ion flux doesn't only happen at zero current. Figure 8 gives a schematic representation of the ionic

flow during zero current, charge and discharge with the corresponding potential difference ($\Delta\phi$). As mentioned earlier, at zero current co-ion (Na^+ and Cl^-) fluxes develop over the bipolar membrane and need to be compensated by counterions (H^+ and OH^-) in order to maintain electroneutrality.
During charge an electric field is applied over the cell, this increases the potential difference over the BPM and start splitting water. The bold arrows indicate the main ionic fluxes. The electric field pulls the cations to the left and the anions to the right, resulting in the formation of HCl and NaOH in their respective compartments. The increased potential difference ($\Delta\phi$) also results in a higher co-ion flux over the membranes as indicated by the broken arrows. Any co-ions at the interface of the BPM are sucked across the membrane and into the accepting solution due to the applied electric field and concentration gradient. This leads to a lower NaCl concentration in the salt compartment as well as the formation of NaCl in the acid and base compartment.
In order to discharge the counterion fluxes is reversed as indicated by the solid arrows and the potential $\Delta\phi$ is decreased. As mentioned earlier water starts to form at the interface and has to diffuse back into the acid and base compartments. There is a limit to this process though, as if one sets the current density too high the formed water will not be able to diffuse fast enough out of the BPM. This will lead to voltage drop and eventually delamination of the bipolar membrane [33]. There is still co-ion flux as indicated by the dashed lines, but the decreased potential difference $\Delta\phi$ will not be the main driving force anymore. In fact the concentration gradient and subsequent diffusion will become a larger factor with co-ions diffusing into the interface, accepting membrane and subsequent acid/base solution. Taking Cl^- as an example: When fully charged with no co-ions in the compartments a potential difference $\Delta\phi$ and a high concentration gradient will establish between the acid, the BPM interface and the subsequent base compartment. The will drive the Cl^- co-ions across the CEM to the interface and the accepting AEM. During charge the electric field will pull the Cl^- across the AEM into the base compartment, but during discharge this is not the case. The concentration gradient is now the main driving force, but as Cl^- builds up in the base compartment during charge-discharge cycles this concentration gradient force will decrease. This in turn will lead to less co-ions breaking through the accepting membrane over time and subsequently build up at the interface and AEM. This has two consequences: First, the buildup of co-ions at the interface which in turn will lead to a voltage drop of the overall potential. Second, Cl^- will start to accumulate inside the AEM, which in turn will increase the resistance of the membrane. For Na^+ is the same situation, but vice versa. By charging these effects can be eliminated again as the electric field will pull the co-ions out of the BPM, but now more Cl^- and Na^+ and accumulated in the base, acid solutions respectively [7][24][34][17].

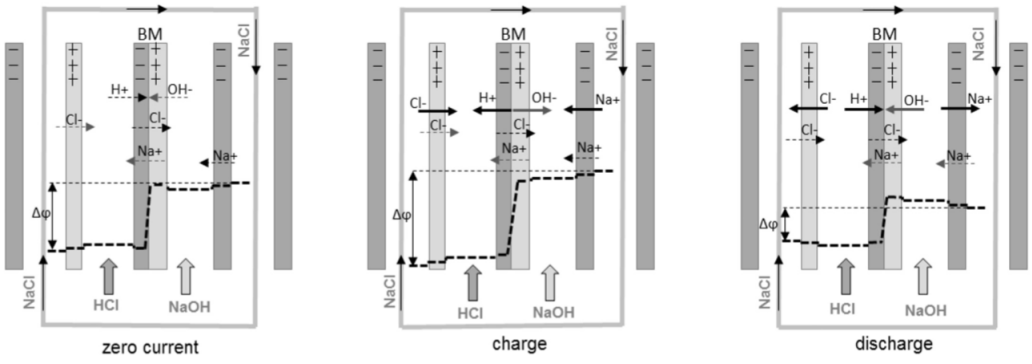

Figure 8: The BPM under zero current, charge and discharge. Under zero current the ionic fluxes are given by the broken arrows. During charge and discharge the counterion flux are given by the bold arrows and co-ion fluxes by the broken arrows. The change in electric potential $\Delta\phi$ is given by the broken line. This figure is reprinted from Jiabing Xia [31].

2.3 Boundary Layer Formation

As mention in Section 2.2, the fixed charge density X and the Donnan equilibrium creates a boundary layer over the membrane which increases the non-ohmic resistance of the cell. This diffusion boundary layer consists out of two smaller adjacent layers that interact with each other as depicted in Figure 9a. On a nanoscale level is the Donnan layer, also known as the Donnan exclusion layer or the Electric Boundary Layer (EDL), where the concentration of counterions is significantly larger than the co-ions. On a micrometer scale the Diffusion Boundary Layer (DBL) is formed [28]. This represents the area where ions are transported from the bulk solution to the interface, or interface to bulk, through diffusion and migration. This change in concentration is accentuated in Figure 9b. Here there is a counterion flux from left to right (just like in Figure 9a). As the ion concentration in the left diffusion layer decreases, this will decrease the conductivity of the solution in the diffusion layer. The reversed can be said for the right diffusion layer, here the ion concentration goes from high to low, meaning the right diffusion layer will have a higher conductivity than the right bulk solution. These combined effects of the DBLs is called concentration polarisation [21][28][32][29]. In essence the resistances change with the ion concentration and in an ideal system these concentration differences will compensate each other. The fact is that the relation between concentration and conductivity isn't linear and they will only compensate partially for each other.

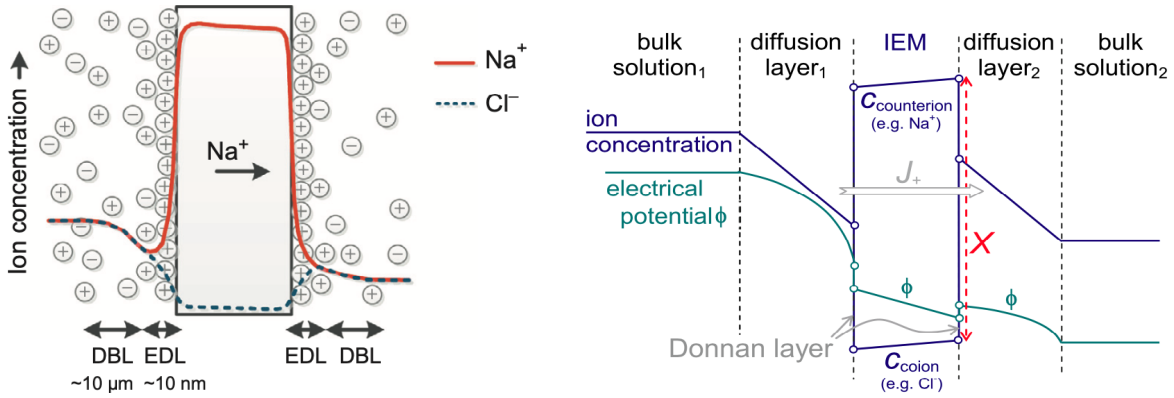

(a) This figure is reprinted from David Vermaas et al. [28].

(b) This figure is reprinted from A.H. Galama et al. [29].

Figure 9: Figure 9a gives a visual representation of how the DBL and EDL is formed. Figure 9b gives a schematic representation of how the ion concentrations and electric potentials change over the diffusion layers. The concentrations and distances are not properly scaled.

Minimizing the effects of concentration polarization can be done by promoting mixing effects in the solution compartments through for example a mesh [35][36]; or by increasing the flow rate of the system [35]. Lastly, it is possible to reduce the effects by reducing the current density during charging, as the Nernst equation is more sensitive to change in the concentrations along the membrane during ED than during RED [36][28]. Note that final point only applies when working with high and low concentrations between solutions, for example 0.5 M and 0.01 M NaCl. This situation is more common in CGFB, as the ABFB hardly operates below the 0.1 M NaCl. It should also be noted that DBL and EBL formation doesn't apply when working with overlimiting currents, where the velocity of ions promote mixing in the boundry layers. This topic goes beyond the scope of this thesis and more information can be found in the works of V. Nikonenko et al. [37] and J. Choi et al. [38].

Non-ohmic resistance consists more than only concentration polarization though, as this only defines

concentration gradients along two axis. A second concentration gradient is formed along the flow axis. The influence of this gradient is dependent on the residence time of the solution in the battery. Figure10 gives a schematic representation of this phenomenon in CGFB systems, but this occurrence is applicable in any flow battery where ions are exchanged over membranes.

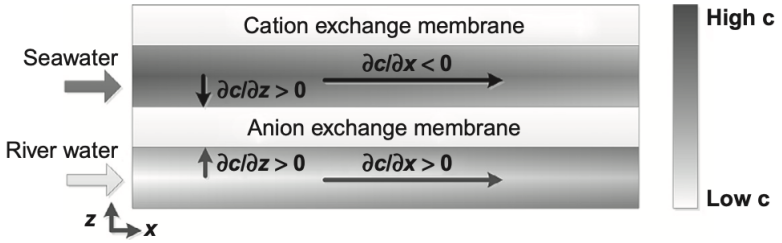

Figure 10: An illustration of how concentration gradients can change over the length of a solution compartment, which is a cause of non-ohmic resistance. This figure is reprinted from D.A. Vermaas [28].

In Figure 10 two solutions flow along the AEM, one with high concentration (seawater) and one with low concentration (river water). Due to the concentration difference a concentration gradient is formed and ions start to diffuse from the high concentration compartment towards the low concentration compartment as denoted by $\delta c/\delta z > 0$. Along the x axis the concentrations depletes in the high concentration solution ($\delta c/\delta x < 0$), while it increases in the low concentration solution ($\delta c/\delta x > 0$). As the concentration gradient decreases over the x axis this will also decrease the membrane voltage. This voltage drop can be scaled to the current density of the system, from which the resistance is obtained. This is also part of the non-ohmic resistance. The significance of the resistance is strongly dependent on two factors: Firstly, the time the solution is in the system exchanging ions; and secondly, the current density during (dis)charge, which drives the amount of ions exchanged over the membrane . This signifies the main difference of non-ohmic resistance compared to normal resistance profiles: The time dependant behaviour that is liked with changes in current [28].
How significant this is can differ between system, as this is largely dependent on the design of the stack. It has been shown that promoting mixing keeps the concentration gradient constant throughout the length of the solution as well minimizing concentration polarization [35]. It is also possible to find a correct ratio between current density and flow rate in order to prevent complete degradation of the concentration gradient, which in turn prevents voltage drop and increase in resistance [28]. Although promoting homogeneous flow has been proven to be the most effective strategy, without compromising the energy efficiency [36]. Part of this is deciding the type flow feed to be used in the system, which can be either co-current, counter current or cross flow. Each of these techniques come with their own advantages and disadvantages. For this study it has been chosen to take the co-current configuration. Co-current flow is preferred in industrial sized units as this avoids local pressure differences and helps minimize leakages, even though from a flow distribution perspective this is the least attractive [36][24].

2.4 Short Circuit Current

As shown in Eq. 9 the resistance of a stack is in fact multiple smaller resistances in series. In Figure 11A is a simplified electrical circuit of a stack. Besides the internal resistance of the stack (R_i) and system also has multiple feed solutions and electrolyte ducts connecting the system with each other, this is represented by the parasitic resistance R_p. This internal resistance will increase linearly with the number of cells a system contains. After a certain threshold it is possible ionic short circuit currents will occur, otherwise known as parasitic currents [39][40]. This is because R_i will become greater than R_p, driving the ions through the path of least resistance. When short circuit currents occur ionic transport of electrical charges will flow through the manifolds of the feed solutions or through the ducts of the electrolyte, in essence 'bypassing' the internal resistance of the stack.

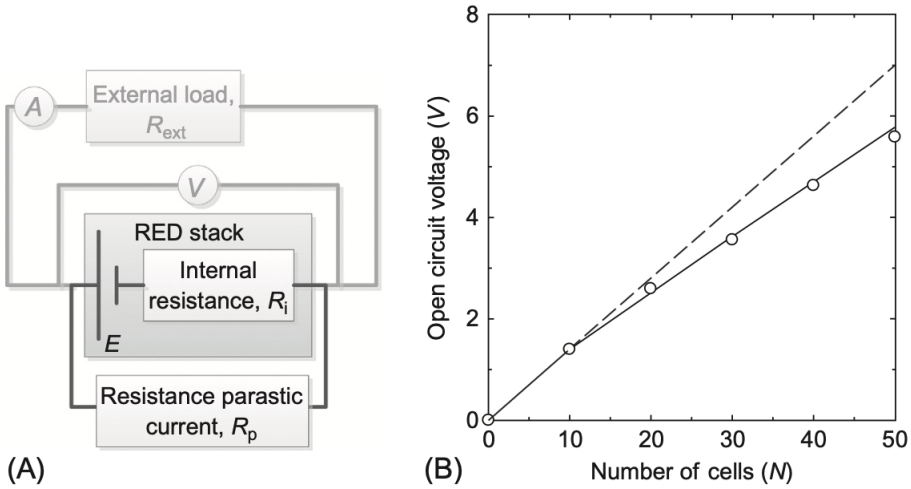

Figure 11: Figure (A) gives the electrical circuit equivalent of battery set up. Internal resistance R_i represents the resistance mentioned in Eq. 9. Resistance parasitic current represents the resistance of all the tubing, inlets, outlets, etc. that is used for the flow of solutions and electrolyte outside the stack. Figure (B) shows how the OCV decreases as the number of cells increase in a stack. This is a general representation and may differ between systems. These figures are reprinted from D.A. Vermaas [28].

As depicted in Figure 11B the effects of short circuit current become greater in proportion to the number of cells in a stack. This is because R_i increases linear, while R_p is non-linearly dependent on the amount of feed manifolds and ducts. If short circuit currents wasn't an issue the OCV line would increase linearly, but this isn't the case and decreases significantly after 20 cells.
In order to prevent short circuit current it is important to properly design the stack in order to prevent this phenomena from happening [40]. It is possible to increase R_p by for example increasing the length of the tubing or reducing the size of the inlets, but this can create problems with pressure drops and flow distribution [35]. Another way reduce the internal resistance of the stack by creating sub divisions of cells that are connected in series with each other and connected in parallel with the rest of the system. The current systems used for this thesis won't exceed the two cells, thus making short circuit current not an issue, but it still important to remember that this can occur in larger systems when designing a battery.

3 Materials and Methods

In this chapter the materials used during the experiments will be discussed, along with the experimental setup for the different types of experiments. Section 3.1 will give details in the required materials needed to assemble the battery and the necessary equipment that was used in order to conduct the experiments. Section 3.2 lists the different experiments conducted, what their parameters are and their intended purpose in order to validate the main research question of this thesis.

3.1 The Small Green Battery

While the practical design of the Green Battery is much larger, with the latest prototype being 50cm x 50cm, this is unpractical for testing concepts in which the chemical process is the most important aspect. This is because this larger battery designs other more practical problems become more prominent, such as: internal and external leakage of solutions from compartments; short circuit currents between compartments thus affecting the voltage output; increased time duration to perform a test due to the larger volumes of solution in the cell; and finally the amount of time needed to (dis)assemble a cell for testing. Therefor this study shall focus on the Small Green Battery (SGB). The SGB is a much smaller design that consists of two Plexiglas end plates of 156mm x 66mm, which house the electrodes and connectors for the in- and output flows. Due to the smaller size this eliminates the short circuit current phenomena as well as minimizing the chances of leakage in the system. The electrodes (Magneto Special Anodes BV, The Netherlands) are constructed from a titanium mesh and coated with iridium and ruthenium, but more abundant materials such carbon and graphite can be used as an alternative [41].

In between the end plates the IEM's and spacers are placed as explained in Section 1.2.2 to create the cell with one or more triplets. The spacers are made in-house and form a mesh for the solutions to flow through, which is sealed by a silicon gasket on the edges of the spacer as shown in Figure 12.
The mesh itself serves two purposes:

- It creates turbulent flow which in turn helps reduce the boundary layer formation along the membrane as discussed in Section 2.
- It prevents the membranes from coming into contact with each other and creates a compartment for the solutions.

These spacers are approximately 500 μm thick with an active area of 0.0022 m^2 and a porosity (γ) of 0.5. The active area represents the area which the solutions flow through and are in contact with the membrane, while the porosity (γ) represents the space the mesh fills in the solutions compartment.

The AEM's, CEM's and BPM's are supplied by Fumatech GmbH, Germany. These membranes consist out of different batches supplied to AquaBattery over the last two years. The quality of these membranes differ considerably between batches and this will be discussed further in Section 4. Table 1 shows the different batches of membranes that were used and their corresponding thickness. The only way of differentiating between same type of membranes is either marking them during the cutting process or measuring their thickness. The thickness of the membrane can also influence the electrical resistance of the membrane, but this goes beyond the scope of this study. When not in use for an experiment these membranes are stored in a 0.5M $NaCl$ solution. It should be noted that when membranes are stored for prolonged periods of time they tend to slightly swell in thickness due to absorbing the solution they are stored in. Therefor the measurements made in Table 1 might deviate 1-3 μm due to swelling. The values given, are an average of multiple measurements.

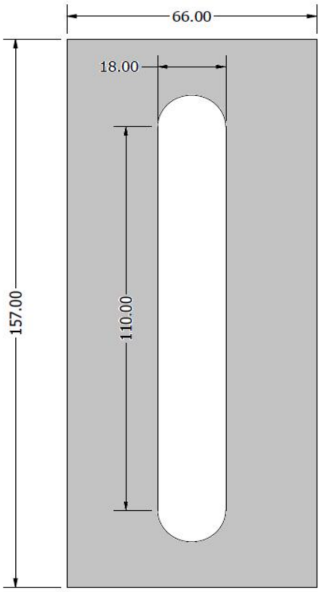

Figure 12: A general schematic drawing of a typical spacer used in the SGB. The solutions flow through the elliptical space in the center and in reality is also filled with a mesh. The outer grey area represents the silicon gasket which seals the compartment. It should also be noted that the in- and outlet holes are not represented in this figure.

Description	**Date**	**Thickness (mm)**
BPM	2017	0.115
BPM	April 2019	0.140
Standard BPM	-	0.165
AEM	January 2019	0.083
AEM	April 2019	0.09
CEM	April 2019	0.085

Table 1: List of membranes used during experiments, their supply date and their corresponding thickness

The solutions are stored in either 2 L or 200 mL external glass bottles (Thermo Fischer Scientific, USA), depending on the type of experiment. The electrolyte in stored in a 2L glass bottle and contains 500 mL of $0.25MFeCl_2/FeCl_3$ mentioned in Section 1.2.2. The electrolyte is replaced at least once a week or before every new set of experiments to keep performance degradation through oxidation to a minimum. The solutions are connected to the battery stack using 6 mm in diameter LDPE tubing with polypropylene connectors (EM-Technik, Germany). Masterflex L/S peristaltic pumps (Cole-Parmer Instruments, USA) were used to pump the solutions and electrolyte. For the Charge Reset Cycle in Section 3.2.3 an Arduino is used to control the pumps, as individual pumps needed to be turned on and off at different time intervals. The Arduino itself has been built by a previous intern at the company, together with a corresponding code as a basis. The code has been expanded to work with the Ivium.

3.2 Experimental Procedure

In order to correctly chart the effects of co-ion transport two types of experiments were conducted: The Characterization tests in Section 3.2.1 and the 50 Cycle test in Section 3.2.2. The Characterization tests are in fact a collection four separate tests that together shed light on the performance of the BPM and at what limits it can operate. The 50 Cycle test represents fifty charge-discharge cycles which should simulate real life operation. During this experiment the degradation of performance over time becomes clear and how this degradation is effected by certain parameters.
The Charge Reset Cycle experiment is conducted in order to find a solution for unwanted Na^+ and Cl^- ions in the acid and base compartments respectively. This is a one of the effects of co-ion transport over time as mentioned previously in Section 2.2.

Depending on the experiment the stack is constructed with either one or two triplets. Experiments with three triplets proved to be unsuccessful, as the the resistance of the SGB was high enough the for the measured voltage to exceed the 10 V, which is the upper limit of the galvanostat. A single triplet contains a AEM, BPM and a CEM, but in order to interact with the electrolyte and convert the ionic current in a electric current a external AEM must be added. The exact configuration depends on the experiment and this shall be further elaborated in its corresponding subsection.
Before each experiment a blank test must be conducted in order to determine the resistance of the electrolyte and the electrodes. This is later subtracted from the final measurements. For this specific setup, the results and how the resistance is determined please refer to Appendix A. For all experiments the electrolyte pump maintains a flow rate of 100 mL/min throughout the entire experiment. This is in order to prevent side reactions from happening in the electrolyte compartments as mentioned in Section 1.2.2.

3.2.1 Characterization

As mentioned earlier characterization in fact consists out of four separate tests: The OCV, IV, IVT and Single Discharge test. For these experiments 100 mL of 1 M HCl and 1 M NaOH, and 200 mL of 0.185 M NaCl solutions are used. These solutions are continuously circulated at a flow rate of about 10 mL/min as can be seen in Figure 13. The solutions are refreshed after each experiment. The other test parameters actually differ per experiment. After the initial run of experiments the IV and the Single Discharge test will be repeated, but with 0.15 M NaCl added to the acid and base solutions. This will mimic the effects of co-ion transport, but in a more advanced stage which under normal conditions needs extended amount of time to build up.

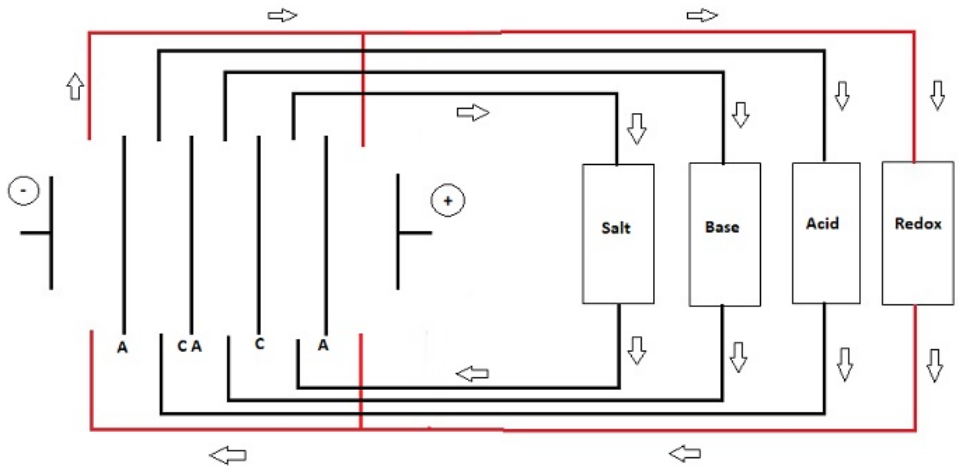

Figure 13: A schematic representation of the setup during the Characterisation Tests. The acid and base containers are filled with 1 M HCl and 1 M NaOH respectively. The salt container is filled with 0.185 M NaCl. During the experiment the acid, base and salt solutions are pumped continuously at 10 mL/min. The redox solution is pumped at 100 mL/min.

Open Circuit Voltage (OCV) test: During the OCV test no actual current is applied. This is so that the Open Circuit Voltage of the system can be measured. As explained in Section 2 the stack represents multiple voltages and resistances in series. In theory the OCV can be calculated using the Nernst equation, which in this case 0.9 V. This test is to determine if there is any deviation from the theoretical value as well as giving any information about the permselectivity of the membranes and short circuit currents [28].

IVT test: For the IVT test a single charge and discharge current of 30 A/m^2 is applied. By subtracting the blank test from the results it is possible to differentiate different resistances from equation 9. This means both the R_{Ohmic} as well as $R_{non-Ohmic}$.

IV test: During the IV test the current density during charge and discharge is slowly increased. Here the behaviour and limits of the BPM is mapped over 15 A/m^2, 45 A/m^2, 60 A/m^2, 75 A/m^2, 90 A/m^2 and 105 A/m^2. From the resulting graphs one can determine how the BPM behaves at different current densities. As mentioned section 2.2, it is entirely possible the voltage will collapse or increase due to co-ion transport or the buildup of water at the BPM interface which in turn will also cause voltage collapse. By running this test more insight is given at which limits the battery can run during normal operation.

Single Discharge: The final test consists out of applying a single discharge current of 15 A/m^2 till the stack reaches 0 V and thus is completely discharged. By plotting the single discharge without background concentration against the graph with background concentration it will become easier to see how co-ion transport has effect on the discharge time and the resulting voltage drop.

3.2.2 50 Cycle Test

The 50 Cycle Test replicates real life operation of the battery in its most basic form. The setup of this experiment is shown in Figure 14. The stack is constructed with two triplets and the acid, base and salt compartments are filled with 0.5 M HCl, 0.5 M NaOH and 0.25 M NaCl respectively. This represents the battery at about 50% SoC. The acid, base and salt compartments are disconnected from the pumps and the input and outputs are sealed.

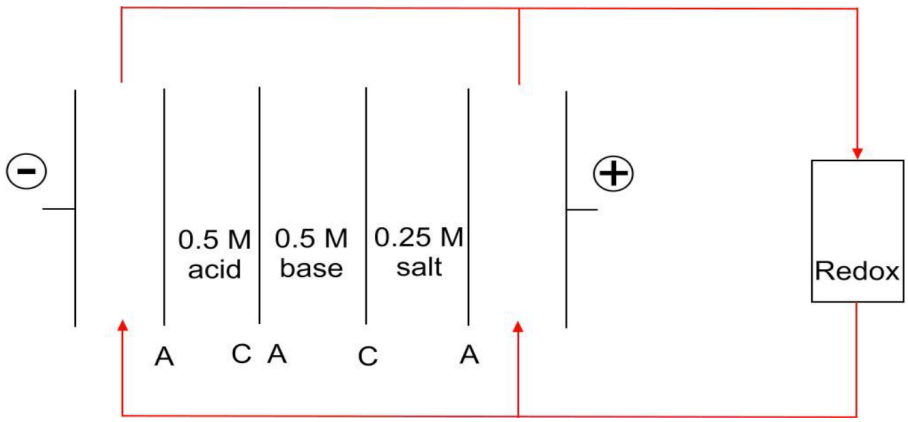

Figure 14: A schematic representation of the setup during the 50 Cycles Test. The acid, base and salt compartments are filled with 0.5 M HCl, 0.5 M NaOH and 0.25 M NaCl respectively after which the pumps are shut off.

With this test two variable parameters can be introduced:

- The charge and discharge current density. This represents how fast the battery will be charged and discharged and will have an effect on the power density in the system. The current density parameters are chosen by studying the behaviour of the BPM during the IVT test, which is part of the Characterization tests and will be explained in Section 4.1.
- The cutoff voltages. By varying the cutoff voltages it is possible to set the upper and lower limits of the SoC. This means that by for example lowering the cutoff voltage range the lifetime of the battery can be increased at the the cost of capacity. This will be explained further in Section 4.2.

First a baseline set of parameters are chosen, in this case a cutoff of 7 V for charging and 0.25 V for discharging as well as charging current density of 100 A/m^2, or 220 mA, and a discharge current density of 30 A/m^2 or 66 mA. With the values measured it becomes possible to plot the change in Round Trip Efficiency (RTE), Power Density (PD) and Energy Density (ED) of the battery over a period of 50 cycles. Furthermore this test can also be used to compare the performance of different BPM's, as the selectivity of BPM's differs between batches. Having a better selectivity means the BPM can block more co-ions from crossing into the wrong compartments, thus better selectivity means the battery will retain its capacity over a longer period of time as the acid and base compartment will contain less impurities.

3.2.3 Charge Reset Cycle

During the Characterization and 50 Cycle Tests efforts are made to prove and minimize co-ion transport effects by extending the lifespan of the battery. Sadly this phenomenon can't completely be eliminated and Na^+ and Cl^- will build up in the acid and base compartments respectively. At a certain point the

battery will fall below 80% of its original ED, which can be considered 'dead' in battery technique terms. One of the advantages of the AB-FB is its ability to 'reset' itself. The purpose of this test is to verify if the cell is able to completely desalinate the salt water and produce as pure as possible demi water. This is useful as in real life operation one can mix the acid and base, which are contaminated with co-ions, to create the salt water used for the reset cycle. By completely desalinating the salt solution it is possible to create new pure acid and base solutions without co-ion contamination.

This cycle is similar to the charge phase of the battery. In Figure 15 the experimental setup shown. By applying current to the electrodes the salt water stream is desalinated, while the acid and base streams become more acidic and basic respectively. The charging current is set to 100 A/m^2 or 220 mA with a cutoff voltage of 7 V. However, instead of switching to the discharge process, the solutions in the compartments are refreshed and the charging process is repeated. All products are collected in different bottles after which the conductivity of the demi water solution is measured. The conductivity is measured (Jumo Aquis touch, Jumo GmbH & Co. KG) to determine the salt concentration in the solution and therefor the effectiveness of the desalination process. The process is done with two triplets and repeated until a sufficient volume for measurement is produced.

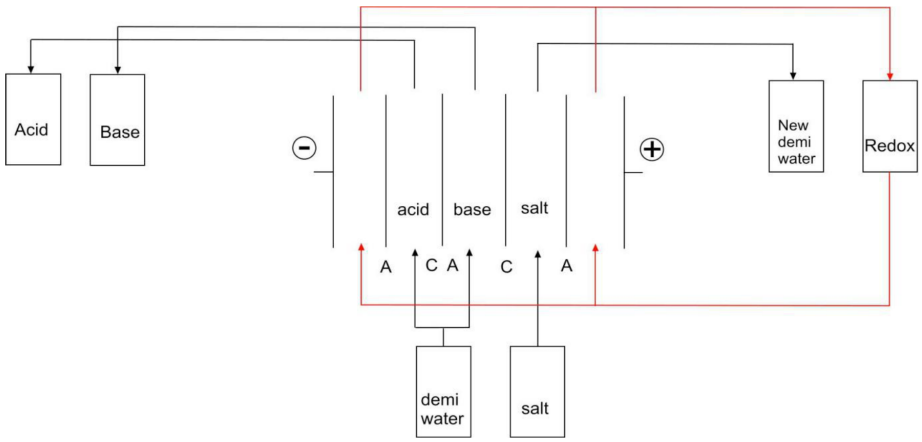

Figure 15: The experimental setup for the Charge Reset Cycle. The stack is filled with pure demi water and 0.25 M NaCl. The Arduino controls the acid, base and salt compartment pumps, while the redox pump operates independently.

The initial salt water concentration is 0.25 M. The demi water and salt water are pumped into the respective compartments as shown in Figure 15 for at least 30 s, this is to make sure the compartments are completely filled and flushed from previous solutions, as this may influence the conductivity measurements. The electrolyte pump is set to 100 mL/min as usual and the other pumps are set to 9 mL/min. During charging the acid, base and salt pumps are turned off for the duration of the charging phase, so only the volume inside the stack is desalinated.
After each charge step the pumps are turned on for a limited amount of time that is specified by the load fraction of the spacer. The demi water and salt pumps are set to 9 mL/min. The loading fraction is a measure of the percentage of the total volume of the spacer that is filled with new solutions. This is done because of preferential flow and how fluid a behaves in noncircular ducts [42]. Knowing the dimensions of the spacer and the flow rate of the incoming stream, the percentage of the solution replaced, or loading fraction of the compartment can be calculated. If one completely refills the volume of the spacer, so a load fraction of above 1, this would mean that part of the salt solution would contaminate the produced demi water bottle and thus influence the conductivity measures. By choosing a low loading fraction part of the desalinated water will in fact be desalinated multiple times and in theory the salt concentration

of the demi water will be even lower.

4 Results and Discussion

As Section 3 has explained the procedure of the experiments, in this chapter the results of those experiments shall be presented and discussed, while also comparing it with theoretical values. The results presented here are a curated sample of a multitude of files as tests were made with multiple BPMs. This is done because BPMs tend to vary in quality even within the same batch. This will be further elaborated in the Appendices. All results are processed using MATLAB.

4.1 Characterization

For the purpose of this thesis the characterization tests are mainly used to gain insights in the basic behaviour of the BPM and how it reacts in relation to co-ion build up in the solutions. For the purpose of this chapter it will stay focused on that approach, but the characterization tests also can be used in a broader more practical way as a tool to compare the quality of bipolar membranes. This is useful because the quality of membranes can vary even when cut from the same sheet. A more comprehensive insight in these differences can be found in Appendix C.

4.1.1 OCV

As mentioned in Section 3.2.1, the OCV test is in fact a simple in which no current is applied and only the Open Circuit Voltage is measured. With this any small side reactions such as short circuit current can be detected as well as determining if the permselectivity is within limits. First the theoretical OCV voltage has to be calculated. Using Eq. 3 - 7, one will find that $U_{cell} = 0.9V$. Due to permselectivity the true value will off course be different. During the test a OCV voltage of 0.88 V was measured. By using Eq. 27 it shows that the permselectivity of all the membranes in the cell average out at around 0.98. This is well within the ranges of the specification sheet given by the producer [25], which range between the 0.94-0.99.

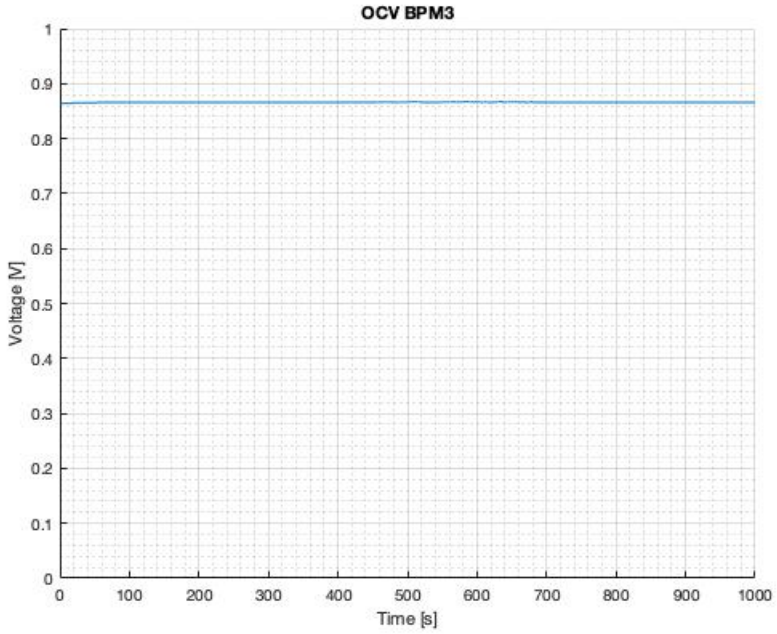

Figure 16: The OCV test over 1000 seconds. The OCV is measured at 0.88 V, which is within the permselectivity limits specified by the manufacturer.

As the test is only conducted with a single triplet short circuit currents isn't an issue. If for example the system contained more than a single triplet and short circuit currents would be occurring, then the easiest way to detect this is if the calculated permselectivity would out of the bounds given by the specification sheet. This doesn't that if the permselectivity with multiple triplets is within the bounds there would be no parasitic currents. If for example one would calculate a permselectivity of 0.94, while the real value is at 0.98, this means that parasitic currents are occurring, but they are so minor it falls within the permselectivity parameters. Therefor it is important to analyse these tests with scrutiny for these phenomena.

4.1.2 IVT

Just like OCV, the IVT test is a relative simple test in order to get better insight in the basic functionality of the stack. In Figure 17 the test starts at approximately the same value as measured in Figure 16. At t=120 seconds a charge voltage of 66 mA is applied for a 120 seconds, then it returns to OCV for a 120 seconds before finally applying a discharge voltage of 66 mA of a 120 seconds. At first glance the time intervals between starting and ending the (dis)charge cycles may seem excessive, but this is actually important at two separate stages for different reasons. First at the first 120 seconds it is to make sure there is completely homogeneous flow throughout the spacer as well as completely flushing the system. If there are inconsistencies with these factors deviation from the OCV would be noticeable. Secondly it is important to get rid of any boundary layer formation. This occurs after the charge cycle and this dissipation can in fact be seen at t= 240s - 260s and t = 480s - 500s by the slight curvature. If this phenomena is not properly dissipated before starting the discharge cycle, then this may in fact influence the reading of the values needed to calculate the resistances.
During the charge and discharge cycle the graph is split into two distinct sections, with the orange line representing the voltages including $R_{electrodes}$ and the blue line without $R_{electrodes}$, which is determined by subtracting the blank test (as explained in Appendix A). At t = 120s and 360s it can be seen that

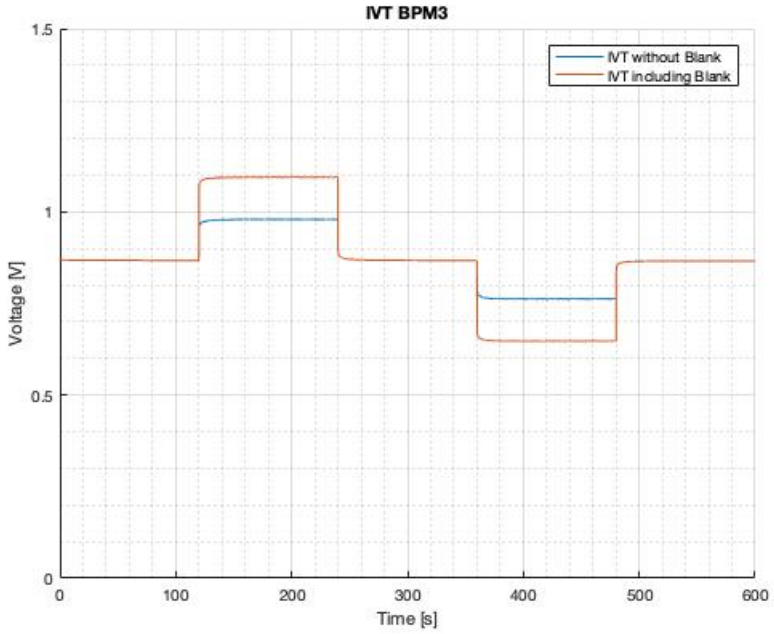

Figure 17: The IVT test plotted over time. The orange line represents the test with $R_{electrodes}$. The blue line represents the results with $R_{electrodes}$ subtracted from the data.

there is only a slight increase ($\pm 0.01V$) in the curvature due to concentration polarization. Keeping this to a minimum is important as this practically eliminates $R_{non-ohmic}$ from Eq. 9 and makes it easier to isolate $R_{electrodes}$ from R_i. If concentration polarization does occur to a large extent (above 5% of the total voltage) it is important to either check the refresh rates and increase it; or reduce the current, as boundary layer formation increases with current. It is also possible the change the setup and apply counter current flow, but this causes other issues as explained in Section 2.3.

A keen eye will also have noticed by now that during and after (dis)charge, the voltages remain practically the same. This is because the charge and discharge current is so low and short in comparison to the volume of the solutions that hardly any change is registered in the concentrations. This makes it easier to determine the resistances.

By reading the values from the graph it can be determined that $R_{electrodes}$ actually represents quite a large part of the voltage. In fact by doing a simple calculation $R_{electrodes}$ represents 68% of the total voltage during charge and discharge. This can be seen as a significant loss and can actually vary a lot when comparing to different tests as can be seen in Appendix C. These losses can be attributed to two main factors: Electrolyte degradation and oxidation on the electrodes, both of which can be minimized by taking the correct precautionary steps.
In relation to the electrolyte the greatest cause of degradation is in fact oxidation over time that occurs by contact with air. The ideal situation to combat this is by using an electrolyte pumping system that minimizes any contact with air, but sadly due to the current setup this is not possible. Therefor it is advised to actually replace the electrolyte at regular basis. Oxidation of the electrodes is also another factor that builds up over time. The best way to combat this is by making the electrolyte solution slightly acidic by adding 0.1 M HCl.

4.1.3 IV

For the first time the effects of co-ions in the acid and base become truly visible during the IV test. In Figure 4.1.3 two distinct lines are plotted. The blue dots represent the charge and discharge of the ABFB under increasing current density with pure solutions, so no co-ions present at the start. After the test experiment is done it is repeated, but then with 0.15 M added to the base and acid compartments. This is in order to replicate conditions in which a large amount of co-ion transport has occurred and study which different effects this has on the BPM and voltage of the system as a whole. This experiment is represented by the orange crosses in the graph. In Figure 18 it is clear that with pure solutions the BPM behaves normally as it increases and decreases linearly during charge and discharge respectively.
The interesting part is that several distinct events have occurred after adding the background concentration. During the charge phase the slope of the graph slightly increases when compared to the pure solutions. This indicates that the resistance of the membrane has increased. One of the most direct explanations for this is the presence of co-ions in the membranes. When the system switches from discharge to charge, these co-ions are still present in the BPM, which temporarily increases the membrane resistance before being pulled out by the electric field and being replaced with H^+ and OH^-. This is discussed in Section 2.2 and has also been encountered in the works of Xia [31]. This isn't the case for this experiment though, because in this experiment charge cycles are run in succession of each other before switching back to the discharge phase.
A more likely explanation for the increased resistance is the change of diffusion forces for Na^+ in the CEM and Cl^- in the AEM. As the amount of $NaCl$ increases in the solution, an increase in the percentage of Na^+ in relation to the H^+ in the CEM will increase. The same occurs in the AEM, but then with Cl^- in relation to OH^-. This change in ion composition in turn increases the resistance of the membranes.

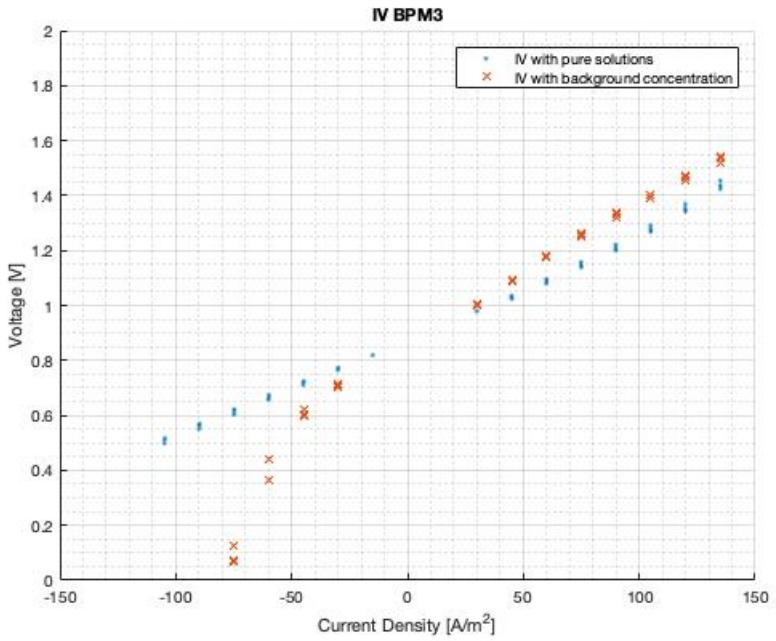

Figure 18: The IV test plotted over -100 to 150 A/m^2 range. The blue line represents the experiment performed with pure solutions. The orange line is the same test performed with 0.15 M NaCl background concentration in the acid and base compartments.

At the discharge phase this same resistance increase occurs as in the charge phase at the interval 0 and -50

A/m^2, but now it is not temporarily. As co-ion transport during discharge is caused by the concentration gradient and diffusion, this driving force is now decreased due to the increased concentration of co-ions in the acid and base solutions. Coupled with the fact that Na^+ and Cl^- are not highly mobile ions when compared to H^+ or OH^- means that during discharge less co-ions diffuse completely through the membrane, and relatively more stay within the membrane than when compared to using pure solutions.

Past -50 A/m^2 rapid voltage drop starts occurring. This can be caused by either two factors: Either the recombination of H^+ and OH^- occurs too rapidly, causing water to build up at the interface of the BPM as it can't diffuse fast enough; or co-ions are accumulating at the interface, which in turn has effect on E_0 of Eq. 7. Both effects will cause the voltage to drop in Figure 18, but are distinctly different processes. When water can't diffuse fast enough, this actually increases the resistance of the BPM, but this phenomena only occurs at higher current densities and is independent from any co-ions in the solutions or interface. As the resistance only increases at higher current densities this will make the graph non linear. The accumulation of co-ions happens not only at high current densities, but at the lower current densities as well. The only difference is that at larger current densities the voltage drop becomes higher as the concentration at the interface is then larger.
In order to determine which of the previous two mentioned situations is happening it is important to compare both plots in Figure 18 with each other. As water accumulation is co-ion independent, this would mean voltage drop would also occur when conducting the experiment with pure solutions. As this isn't the case it can be concluded that the voltage drop is caused by co-ions.

The situation presented here shows two extremes in the behaviour of the BPM and that co-ions have the most effect on the BPM during discharge. During normal operation co-ions will slowly build up in the system, thus the lines will slowly shift from the starting situation with pure solutions towards the curve containing background concentrations.
To finalize, Figure 18 shows how operating under different current densities comes with its own trade offs. During discharge it is possible to operate under high current, thus obtaining high power densities, but this will make the system more susceptible to the voltage drop due to co-ions. On the other hand, operating at low discharge current densities will decimate the aforementioned power density. During charge the bipolar membrane doesn't seem to be effected as much by the background concentration as during discharge. This reinforces the theory that the electric field has a strong effect on the co-ions. In reality, there is a substantial amount of co-ion transport during charge, but this will only directly be measurable in the solutions and not in the performance of the membrane. This brings the system in a vicious circle as the membrane still performs well at high charge current densities, but in turn will decrease the membrane performance at discharge. Therefor a balance must be found, which will be investigated further in Section 4.2.

4.1.4 Single Discharge

In comparison to the IV experiment, the single discharge test represents a more practical visualization of how co-ions can effect the performance of a stack. Once again the orange and blue line represent the same experiment with and without background concentration. Both decrease in voltage until it is fully discharge at 0 V. Figure 19 shows the experiment ending just above 0.1 V. This difference is caused by the subtraction of the blank test from the measured end results.
As can be seen in Figure 19 the expected voltage collapse occurs and causes the system to finish discharge 35% earlier than when operating with pure solutions. As already explained in Section 2.2 and 4.1.3 the premature collapse of the discharge curve is because of co-ions entering the membrane. The presence of the background concentration has lowered the concentration gradient between the BPM interface and the solution. This reduced ratio means that one of the main driving forces for co-ions to leave the interface of the BPM and enter the accepting solution has been decreased. This means more Na^+ and Cl^- stay at the interface and in the membrane itself. The concentration increase in the membrane causes an increase

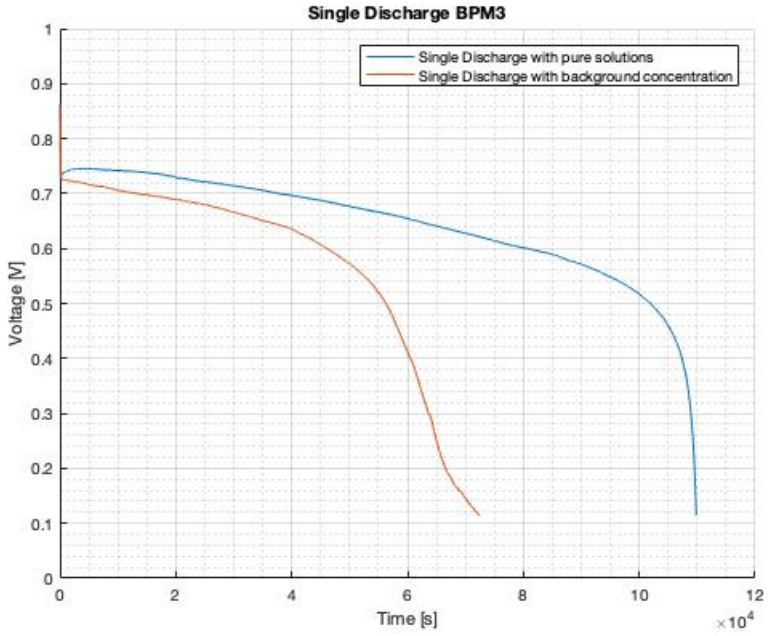

Figure 19: The Single Discharge test plotted with voltage over time. The blue line represents the test performed without background concentration. The orange line is the same experiment with 0.15 M NaCl added to the acid and base solutions.

in resistance, as a consequence the measured potential drops. The increase of co-ions at the interface causes a change in the concentrations used in the Nernst equation, which in turn changes U_0 and thus also the measured potential U_cell. The increase in resistance can be seen in the increased slope which already starts forming at the beginning of the experiment. This represents co-ions diffusing into the membrane from the interface, increasing R_{BPM}. As more ions enter into the membrane the concentration gradient decreases further over time and after a certain point this force becomes so small the co-ions increasingly start to build up at the interface. This situation can easily be illustrated by adding a small amount of co-ions (0.005 M) to Eq. 3 and 4:

$$U_{BPM-AEM} = \frac{RT}{zF} ln \frac{[OH^-]_{BPM} + [Cl^-]_{BPM}}{[OH^-]_{BASE}} \approx \frac{8.314 \cdot 298}{-1 \cdot 96485} ln \frac{10^{-7} + 0.005}{0.5} = 0.118V \tag{30}$$

$$U_{BPM-CEM} = \frac{RT}{zF} ln \frac{[H^+]_{ACID}}{[H^+]_{BPM} + [Na^+]_{BPM}} \approx \frac{8.314 \cdot 298}{1 \cdot 96485} ln \frac{0.5}{10^{-7} + 0.005} = 0.118V \tag{31}$$

The resulting 0.118 V is a 70% decrease from the original value of 0.396 V without co-ions at the interface. This same occurrence starts happening in Figure 19 at around $5 \cdot 10^4$ seconds when the curve rapidly starts declining towards 0 V. Thank to this even though the voltage has reached 0 V, this doesn't mean the battery is actually completely discharged. In reality, if one was to measure the $[H^+]$ concentration it will actually be less discharged than in theory.

4.2 50 Cycle Test

With the basic properties and limits determined in the characterization experiments, the 50 cycle tests can be conducted to research the actual long term stability and efficiencies of the AB-FB setup. This

experiment is divided into 3 sub experiments. Between each test one of two parameters is changed, either the cut off voltage or the current density during charge and discharge. When the battery falls below 80% of its original energy capacity it is considered 'dead', after which the solutions will have to be replaced or treated with the reset cycle. As with all tests $R_{electrodes}$ is subtracted from all results, so degradation of the electrolyte or corrosion of the electrodes will not influence the graphs. The cation and anion membranes are from the 2019 April batch and the bipolar membrane comes from the Standard BPM batch. Tests with other BPMs have been conducted in which difference in efficiency and lifetime can be found, most notably between the 2017 batch and the one used in this experiment. These results can be found in Appendix D. The respective parameters are as following:

- 7V - 0.25V Cut off: First a baseline test is conducted in order to compare all following results after this test. This experiment will have its cut off voltages set between 7 and 0.25 volts. As will be seen in the graphs in this section, this represents a high depth of charge. The system will have a charge current density of 100 A/m^2 and a discharge current density of 30 A/m^2. This is based of Figure 18, in which the discharge current density is kept intentionally low in order to prevent large voltage drops.
- 3.5V - 0.6V Cut off: With the baseline established the cut off voltages are reduced. In practical terms this mean the battery will charge and discharge not as deep as in the previous experiment. The charge and discharge current densities remain the same. By reducing the cut off voltage it is expected the efficiencies will go up. It is also expected that the energy density will go down, but the lifespan will increase.
- 3.5V - 0.6V Cut off with 50 A/m^2: For the final experiment the cut off voltage stays the same, but the charging current density is reduced to 50 A/m^2. The theory here is that with a weaker electric field the amount of co-ion transportation will be reduced.

Of each test the corresponding efficiencies and power/energy densities will be calculated per cycle. This way a comprehensive view can be formed how the battery degrades.

4.2.1 7V - 0.25V Cut Off

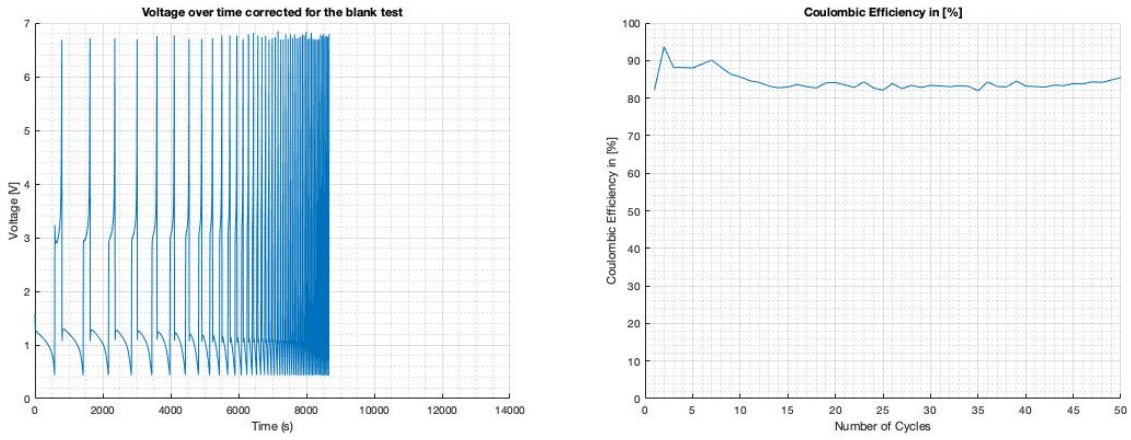

(a) (b)

Figure 20: Standard BPM with 7V - 0.25V cut off voltage and 100 A/m^2 and -30 A/m^2 current density. Figure 20a represents the voltage over time and Figure 20b represents the coulombic efficiency for each cycle.

Examining Figure 20a a clear degradation in the cycles can be observed. It takes the battery just short of 9000 seconds to complete fifty cycles of charge and discharge, with each cycle becoming shorter. In fact, only the first cycle seems to have discharged and charged properly. This can be seen in the small 'U' shape the first charge cycle makes. When a AB-FB is properly discharged the acid and base compartments will mainly be containing demineralized water. This type of water has a low conductivity and will increase the resistance in the salt compartment. Once the system starts charging the system starts shifting to a state that all compartments contain a roughly equal amount of Na^+ and Cl^-, decreasing the overall resistance, before the NaCl concentration in the salt compartment becomes completely depleted. This final phase can be seen in the massive spike in the final seconds of the charge cycle as resistance builds up. This rapid degradation can seen in low coulombic efficiency of the system presented in Figure 20b. It is only in the first 2 cycles the system achieves above 90% efficiency before quickly degrading to around 80%. To put this efficiency into a different perspective, the coulombic efficiency of lithium ion batteries is around the 99.1-99.5% [43]. This means the AB-FB is significantly charging more than it is discharging and currently isn't a stable system beyond 2-3 charge discharge cycles.

This low coulombic efficiency is also reflected in the RTE and VE in Figure 21, with RTE and VE both forming a peak at around 30% before also quickly degrading to below 20%. This is much lower than other flow batteries, with for example vanadium redox flow batteries reaching VE ranges of 85% to 95%[44]. This low VE can be explained by the high resistances forming in the final stanges during charge and discharge, as can be seen in 20a. The area covered under the curves of this voltage peak is far smaller compared to the rest of the cycle. This means it takes the system a lot of effort to reach the final limits of the SoC, which is caused by the high resistance of the demineralized water that is formed in these upper limits. Another explanation is the possibility of high internal resistance in the system such as the electrodes and electrolyte. After all, this has been shown in Figure 17 where it can take up to 68% of the total resistance the system is experiencing. This isn't the case though, as the results shown here have been corrected for the blank test and thus excludes $R_{electrodes}$ and $R_{electrolyte}$. These resistances would also effect the graph in its entirety and not just the final stages of charge. The RTE is low because the VE is low. In order to improve the RTE is is important to reduce the upper and lower limits of the SoC.

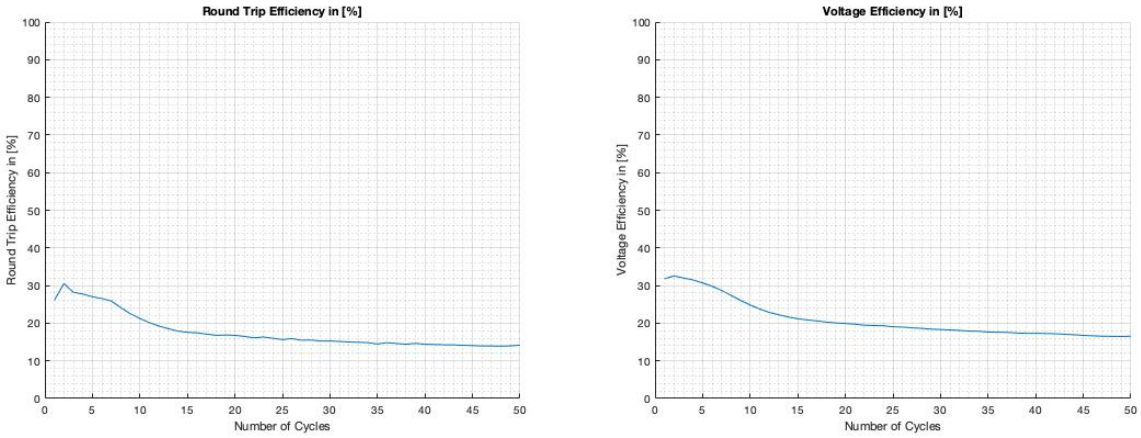

(a) (b)

Figure 21: Standard BPM with 7V - 0.25V cut off voltage and 100 A/m^2 and -30 A/m^2 current density. Figure 21a represents the round trip efficiency and Figure 21b represents the voltage efficiency for each cycle respectively.

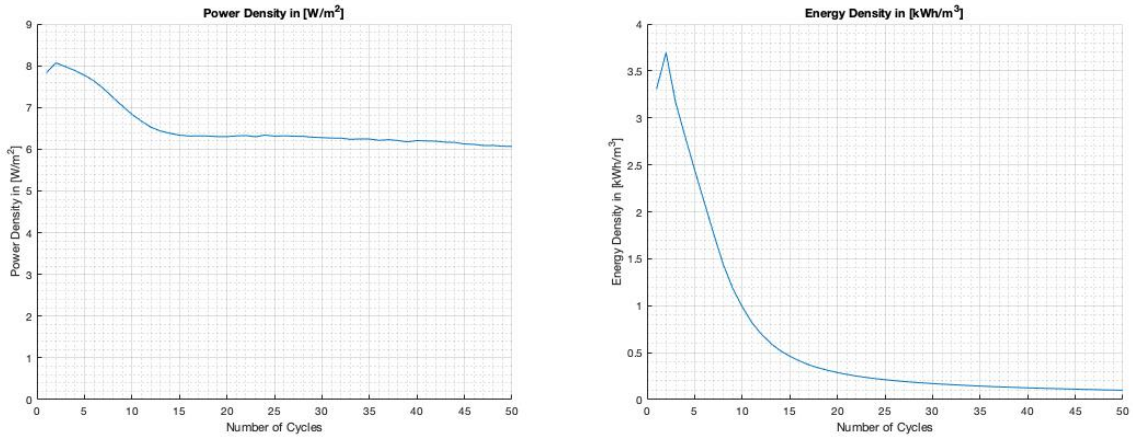

(a) (b)

Figure 22: Standard BPM with 7V - 0.25V cut off voltage and 100 A/m^2 and -30 A/m^2 current density. Figure 22a represents the power density and Figure 22b represents the energy density for each cycle respectively.

As mentioned earlier in this section, when the battery falls below 80% of its original ED it is considered 'dead'. In Figure 22b the degradation of the energy density is plotted for each cycle. First the energy rises to 3.7 kWh/m^3, this represents the first cycle of the battery in which it has to charge to its full capacity. By maintaining the 80% definition, this means that when the energy density falls below 3 kWh/m^3 it has degraded too far and needs to be reset. By reading the graph in Figure 22b, this means that after 3 cycles the ED has fallen too low. It has to be noted though that an energy density of 3.7 kWh/m^3 is actually an improvement over earlier research, with van Egmond et al. reporting only 2.9 kWh/m^3 [17]. Although in both cases this is still far lower than the theoretical energy density of 11 kWh/m^3. The system also compares quite favourably with other storage systems such as compressed air (2-6 kWh/m^3) and pumped hydro systems (0.5-2 kWh/m^3), with its power density exceeding both. Combine this with the fact that the AB-FB is scalable and not constricted to geographical features makes this system an interesting alternative for long term storage with further improvements.

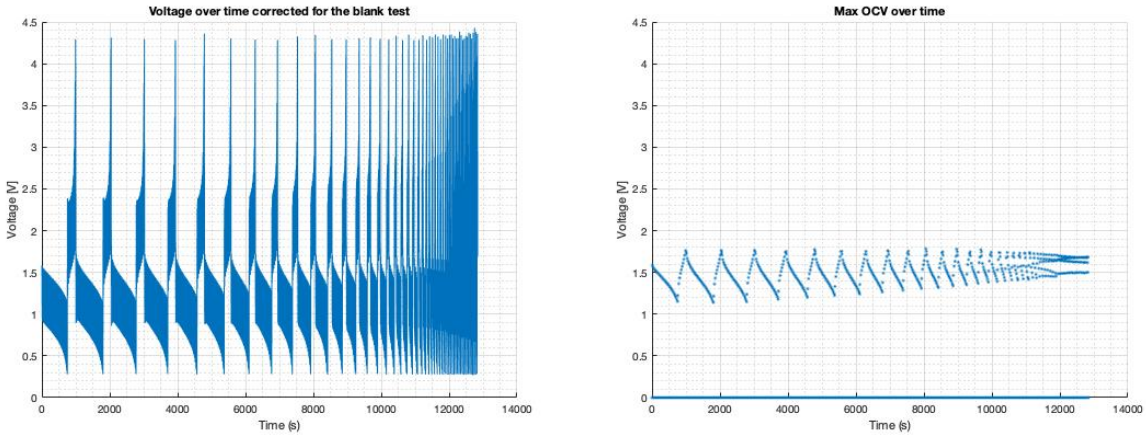

(a) (b)

Figure 23: Standard BPM with 7V - 0.25V cut off voltage and 100 A/m^2 and -30 A/m^2 current density. Figure 23a represents the voltage over time with repeating intervals of 20 seconds in which the OCV value is measured. Figure 23b shows the OCV value over time.

In order to gain better insight in how the concentrations develop in the solutions the same 7V - 0.25V test was conducted, but now with short OCV intervals every 20 seconds during charge and discharge. Another benefit of this experiment is it also shows the development of the internal resistance R_i. The result of this experiment can be found in Figure 23. When comparing Figure 23a with Figure 20a the first thing that is noticeable is the shaded blue areas. This is in fact the internal resistance R_i as the voltage quickly switches between OCV and operational voltage. In order to make the picture more clear Figure 23b is plotted. The plot in this figure is development of the OCV over time. What happens here is that the max OCV value during discharge is slowly increasing. This is actually the state of charge increasing and this is because of voltage collapse caused by co-ion transport during discharge. This phenomena is already explained in Section 2.2, 4.1.3 and 4.1.4. In Figure 23a it can be seen that the discharge times are getting increasingly shorter due to voltage collapse, this gives the system continuously less time to discharge, thus raising the SoC. With the SoC slowly rising the system also experiences increasingly shorter charge times as it reaches the max voltage sooner. Even though the charge cycle becomes faster, co-ion transportation is still occurring, thus accelerating the discharge cycle voltage collapse. After a certain point voltage collapse happens so fast, the system is hardly or even at all discharging.

4.2.2 3.5V-0.6V Cut Off

With the knowledge gained in Section 4.2.1 it is decided to decrease the cut off voltages. This basically means decreasing the depth and height of charge. By doing this is it is theorized that the efficiencies will increase, while the energy density will decrease. It is also suspected that co-ion transport will also decrease, but this has more to do with the fact that the amount of time in which co-ion transport can occur is reduced.

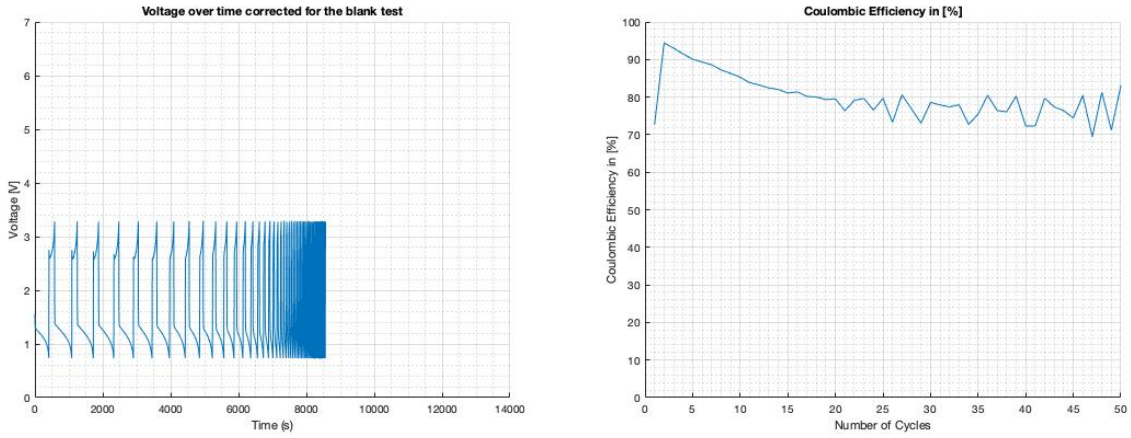

(a) (b)

Figure 24: Standard BPM with 3.5V - 0.6V cut off voltage and 100 A/m^2 and -30 A/m^2 current density. Figure 24a represents the voltage over time and Figure 24b represents the coulombic efficiency for each cycle.

For the first five cycles the voltage profile in Figure 24a shows improved charge/discharge cycles, with the metaphorical 'U' shape appearing, indicating the system discharging to a reasonable level. Shifting the attention to the coulombic efficiency in Figure 24b, it is once again above 90%. The key difference now is that the battery stays above 90% coulombic efficiency for a increased amount of time, only dropping below this level after five cycles. This indicates that the system stays more stable for a longer period with less side reactions occurring during this time. After the 20th cycle the coulombic efficiency starts to increasingly vary. This is probably because the cycles become so short it becomes hard to properly process the data.
Proceeding towards Figure 25, it shows that the voltage efficiency has increased significantly from around 30% up to 40%. As mentioned earlier, this was expected, as a significant portion of the voltage input was cut off during the charge cycle compared to Figure 20a. This shows that just like other batteries such as lithium ion it is actually rather inefficient to go to 100 or 0 % SoC. In the case of the AB-FB it means transferring the very last ions in a solution at the cost of high voltage input. Naturally the RTE increases as well, as both the CE and VE has shown improvement.
This trend of improvement continues to both the PD and the ED in Figure 26. The energy density plot in Figure 26b shows a drop in peak energy density, which was expected as the range of charge for the battery has decreased. As a trade off the energy density drops past the 80% at the sixth cycle at 2.56 V. Compared to the ED in Figure 22b this is a improvement of 3 cycles, which means the lifetime is effectively doubled. With the adjustment of the cut off voltages less counterion transport occurs over the BPM, which in turn also means less co-ion transport. Is possible to make the cut off voltage range even smaller, but then the ED will decrease even further. This creates a balance in the system as a longer lifespan comes at the cost of energy density. In Figure26a the power density has also improved over the previous test. The cause of this is most likely the fact that the system is actually operating closer to its max power point as the mean discharge voltage is decreased.

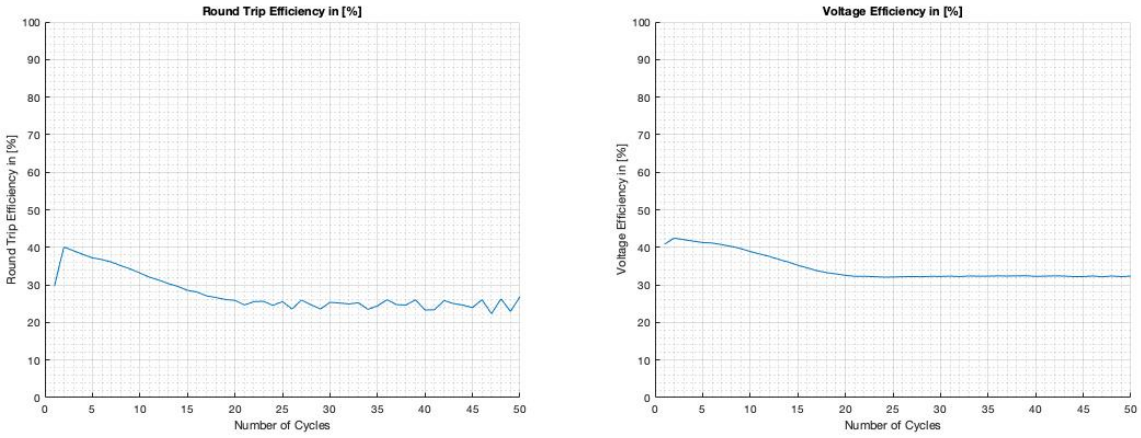

(a) (b)

Figure 25: Standard BPM with 3.5V - 0.6V cut off voltage and 100 A/m^2 and -30 A/m^2 current density. Figure 25a represents the round trip efficiency and Figure 25b represents the voltage efficiency for each cycle respectively.

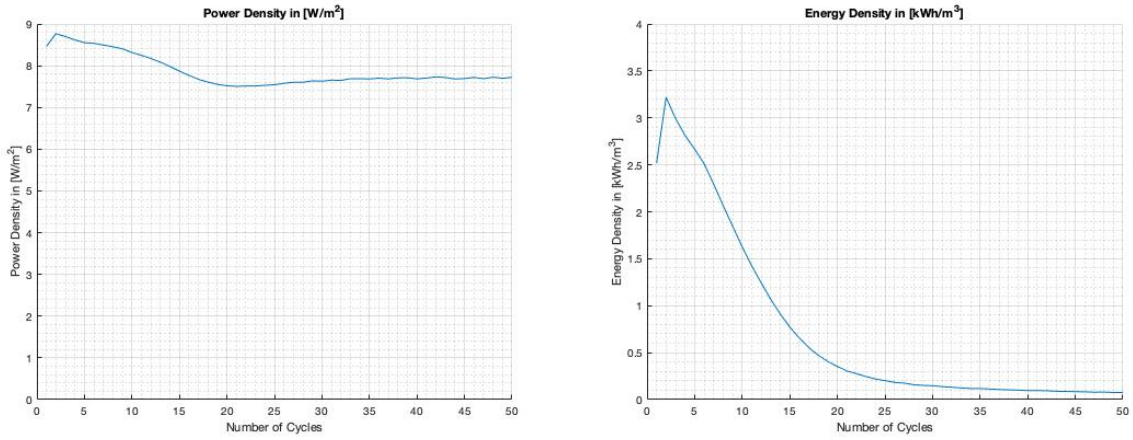

(a) (b)

Figure 26: Standard BPM with 3.5V - 0.6V cut off voltage and 100 A/m^2 and -30 A/m^2 current density. Figure 26a represents the power density and Figure 26b represents the energy density for each cycle respectively.

4.2.3 3.5V - 0.6V Cut Off with 50 A/m^2 charge current density

For the final sub experiment of this section the charge current density was reduced from 100 A/m^2 to 50 A/m^2. This means that besides reducing the SoC range, it also takes the system longer to charge to its designated level. Figure 27a shows that the charge cycles have effectively doubled in time, while keeping the discharge cycles the same.. The reduction in charge current density has had a negative effect on the CE, as can be seen in Figure 27b, and has decrease by 2.5% in comparison to Figure 24b. The significance of this decrease is up for debate though, as this change can quickly be affected by minor

unforeseen changes in the system. This for example can be things like slight deviations in the solution concentrations or variations in the membranes, thus affecting their performance.

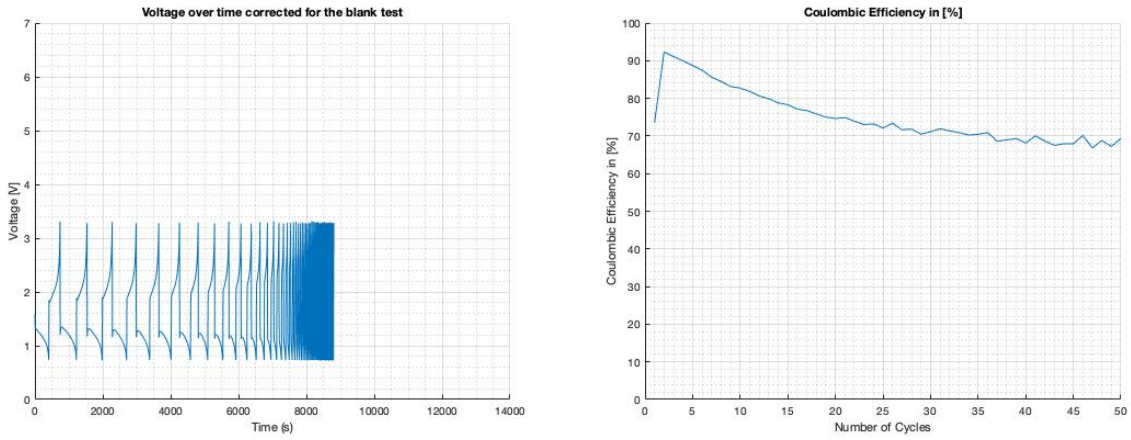

(a) (b)

Figure 27: Standard BPM with 3.5V - 0.6V cut off voltage and 50 A/m^2 and -30 A/m^2 current density. Figure 27a represents the voltage over time and Figure 27b represents the coulombic efficiency for each cycle.

Figures 28 both show great increase in efficiencies, with the round trip efficiency shortly rising above 50%. As the coulombic efficiency has hardly changed this would indicate that by reducing the charge current density this has minimal effect on the side reaction occurring in the battery, but actually improves the battery charging. This improvement in round trip efficiency reflects back on the voltage efficiency as these two results are linked to one other. It could seem that changing the charging current density only has affect on the round trip efficiency and voltage efficiency, because upon close inspection there is hardly no change in both the power density as well as the energy density in Figure 29. This does deviate with the theory though as a lower charging current density should have a more profound effect on the CE. In theory as lower charging density would have a negative effect on the CE. This has to do with the fact that during charge besides counterions, there are also co-ions moving through the BPM. Referring to Section 2.2; during high charge current density the potential difference over the BPM increases, this means that more counterions will be transported over the BPM in comparison to the amount of co-ions. If the charge current density is decreased, the potential difference over the BPM decreases as well. This leads to more co-ion transport in relation to the counterion transport over the BPM and will have a negative effect on the CE. Why the lower charge density hasn't had a more profound effect on the CE was discussed. Apparently 50 A/m^2 is around the lowest limit possible before the charge density has a greater effect on the coulombic efficiency.

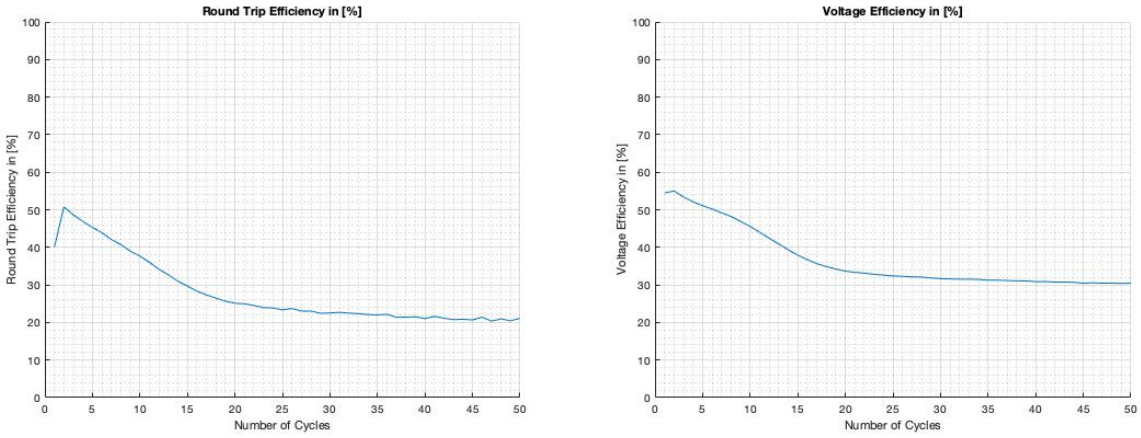

(a) (b)

Figure 28: Standard BPM with 3.5V - 0.6V cut off voltage and 50 A/m^2 and -30 A/m^2 current density. Figure 28a represents the round trip efficiency and Figure 28b represents the voltage efficiency for each cycle respectively.

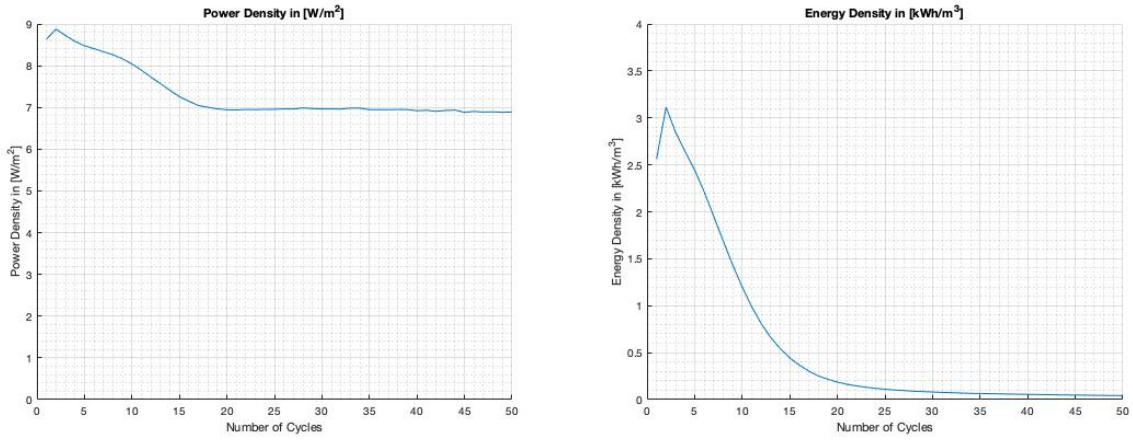

(a) 1 (b)

Figure 29: Standard BPM with 3.5V - 0.6V cut off voltage and 50 A/m^2 and -30 A/m^2 current density. Figure 29a represents the power density and Figure 29b represents the energy density for each cycle respectively.

4.3 Charge Reset Cycle

By going through the results and theory presented up till now it is safe to say that co-ion transportation can be seen as an issue that will inevitably happen in a flow battery. The charge reset cycle is therefore set up in order to validate the possibility for an ABFB to reset itself and recover a certain amount of its original energy density. As explained in Section 3.2.3 this is done by mixing the degraded acid and base, which creates salt water. This salt water then undergoes electrodialysis with the goal of making as pure as possible demi water coupled with high molarity acid and base solutions. As the current setup

lacks any pH meter first test samples were made in order to find the relation between conductivity and concentration. This can be found in Section B.

During initial tests it was quickly discovered that the quality of produced demi water varied between batches of AEMs. The explanation for this is that during desalinating the salt water makes use of the cation and anion exchange membranes. These same fluctuations in quality can be found in the characterization of the BPMs in Appendix C and in the concluding parts of this section. Therefor this experiment can also be used in order to test the quality of the aforementioned membranes. As it is important to produce the highest quality of demi water experiments were first conducted between AEMs to determine which gave the best desalination. This wasn't done for CEMs because at the moment of conducting these tests there was only one batch available, that from April 2019, as can be seen in table 1. Next, the load fraction has to be optimized for the solutions inside the compartments. The reason for this is that flow within the stack isn't homogeneous. The flow through the spacers has been modeled with a CFD analysis, but no improvements had yet been implemented to the spacers during the time of this study. A sample of this CFD analysis can be found in Appendix E. Finally, once these parameters are established, the concentration of the produced acid and base is measured with the goal of trying to get as high molarity as possible.

The starting solution for desalination is a 0.25 M NaCl solution with a corresponding conductivity of 23.6 mS/cm. The industrial produced demi water used for the acid and base compartments has a conductivity of 0.033 mS/cm, with the assumption that it contains 0 M NaCl. After each experiment the produced demi water is collected and measured, using Eq. 34. For the first step of determining the quality of the AEMs a stack of two triplets was used with a loading fraction of 100%. These results are presented in table 2.

Description	**Thickness (mm)**	**Conductivity** ($mScm^{-1}$)	**Concentration** ($molL^{-1}$)
Reference NaCl	-	0.033	0
Reference NaCl	-	23.6	0.25
AEM Jan. 2019	0.083	11.2	0.11
AEM Apr. 2019	0.078	5.6	0.045

Table 2: Measured conductivity values of the reference NaCl solutions and the different batches of AEM. The thickness presented here differs from table 1 due to swelling and use.

Based on the conductivity values of table 2 it shows that the April 2019 batch give the best performance. As the conductivity is only 5.6 mS/cm next steps have to be made to further reduce the concentration of Na^+ and Cl^- ions in solution, as the less ions in the demi water means higher concentrations of produced acid and base, which in turn gives the battery a higher SoC when resuming operation.

Before proceeding in determining the load fraction, experiments were conducted in order to establish whether it was better to keep the stack at two triplets or reduce it to a single triplet. Having a single triplet has several distinct advantages. To start, having a single triplet would decrease the resistance of the system, as there are less membranes, spacers and overall solution. To add on top of that, running single triplets eliminates any possible short circuit current. Finally, it abolishes that chance of preferential flow between triplets. This means that, due to slight variations in spacer thickness, flow speed varies between triplets. On the other hand, running two triplets would drastically decrease the time needed to produce a measurable amount of demi water, decreasing the run time of the experiment. In addition, with two triplets the influence of $R_{electrodes}$ and $R_{electrolyte}$ on the overall resistance decreases. This will reduce the margin of error per triplet when subtracting the aforementioned resistances from overall equation (i.e. subtracting the blank test from the results). The voltage over time relation between one

and two triplets, along with a close up of a single charge cycle can be found in Figure 30 and 31:

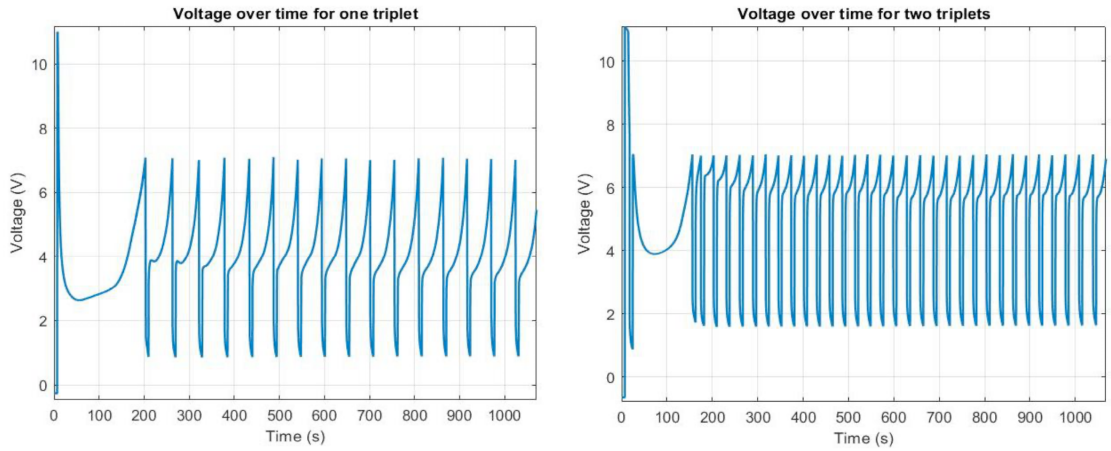

Figure 30: Voltage over time plots with one triplet on the left and two triplets on the right. In order to produce a measurable amount of demi water tests could last up to 3 hours. Only the first 1000 seconds are presented here for clarity. This experiment had a load fraction of about 0.4

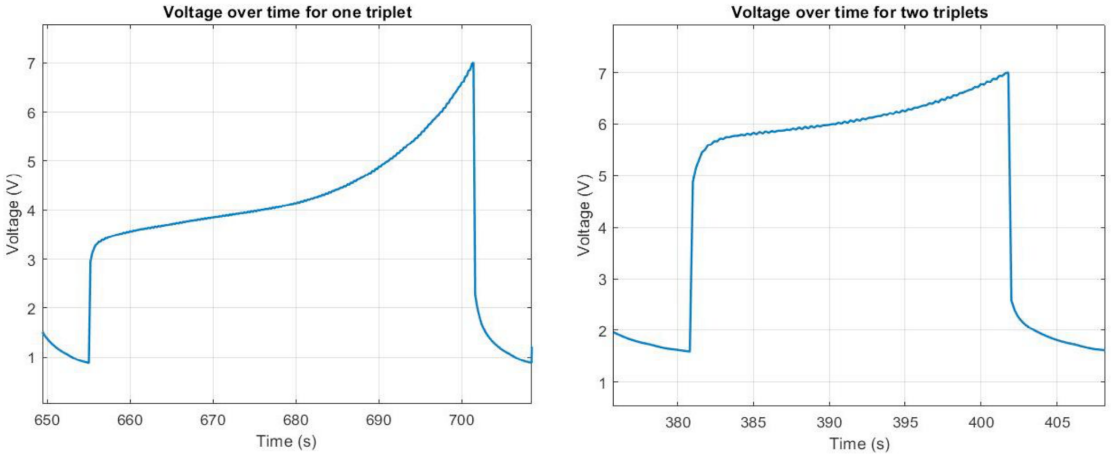

Figure 31: A close up of the 10th cycle presented in Figure 30. Both experiments have a cut off voltage of 7 V and a constant current of 220 mA. As to be expected the starting OCV value before applying current is roughly double for two triplets compared to one triplet. The same applies for the resistance of the stack. This is of course because multiple triplets are in series of each other.

Figure 30 shows that the charging cycle for two triplets is much shorter than charging with a single triplet. When zooming in on the 10th cycle in Figure 31 it becomes clear that a normal cycle with one triplet last about 46 s, while a normal cycle with two triplets last approximately 22 s. This would insinuate that with less time, less desalination would take place, leading to a higher conductivity in the demi water solution. Another difference is the higher starting voltage for two triplets. The one triplet stack starts desalination at around 3.5 V, while the two triplet stack starts at about 5.5 V. This means that for a two triplet setup the cycle starts closer to the cut off voltage, which means a shorter duration of the charging cycle and thus worse desalination. For two triplets to properly operate a cut off

voltage of 14 V is need, although in reality this will probably be higher as it is also important to take $R_{electrodes}$ and $R_{electrolyte}$ into account. These two resistances are subtracted from the results shown here.

Upon closer study of the charge cycles a common path can be followed in the process. First the voltage shoots up towards 10 V after which a very long initial charge curve develops. In the case of two triplets this initial voltage even shoots above 10 V and past the limit of the Ivium galvanostat. This is caused by the initial large presence of demi water in the acid and base compartments which has a very low conductivity. Once the charge current is applied this demi water becomes acid and base, which has a higher conductivity and thus lowering the resistance of the stack. As the load fraction is only 0.4, not all acid, base and salt solution is pumped out of the system after this initial cycle. This means that the fresh demi water in the acid and base, and the salt water solution in the salt compartment, mixes with part of the already desalinated solution. Therefor each cycle after the initial cycle, the acid and base probably contains around 0.1-0.2 M HCl and NaOH respectively, and the salt compartment probably averages out at 0.1-0.2 M. This as a whole raises the conductivity of the system and how much mixing occurs depends of the load fraction. This phenomena can be seen in Figure 30 in the cycles after the initial cycle where the first 2-4 charge cycles have a higher starting charge voltage than the subsequent cycles after in which an equilibrium is established. At this point it shows that with the current setup, if quality was the goal, it would in fact be better to run the experiments with one triplet until a galvanostat that can reach higher voltages is used. In other cases it was deemed better to use two triplets as this drastically shortened the experiment run time before a measurable amount of solution was produced.

As resistance of the solutions in the stack proved to be one of the larger obstacles remaining with one triplet remained the preferred method for this experiment. In order to strike a compromise between one and two triplets, a single triplet with double salt spacer is constructed in the stack. By doing this the stack operates with the advantages of one triplet, while producing the same amount of demi water comparable with two triplets. Only the salt spacer is chosen, because in this stage of the experiment desalination of the salt water has priority over producing good quality acid and base. This slightly increases the electrical resistance of the stack, as the volume in the salt compartment is doubled, but increases the amount of salt water that is processed in each cycle and speeds up the process. This also halves the load fraction as this value is determined by the pumping time and the volume in the compartment, assuming the pumping time remains unchanged. Decreasing the pumping time would mean a lower volume of the salt solution is refreshed, from which a mixed solution of salt and demi water forms as discussed earlier in this section. As only a fraction of the solution is replaced each pumping cycle, a fraction of the same amount will actually be desalinated multiple times, resulting in a lower NaCl concentration.
The whole reason of using low loading fractions in the end is to combat preferential and non-homogeneous flow appearing inside the compartments. This means that part of influent reaches the compartment exit point faster than other parts of the flow, meaning that even for loading fractions lower than 1 there can still be salt water in the effluent flow. Table 3 represents the results for the charge reset cycles with one or two salt spacers, are conducted with two triplets and have varying load fractions. These comparison experiments were run in order to validate if double salt spacers could be used with the current setup.

	Pumping time (s)	Loading fraction (-)	Conductivity ($mScm^{-1}$)
Single salt spacer	2	0.27	2.4
	3	0.41	1.7
	4	0.55	2.2
	5	0.68	2.7
	9	1.23	7.4
Double salt spacer	2.5	0.17	0.89
	3	0.20	0.93
	4	0.27	2.4
	7.33	0.5	4.0

Table 3: Produced demi water with their corresponding conductivity values, load fraction and the applied pumping time. The cell contains two triplets and one or two salt spacers.

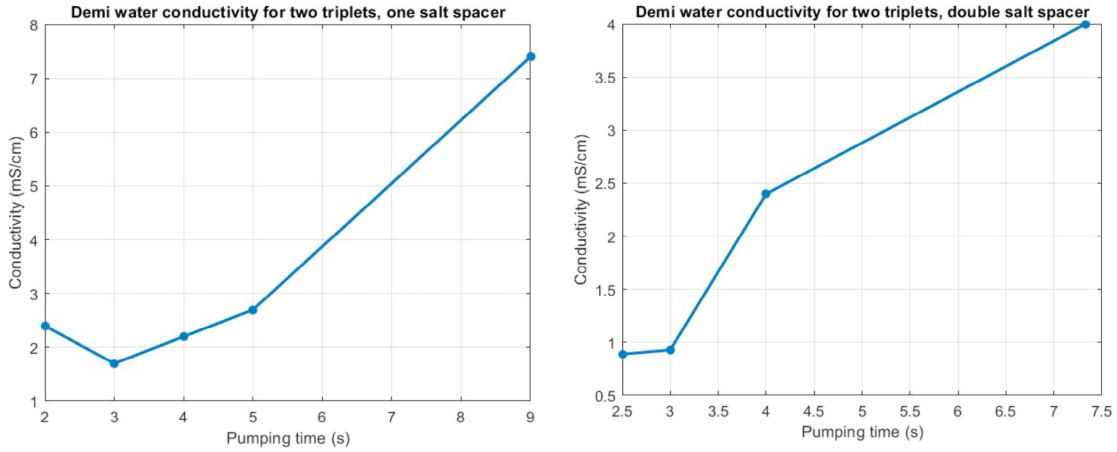

Figure 32: Results from table 3 plotted with the pumping time on the x axis and the corresponding conductivity on the y axis.

Figure 32 and table 3 shows that the load fraction is the dominating factor in determining the conductivity of the effluent solution, with lower load fraction reducing the conductivity. By comparing results in table 3 also shows that even though the lower load fraction leads to lower conductivity, the resulting conductivity still tends to vary. This can be seen when comparing 0.5 load fraction with one and two salt spacers, which is 2.2 and 4 mS/cm respectively. This can be caused by a multitude of reasons as the same non-homogeneous flow and hydraulic resistance isn't guaranteed between experiments. Still the difference between the resulting conductivity's can be seen as minimal as this often means a difference of 0.01 mol/L. It should be noted that even though 2.5 seconds provided the best quality demi water, the test was also deemed unreliable. This is because the pumping cycle proved to be so short that the electrical resistance of the salt compartment builds up over time. This is because only a minute amount of solution is replaced and the $NaCl$ concentration at the start of each cycle declines. After a certain period the electrical resistance in the compartment becomes so high it even exceeds the 10 V galvanostat limit. The practicality of using a double salt spacer should also be questioned. For these sets of experiments it was a useful solution, but impractical in a real life situation as it isn't possible to change the amount of salt spacers for a separate process. The effect of a double salt spacer in normal operation is also at the time of writing this thesis unknown and could be researched further.

Even though the use of double salt spacers is not a true reflection of real life use, it bypasses the current limitations of the set up and allows further investigation of the limits of the charge reset cycle. Once the stack is combined with a system that can tolerate higher voltages the previous conclusions should still be relevant, with only the load fractions differing.
In order to mimic real life long time use a 30 hour test was set up based on the knowledge gained in the previous two experiments. This is meant to replicate the system producing large amounts of acid and base for future use after the energy density has dropped past 80% of its original value. The stack is constructed with one triplet and two salt spacers in order to stay well within the boundaries of the galvanostat and achieve longer desalination times. The cation and anion exchange membranes are taken from the April 2019 batch and the BPM from the 2017 batch. The pumping time was set to 3 seconds, i.e. 0.41 load fraction, as this provided the best results according to table 3 (One triplet with double salt spacer is the same volume as two triplets with one salt spacer). At the end of the experiment the acid, base and salt solutions is measured. These results and the first 1000 seconds of the corresponding graphs is presented in table 4 and Figure 33 respectively.

Solution	**Conductivity** ($mScm^{-1}$)	**Concentration** ($molL^{-1}$)
Salt	0.0815	0
Acid	74.3	0.183
Base	46.9	0.216

Table 4: Measured conductivity values of the 30 hour charge reset experiment with corresponding concentrations

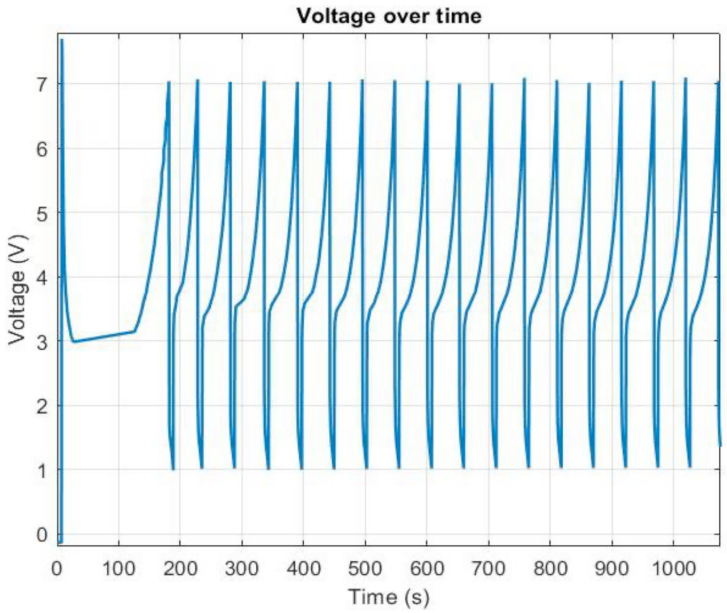

Figure 33: A plot of the voltage over time for the 30 hour charge reset experiment. This was conducted with one triplet and two salt spacers. Only the first 1000 seconds is presented here for a clear image.

Based on the results in table 4 the experiment was able to achieve excellent results with conductivity's of 0.0815, 74.3 and 46.9 mS/cm for the demi water, acid and base respectively. No leakages both internally

and externally were detected and the stack performed almost 2500 cycles. The produced demi water approached almost industrial grade demi water of 0.033 mS/cm, which is close to 0 M concentration. The resulting concentrations of the acid (0.183 M) and base (0.216 M) would seem out of place as that would mean Na^+ and Cl^- ions would have disappeared. This deviation from the expected 0.25 M can be caused by two different phenomena, either co-ion transportation or osmosis. Osmosis can occur when the acid and base compartment contains higher concentrations of Na^+ and Cl^- ions, after which demi water flows from the salt compartment to the acid and base. This would of course reduce the concentration of the acid and base compartment. If this was actually occurring can't be concluded definitely as the possibility of osmosis wasn't considered until writing this thesis. An easy way to detect osmosis is if there is a change in the volume of the solutions. This hasn't been detected, but this check is done for detecting leakage and not osmosis. As discussed earlier in Section 2.2, co-ion transportation also occurs during charging, which is the same process as used during this experiment. With co-ion transport occurring, this would mean the acid and base concentrations will deviate from the desired 0.25 M and Na^+ and Cl^- would flow to the acid and base compartments respectively. The difference in concentration between the two compartments is still an oddity though, as this doesn't conform with the mass balance of the ions in the system. Here it is theorized that this could be because of the use of a conductivity sensor to determine the molarity of the solutions. As of writing this thesis it is not known how much influence Na^+ and Cl^- co-ions have on the conductivity measurements of the acid and base solutions. It is plausible that these differ between Na^+ and Cl^-. This shows a possible downside of needing to first measure the conductivity in order to determine the concentration, instead of being able to directly measure it. Additionally, how the setup is used in this experiment isn't practical for future use as it takes 30h to produce only 700 mL of demi water. Once again, this issue can be solved with a larger system that is able to sustain higher voltages.

Finally an attempt is made to improve the produced acid and base concentrations in order for the battery to start at a higher SoC once it resumes operation after resetting itself. The experimental setup stays the same, but the pumps that are used to refresh the acid and base compartments are programmed to refresh only once every two cycles. Under ideal conditions this would mean that with 0.25 M NaCl, 0.5 M HCl and NaOH can be produced as the amount of ions transferred to these compartments is doubled. The experiment is conducted with almost the same setup as the 30 hour test. What stayed the same was the AEMs and CEMs from the April 2019 batch, double salt spacers and the use of a single triplet. Variation were made in the cut off voltage (7 to 9 V); the use of double spacers in the acid and base compartments; and the BPMs. This was done in order to find out if any of the parameters have any affect on the end concentrations. These results can be found in tables 5 - 8:

Solution	**Conductivity** ($mScm^{-1}$)	**Concentration** ($molL^{-1}$)
Salt	0.074	0
Acid	135.7	0.367
Base	68.8	0.332

Table 5: Measured conductivity and concentration values for the **2017 BPM**, 7 V cutoff voltage, double salt, acid and base spacers.

Solution	Conductivity ($mScm^{-1}$)	Concentration ($molL^{-1}$)
Salt	0.087	0
Acid	153.9	0.422
Base	71.8	0.348

Table 6: Measured conductivity and concentration values for the **2017 BPM**, 9 V cutoff voltage, double salt, acid and base spacers.

Solution	Conductivity ($mScm^{-1}$)	Concentration ($molL^{-1}$)
Salt	0.21	0
Acid	134.2	0.363
Base	63.9	0.306

Table 7: Measured conductivity and concentration values for the **2019 BPM**, 7 V cutoff voltage, double salt, single acid and base spacers.

Solution	Conductivity ($mScm^{-1}$)	Concentration ($molL^{-1}$)
Salt	0.232	0
Acid	66.9	0.161
Base	36.2	0.159

Table 8: Measured conductivity and concentration values for the **Standard BPM**, 7 V cutoff voltage, double salt, single acid and base spacers.

Based off the results in tables 5 - 8 it becomes clear that the Standard BPM performs the worst of the bipolar membranes, while the 2017 BPM proved to be the best. This supports the theory mentioned earlier that co-ion transport is occurring during this experiment, as the quality of the membrane represents a large factor in the amount of co-ion transportation taking place. Similar results in quality difference between membranes are presented in Appendix C and D. This is actually a note of concern for a technology so dependent on the quality of its membranes. Using two spacers for the acid and base compartments proved to make no difference in improving the concentrations. An expected outcome as doubling the spacers mimics the volume of two triplets, while still operating with the advantages of one triplet. By doubling the acid and the base spacers the electric resistance in the system will also increase, with only the membrane resistance staying the same. Increasing the cutoff voltage does slightly increase the resulting concentrations, but this is anticipated as the electrodialysis process takes longer. Although at 7 V cutoff the salt concentration is already practically 0 M, so the amount of desalination actually occurring in the 2 V difference is questionable. Finally, the concentration of the acid and base is once again below the expected value, 0.5 M in this case. An indication that osmosis and/or co-ion transport can be occurring during this process, for the same reasons noted for the poorer acid and base quality during the 30 hour experiment. With the Standard BPM batch not even passing the 0.25 M concentration, even with a adjusted pumping ratio. In order to properly validate whether osmosis or co-ion transport is an issue future experiments need to be conducted in which the concentrations of ions can directly be measured. If co-ion transport is an issue then this can hamper the effectiveness of the charge reset step. When a system is supplied with the same quality membranes as the 2017 batch, it is probably possible to recover much of the original energy density with this process, assuming a more robust and optimized system is used.

5 Conclusions and Recommendations

The goal of this thesis was to identify what the influence of co-ion transport is on the AB-FB and find ways to minimize or neutralize the occurrence. This was done by splitting the main question up into several sub questions: Identifying any additional losses in order to remove them from the analysis, gain insight in how co-ion transport differs between the charge/discharge cycle, how co-ion transportation influences the lifetime of AB-FB and eventually researching a method to 'reset' the AB-FB.

Three different additional losses were found: Boundary layer formation, short circuit current and the ohmic resistance in the electrolyte and electrodes. Boundary layer formation is discussed in Section 2.3 and 4.1.2. It is most important to note that boundary layer formation is highly dependent on current density, flow turbulence and flow speed. Larger current densities during charge/discharge means larger boundary layer formation, which in turn increases the electrical resistance of the system. This can be mitigated by either increasing the flow speed of the pumps, or promoting turbulent flow in the solutions. As a loss factor, boundary layer formation was easily mitigated during the experiments of this thesis, but it is important to be able to recognise when it is occurring to a greater degree.
Short circuit currents has shortly been discussed in Section 2.4, but is the only instance that it is mentioned in this thesis. This is because short circuit currents only start occurring when running such a number of triplets that the internal resistance of the cell becomes greater than the resistance of the feed solution manifolds. As all experiments have been run with one or two triplets, short circuit currents have never been an issue. Finally, during the IVT test in Section 4.1.2 it becomes clear that R_{ohmic} losses due to the electrolyte and electrodes can become quite significant. Taking up to 68% of the total voltage during charge and discharge. These losses can be attributed to two main factors: Electrolyte degradation and oxidation on the electrodes. By conducting the blank test in Appendix A it is possible to subtract this loss factor from the results.

In Section 2.2 it is discussed that co-ion transport occurs due to membranes not being perfectly selective. This phenomena occurs during the charge and discharge phase, but due to different reasons. During the charge phase co-ion transport is driven by the electric field, while in the discharge phase it is driven by diffusion forces. What this does is shown in Figure 18. In this figure it can be seen that during the charge phase hardly any change can be observed in the voltage curve, as all the co-ions are pulled through the BPM into the corresponding solutions. During discharge the story is different and can be seen in Figure 18 and 19. With the presence of co-ions in the background of the acid and base the diffusion forces decrease. This in turn leads to buildup of co-ion at the interface of the BPM and inside the membrane itself. Co-ion buildup at the interface can be spotted by a rapid voltage drop, this is represented most clearly in Figure 19. Due to co-ion presence with the BPM itself the electrical resistance of the BPM will increase as well, this in turn will lead to further decrease in voltage. Resistance increase in the BPM can best be spotted in the increase of the slope in Figure 18. When the charge phase is initiated again all co-ions present in the membrane are pulled out of the BPM into the corresponding solutions. This causes the co-ion background concentration to increase even further and creates a self reinforcing loop, as this increase will decrease the diffusion forces even further in the subsequent discharge phase.

By conducting the 50 Cycle experiment in Section 4.2 it becomes clear what for effect co-ion transportation has on the lifetime of the battery. As can be seen in Figure 20a. The initial test, with 7 V - 0.25 V cut off voltage, is to establish a baseline for comparison. This only reaches a RTE of 30 % in its first cycle, with an ED of 3.7 kWh/m^3. While the ED is an improvement over the 2.9 kWh/m^3 published in Egmond et al, it degrades below 80 % of its original energy density after 3 cycles. This ED degradation is caused by the co-ion transportation described in the previous paragraph. The co-ion buildup in the solutions of the acid and the base causes the voltage to drop faster with each cycle. On

paper it would seem the system is discharge faster, but this is not true. In reality with each consecutive the voltage drops faster, but it doesn't discharge as deep as the previous cycle. Subsequently, during the charge phase the system reaches its upper limit faster and as co-ions build up cycles becomes increasingly shorter. As can be seen in Appendix D, the lifespan varies greatly between BPMs, which is an indication of much influence the permselectivity of a membrane is on the amount of co-ion transportation. Sadly membrane quality is something that is dependent on suppliers, but by changing the current density and SoC limits co-ion transport can be reduced and thus improving the battery lifetime. To start, the SoC limits were reduced to 3.5 V - 0.6 V cut off voltage. Changing this parameter has had a substantial effect on the longevity of the system, with the system being able to run six charge/discharge cycles before dropping below 80 % of its original ED. The RTE has also improved from 30 % to 40 %, but as a trade off the ED itself has dropped from 3.7 kWh/m^3 to 3.2 kWh/m^3. With the adjustment of the cut off voltages less counterion transport occurs over the BPM, which in turn also means less co-ion transport. This gives the operator of the AB-FB a choice: either go for maximum depth of charge in order to be able to store more energy, but increase the degradation of the AB-FB; or reduce the upper and lower limit of the SoC, which also reduces the energy density, but also increases the lifespan of the system. While keeping the 3.5 V - 0.6 V cut off voltage limits, the charge current density was reduced from its original 100 A/m^2 to 50 A/m^2. Compared to the previous test, no significant changes has been observed in the ED. In addition, the system runs the same amount of cycles before degrading below 80 % of its initial ED. When looking at the efficiencies the RTE has increased from 40 % to 50 %, while the CE has stayed roughly the same. By reducing the charge density it seems the system is able to charge more efficiently, but the equal CE differs from expectations. By lowering the charge density the potential difference over the BPM is lowered as well, which would mean that more co-ions should enter the membrane in relation with the counterions. This should lower the CE, but in this experiment this wasn't the case. It is theorized that the limit before CE degradation is noticeable is at 50 A/m^2. In order to prove this more experimentation with charge current densities below the 50 A/m^2 should be performed. Unfortunately due to time constraints and the global pandemic this wasn't possible and should be investigated further in the future. Research into the effects of changing in the discharge density should also still be conducted. Most notably increasing the discharge density, as the experiments run during the 50 Cycle tests were discharged at 30 A/m^2, which is already very low. It is expected that increasing the discharge current density will actually increase co-ion transport as the potential difference over the BPM is lowered even further during discharge. The theory behind this is mentioned in Section 2.2.

From the previous paragraph it is concluded that the most effective way to minimize co-ion transport, besides using membranes with improved permselectivity, is by reducing the upper and lower limit of the SoC. This comes at the cost of the ED of the system. After a certain period the ED has reduced too far and needs to be reset. For this the Charge Reset Cycle has been devised. By combining the acid and base solutions, a NaCl solution is created. This solution is pumped through the salt compartment with demi water in the acid and base compartment, after which electrodialysis is performed. With this process pure acid, base and demi water should be produced suitable for use in the AB-FB. Eventually it was possible to create 0 M demi water, but the acid and base solutions never exceeded the 0.422 M and 0.348 M respectively. A hypothesis is that this is either because of co-ion transport or osmosis. In order to definitely conclude if it is because of co-ion transport accurate measurements should be take of the co-ion concentration. During this thesis this is done via conductivity measurements, after which the concentration is extrapolated in Appendix B. Unfortunately it is currently unknown how much influence co-ions have on the conductivity of the solutions. If the concentration difference is because of osmosis should also be tested in a future date, as this theory was conceived during writing of this thesis. The process shows merit as the goal was to create 0.5 M acid and base and the resulting solutions is still usable for the system. By further refining the process it should be possible to reach the intended goal. This can be done by for example minimizing non-homogeneous flow or adjusting the acid/base - salt pump ratios.

A Blank Test Results and Discussion

The blank test represents a simple test in order to determine the $R_{electrodes}$ of the cell, with $R_{electrodes}$ representing the resistance of the electrodes, electrolyte solution and the electrical wiring used to measure the battery. Both the electrolyte solution and the electrodes will degrade over time due to oxidation, which will effect $R_{electrodes}$ and increase the resistance. Therefore it is important to perform the blank test before every set of experiments, when the electrolyte is refreshed or a single experiment has run for a long time (6+ hours). In order to perform the test only an AEM will be placed between the electrode end plates. Technically the resistance of the single AEM will contribute to the $R_{electrodes}$ measurement, but this is considered negligible. A schematic representation of the blank test can be found in Figure 34.

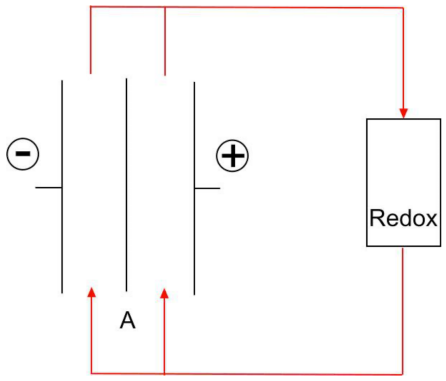

Figure 34: A schematic representation of the Blank Test. Between the two end plates resides only a single AEM. The electrolyte solution is pumped continuously at 100 mL/min.

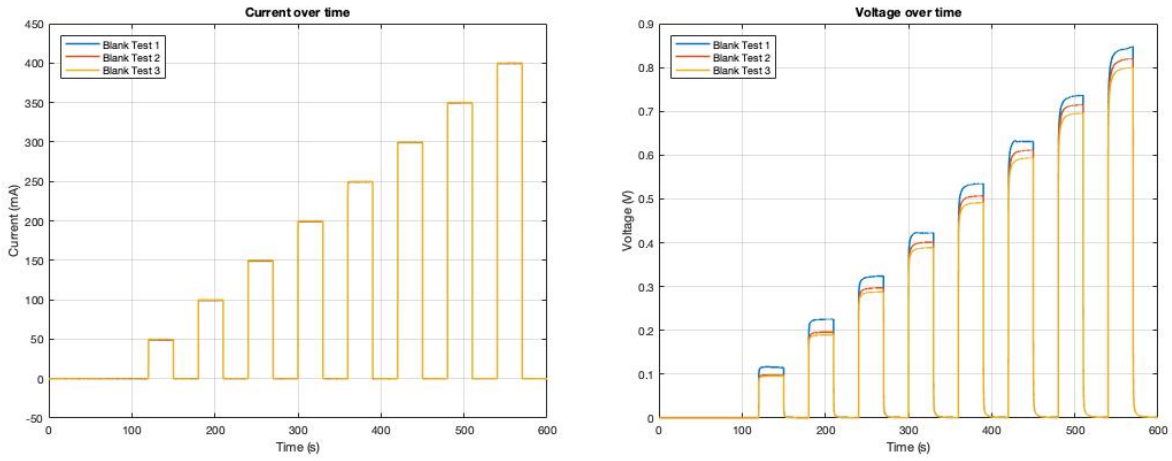

Figure 35: The blank test plotted in two different graphs. The left graph is the current over time and the graph on the right is the voltage over time. Over a period of ten minutes the applied current is gradually increased.

In Figure 35 an example is shown of a typical blank test. Over a period of ten minutes the current is incrementally increased with short OCV intervals in between, from there the resulting voltage is measured. This test is repeated three times. As can be seen in the right graph in Figure 35, the resulting voltages actually differ between tests. The scope of this difference actually differs between each test set and it is speculated that this is caused by degradation of the electrolyte.

Once the set of three tests is complete an I-V curve can be plotted from which a polynomial can be determined in MATLAB. As there are three differing voltages to choose from to plot the I-V curve with, the average voltage must be calculated between these three voltage plots. It is also possible to take the worst or best voltage plot, but as it is unknown if the resistance resembles the worst or the best plot once the actual test is running, it is deemed safest to compromise and take the average. Note, the example shown in Figure 35 is an extreme example amongst all results. Typically all three voltage plots are plotted much closer together. By creating a polynomial of the I-V curve it becomes possible to derive an equation of the voltage as a function of the current or determining $R_{electrodes}$ as a constant. With $R_{electrodes}$ known, it can be subtracted from the results of subsequent experiments and thus eliminating this loss factor from the results.

Close inspection of Figure 35 does show another peculiar oddity: The effects of concentration polarization. Looking over the voltage over time, the voltage graph shows slight curvature at the start of each application of current. The curvature eventually flattens out, but at higher current densities is either doesn't flatten out or it takes longer. This is because the concentration polarization is significantly larger or hasn't even reached steady state yet. Most notably the final voltage curve is still rising before it is cut off. This can actually influence the determination of $R_{electrodes}$ as that current density as the voltage hasn't reached its final value. In order to combat this the pumping speed of the electrolyte has to be increased. When doing this the piping and manifolds must also be checked to make sure it can handle the increased pressure and pressure drops of the increased flow. The pump speed was left at 100 mL/min for the purpose of this thesis as the highest operating current in all experiments in 220 mA, well within range in which the curve flattens out.

B Conductivity vs Concentration

Due to limitations in materials and set up it was only possible to determine the concentration by correlating it with the conductivity of the solution. By knowing the relation between conductivity and concentration it was possible to determine the extent of desalination of the salt compartment. This does have limitations though, as measuring the conductivity assumes that the solution only contains the produced ions. Therefor this reference is best used to measure the purity of the desalinated salt solution (i.e. demi water).
Reference solutions of predetermined concentrations were prepared for HCl, NaOH, NaCl and their conductivity was measured. These results are shown in Table 9. After measuring the solutions an equation for the conductivity of each solution was derived which are represented by Eq. 32 - 34.

Solution	**Concentration** ($molL^{-1}$)	**Conductivity** ($mScm^{-1}$)
HCl	1	341.0
	0.5	186.8
	0.25	98.2
	0.1	40.8
NaOH	1	192.7
	0.5	102.8
	0.25	54.4
	0.1	22.5
NaCl	1	84.4
	0.8	73.3
	0.6	57.9
	0.4	39.7
	0.2	20.6
	0.1	11.7
	0.05	5.3
	0.02	2.3
	0.01	1.1
	0.0	0.033

Table 9: Measured conductivity values for the respective concentration of each solution

$$\textbf{HCl} \quad y = 0.0030x - 0.0397 \tag{32}$$

$$\textbf{NaOH} \quad y = 0.0053x - 0.0325 \tag{33}$$

$$\textbf{NaCl} \quad y = 0.0114x - 0.0189 \tag{34}$$

For Eq. 32 - 34 y represents the concentration and x is the conductivity of the solution. Now that the relations are known between conductivity and concentration it becomes easier to determine the quality of any produced acid, base and demi water.

C Results of the Characterization tests

In this appendix graphs are presented in which can be seen how much results can differ between membranes, thus indicating a difference in quality. The membranes presented here are named BPM 1, 2 and 3. BPM 1, 2 and 3 are bipolar membranes cut from the 'Standard' batch from Fumatech supplied in Januari 2020. All membranes are cut from the same sheet. All experiments are run back to back with blank tests performed before and after in order to get the most accurate and comparable measurements.

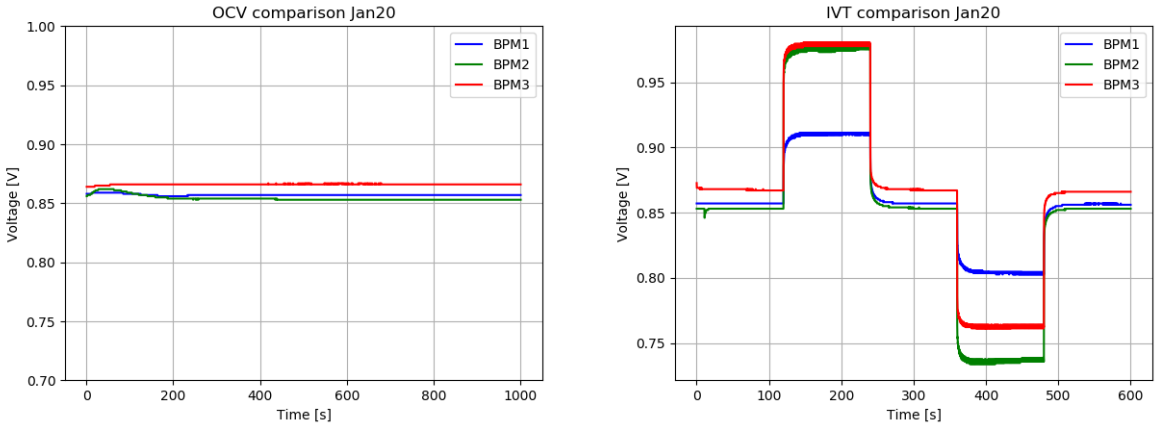

(a) (b)

Figure 36: The OCV and IVT test with BPM 1, 2 and 3 compared to each other using pure solutions. This experiment has bee corrected for the blank test, so $R_{electrodes}$ has already be subtracted.

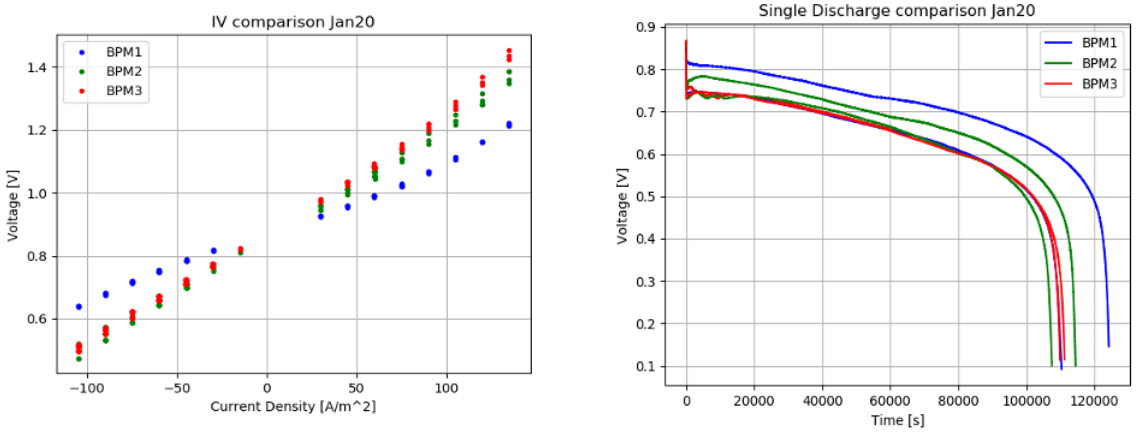

(a) (b)

Figure 37: Figure 37a and 37b represent the IV and Single discharge experiments run with pure solutions.

Figures 36 and 37 represent the Characterisation experiments done with pure solutions and no background concentrations. As mentioned earlier all the BPMs are cut from the same sheet and still deviations between BPMs can be noted. The most significant difference can be seen in BPM 1 compared to BPM 2 and

3. Throughout all experiments BPM 1 has significantly less membrane resistance compared to the rest. This can most profoundly be seen in Figure 36b and 37a. An explanation for this is possible deviations of thickness and composition in the membrane sheets. These deviations have already frequently been noted between batches and with this set of experiments basic proof can be found that it even happens on the same sheet itself. In order to verify this further research must be conducted with a microscope and accurate thickness measurements.

The following Figures 38 - 40 show the IV and Single Discharge experiments with 0.15 M NaCl background concentration. Figure 41 compares them all in one figure together the the graphs from the pure solution experiments.

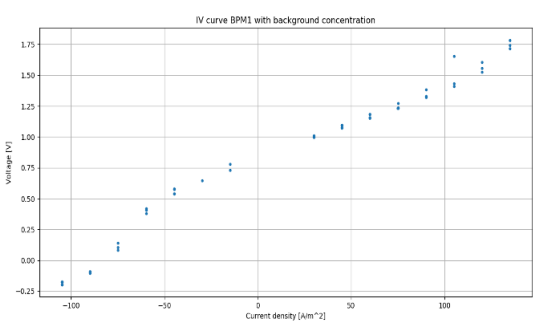

(a)

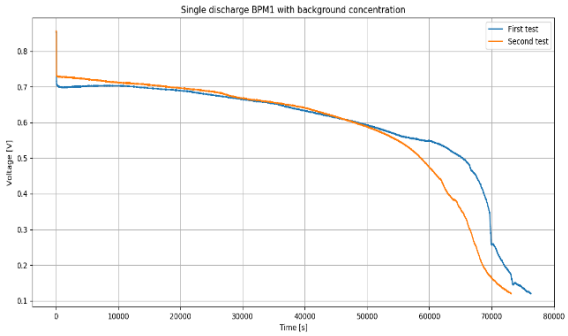

(b)

Figure 38: Figure 38a represents the IV test with 0.15 M NaCl. Figure 38b represents the Single Discharge test with the same amount of background concentration. The Single Discharge experiment was conducted twice as this experiments tends to show deviations, as can be seen in the graph.

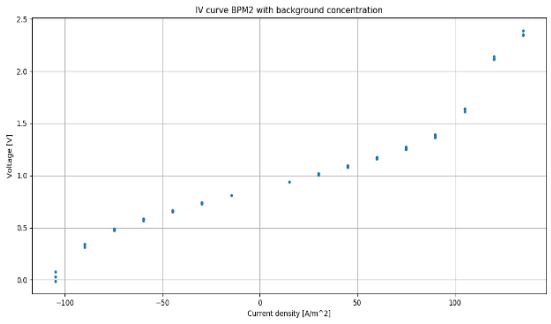

(a)

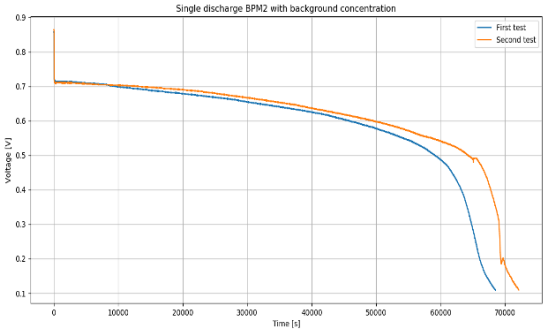

(b)

Figure 39: Figure 39a represents the IV test with 0.15 M NaCl. Figure 39b represents the Single Discharge test with the same amount of background concentration. The Single Discharge experiment was conducted twice as this experiments tends to show deviations, as can be seen in the graph.

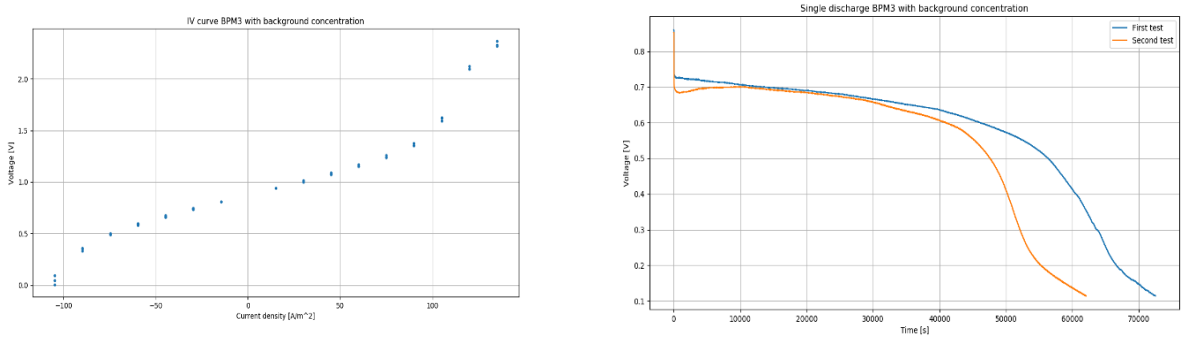

(a) (b)

Figure 40: Figure 40a represents the IV test with 0.15 M NaCl. Figure 40b represents the Single Discharge test with the same amount of background concentration. The Single Discharge experiment was conducted twice as this experiments tends to show deviations, as can be seen in the graph.

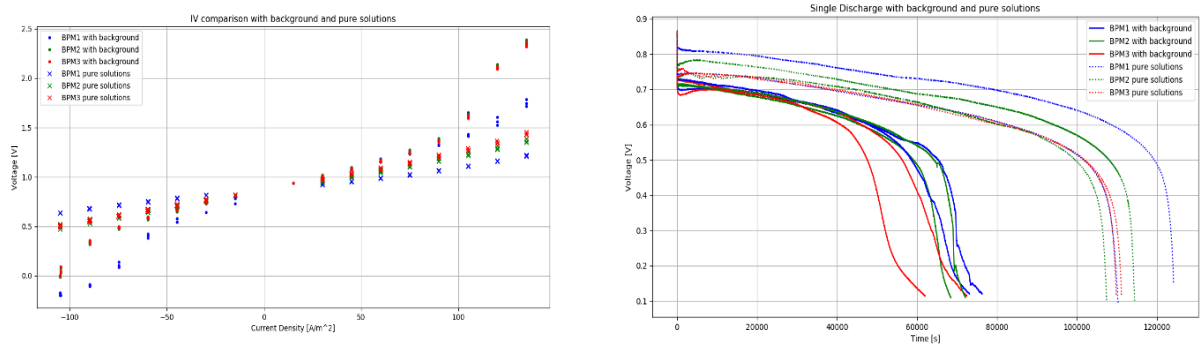

(a) (b)

Figure 41: Figure 41 shows all the results from Figures 37 - 40 together in their corresponding graphs.

As can be seen in Figure 41a, BPM 1 is once again the largest outlier compared to the other tested bipolar membranes. During the charging phase it shows less resistance both with and without background concentration. As for the discharge phase, it slight differs depending if there is or isn't background concentration in the solution. Following the line of the pure solutions, it can be seen that BPM 1 shows less resistance compared to BPM 2 and 3. When adding background concentration the results contradict expectations, with BPM 1 actually experiencing more resistance and voltage drop than BPM 2 and 3. This is strange as this would indicate that BPM 1 experiences more co-ion transport, but Figure 41b contradicts this. If BPM 1 was experiencing more co-ion transport during discharge, this would mean that it would show a steeper slope and ealier voltage drop in comparison to the other membranes. This is not the case, as it experiences less or equal voltage drop. One thing to note is that the system discharges only at 15 A/m^2 during the Single Discharge test. As can be seen in Figure 41a this is on the low side of the measured discharge range, where the differences are less extreme than the upper ranges of 50 A/m^2 and above. Still, even in these lower ranges BPM 1 experiences more co-ion transport which isn't seen in Figure 41b. Next to inconsistencies in thickness and composition it might also be possible that BPM 1 has been damaged or suffered from membrane poisoning from the electrolyte. Membrane poisoning from

electrolyte can occur when electrolyte leaks into the acid and base compartment. This can cause the electrolyte to become embedded in the BPM, thus effecting its performance. The possibility that this is the case is considered small though, as this was a freshly cut membrane and no leakages have been registered. No surface damages have been detected by eye, but it is possible microscopic deviations can be found when examined under a microscope.

D Results of the 50 Cycle tests

For the final appendix entry, the remaining useful results are presented of the 50 Cycle Experiments. Figures 42 - 44 represent the 50 Cycle tests done with the BPM from January 2019. Figures 45 - 47 show the graphs of the experiments done with the 2017 BPM. As mentioned in earlier sections, there can be quite significant differences between the quality of the membranes. In practical terms this means membranes of better quality last more cycles before degrading below 80 % ED. This degradation is coupled with the amount of co-ion transportation occurring in the system. As can be seen in the following graphs the difference between the 2019 and 2017 BPMs can be marked as quite significant. As this section is only meant in giving insight in the performance differences between membranes, only a short concluding comparison explanation shall be given. All tests are corrected with the blank test, so $R_{electrodes}$ has been subtracted.

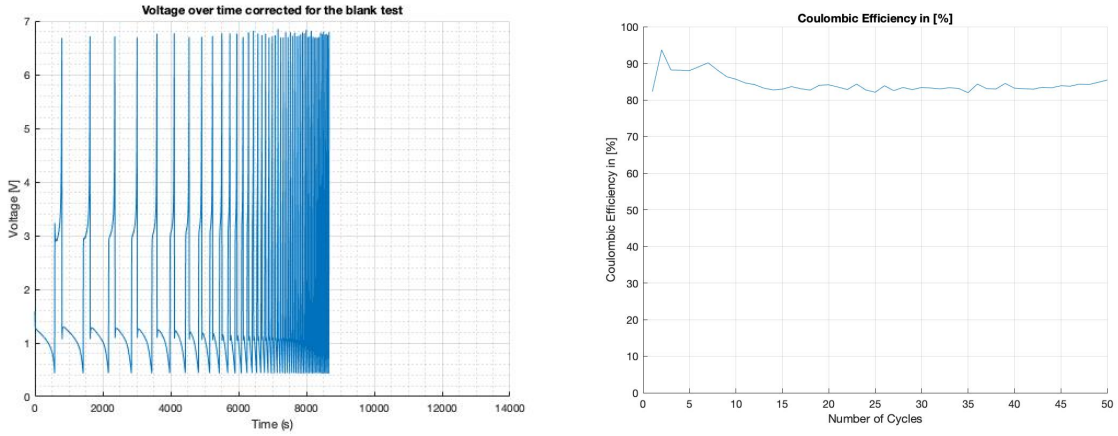

(a) (b)

Figure 42: Figure 42a represents the voltage over time. Figure 42b is the coulombic efficiency for each cycle.

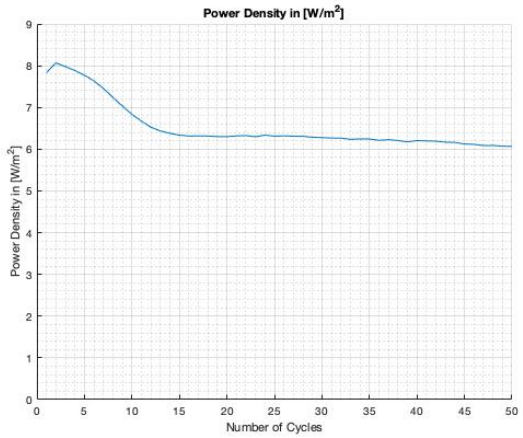

(a)

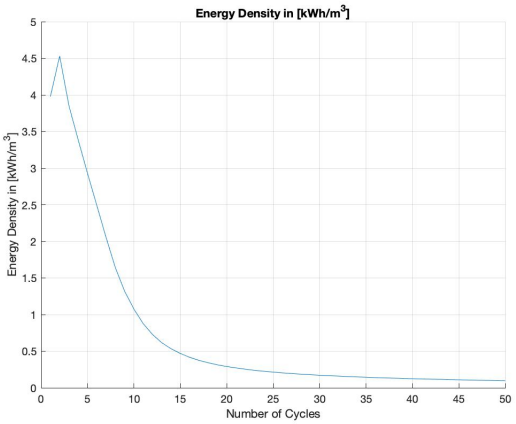

(b)

Figure 43: Figure 43a shows the PD development over each cycle, while Figure 43b shows the corresponding ED.

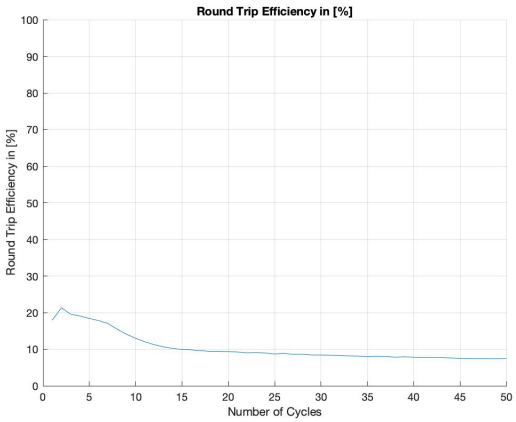

(a)

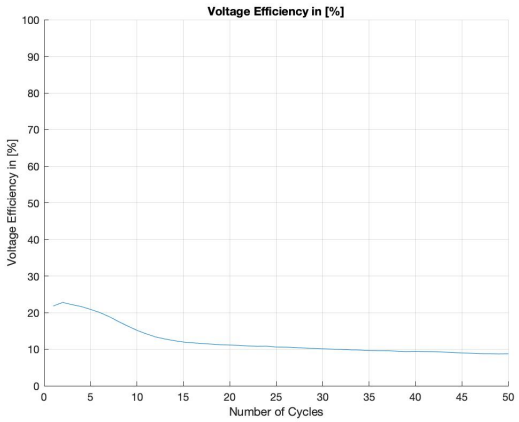

(b)

Figure 44: The RTE efficiency is presented in Figure 44a. The corresponding VE can be found in Figure 44b.

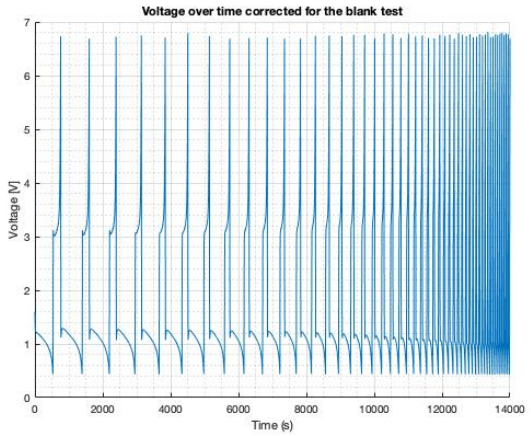

(a)

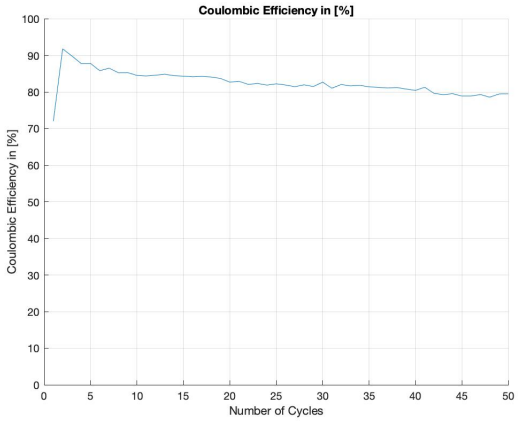

(b)

Figure 45: Figure 45a represents the voltage over time. Figure 45b is the coulombic efficiency for each cycle.

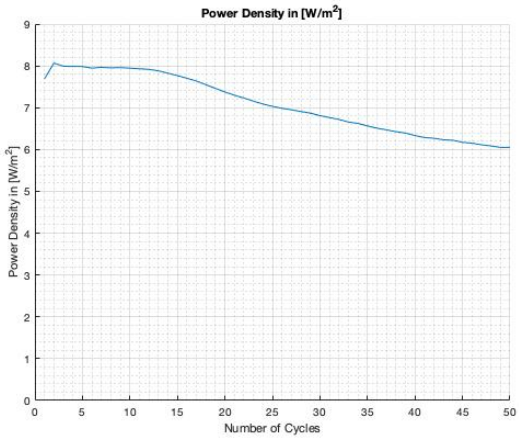

(a)

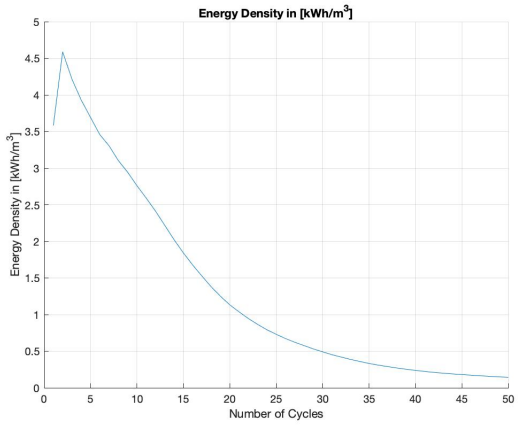

(b)

Figure 46: Figure 46a shows the PD development over each cycle, while Figure 46b shows the corresponding ED.

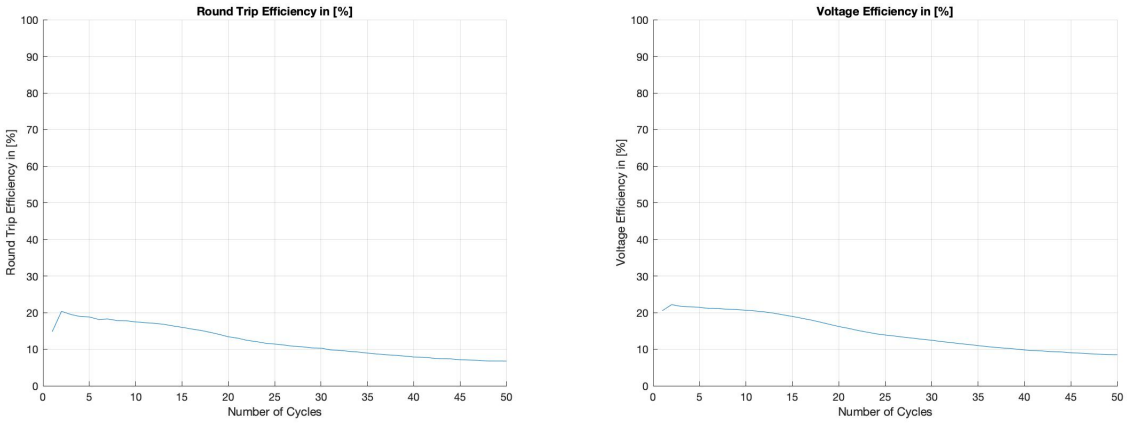

(a) (b)

Figure 47: The RTE efficiency is presented in Figure 47a. The corresponding VE can be found in Figure 47b.

When reviewing the above figures it become clear the BPM has no influence on the efficiencies of the system. Both Figures 44 and 47 show similar RTE and VE. This gives indication that in order to improve these properties, changes to the DoC and current densities must be made. The most interesting observations can be found in Figure 42 and 45 with their corresponding PD/ED graphs, which are Figures 43 and 46 respectively. When comparing Figure 42a to Figure 45a, it shows the 2017 BPM last for almost twice as long before completing its fifty cycles. This is further supported when comparing related ED and PD in Figures 43 and 46. While both the 2017 and 2019 BPM peak at 8 W/m^2, the 2017 BPM only starts to degrade below this number after ten cycles compared to only four cycles for the 2019 BPM. This trend continues when comparing ED. The 2019 BPM lasts only three cycles before degrading below 80 % of its max value of 4.5 kWh/m^3. This is in stark contrast with Figure 46b, where the system with the 2017 BPM lasts six cycles before deteriorating.

These figure show that the 2017 BPM has a significantly better permselectivity (α) and fixed charge density X. This supports the theory written in Section 2.2, where it is mentioned that these properties are heavily influenced by the composition of the membrane. As the technology is still in development, these variations will probably be an issue in the foreseeable future. It is therefor important to continue studying further possibilities in limiting or bypassing these variations in the different BPMs.

E CFD Analysis

In this section a small visualisation of the flow distribution through the spacer is given. This is to give a general idea in how the solutions flow through the system. As there is no solution implemented to distribute the flow more evenly, the load fraction is used to combat the effluent from exiting before it is properly treated. These images have been provided by AquaBattery B.V.

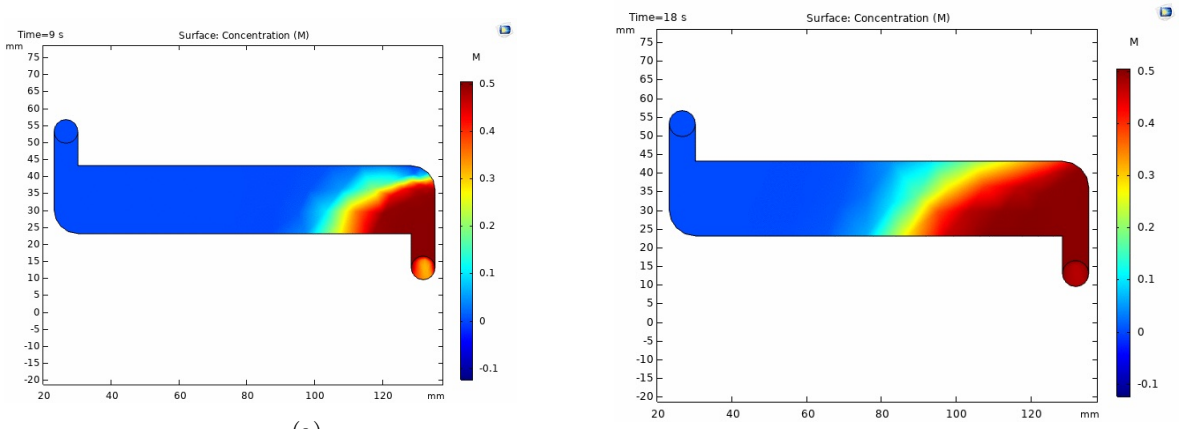

(a) (b)

Figure 48: The flow distribution at the initial stages.

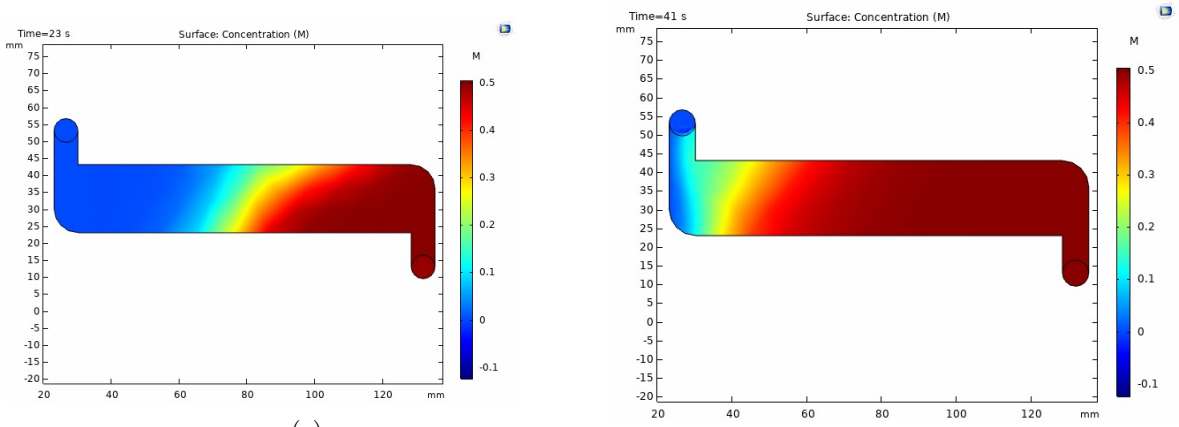

(a) (b)

Figure 49: The flow distribution approaching the exit of the spacer. It can be seen that initial concentrations of effluent have already reached the exit, long before the main body.

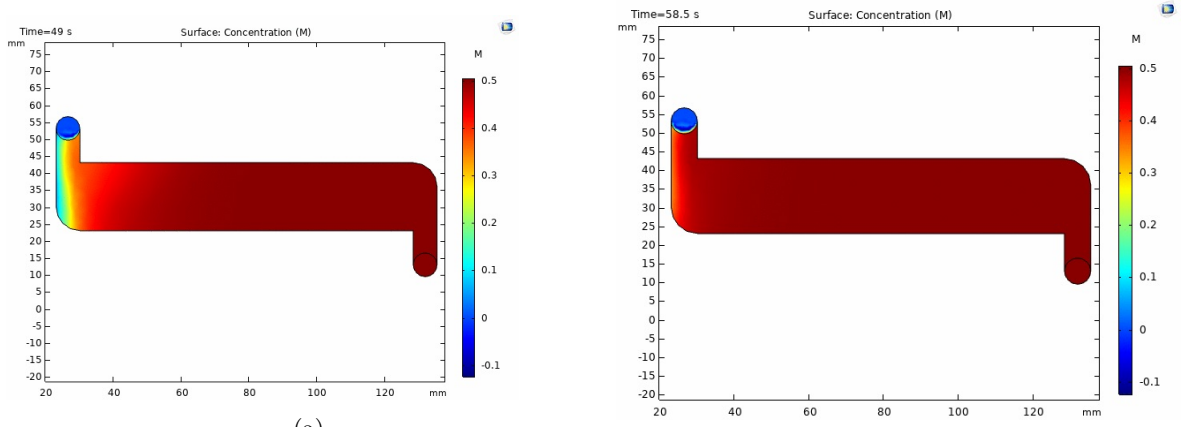

Figure 50: The final stages of the flow distribution. Here it can be seen that the most upper part of the spacer (the left side) still requires time to evenly distribute.

As can be seen in Figure 48, in the initial stages the flow distribution is very uneven. As can be expected the concentration spreads faster on the side of the input, as that is the closest point. This means it takes longer before the far side is filled with new concentration. Figure 49 shows that a more even distribution starts to form when approaching the exit. This is because the difference in distance of the fresh solution front is less than at the start. Finally, Figure 50 shows the entire spacers evenly filled except the final most left part of the spacer. This is because it is farthest from in input and exit, as the solution has a preference to take the shortest route from input to output. By implementing a load fraction as mentioned in Section 3.2.3, it is aimed to combat this uneven flow distribution and prevent any solution from the influent.

F Matlab Code for 50 Cycle Experiment

```
close all; clc; clear all;

BPM = '2017 BPM';
%% Loading the experimental results

%Blank Test
Excel_Blank = readtable('SGB_XG_25112019_BlankTest.xlsx');
BlankTest = table2array(Excel_Blank);

Time = BlankTest(:,1);

% First Blank Test
Current_1 = BlankTest(:,2); %[mA]
Voltage_1 = BlankTest(:,3); %[V]

% Second Blank Test
Current_2 = BlankTest(:,5); %[mA]
Voltage_2 = BlankTest(:,6); %[V]

% Third Blank Test
Current_3 = BlankTest(:,8); %[mA]
Voltage_3 = BlankTest(:,9); %[V]

%% Load main test that has to be analysed

Excel_Cycling = readtable('
    SGB_XG_20112019_AcidBaseCyclingTest_2triplets_2019StandardBatch.xlsx');
Cycling_Test = table2array(Excel_Cycling);

Cycling_Time = Cycling_Test(:,1); %[s]
Cycling_Current = Cycling_Test(:,2); %[mA]
Cycling_Voltage = Cycling_Test(:,3); %[V]

%% Set constants of the system

R_i = 3.48; %Ohm
I_Charge = 110; %charge current [mA]
I_Discharge = 66; %discharge current [mA]
M = 4; %number of membranes in the triplet
A = 22*10^-4; %Surface area of the membrane [m^2]
V_acid = 500e-6*11e-2*2e-2; %thickness spacer*length*width mesh in spacer
V_base = 500e-6*11e-2*2e-2;
V_salt = 500e-6*11e-2*2e-2;
y_spacer = 0.5; %Porosity of the spacer
N = 2; %The amount of cells in the stack
V_solution = N*((V_acid+V_base+V_salt)*y_spacer); %m^3

%% Plotting Blank Test
```

```
48 % Plot Current over time
49 figure(1)
50 plot(Time,Current_1,'linewidth',1.5)
51 grid on
52 hold on
53 plot(Time,Current_2,'linewidth',1.5)
54 plot(Time,Current_3,'linewidth',1.5)
55 title('Current over time');
56 xlabel('Time (s)');
57 ylabel('Current (mA)');
58 legend('Blank Test 1','Blank Test 2','Blank Test 3', 'Location', 'northwest
       ');
59 hold off
60
61 % Plot Voltage over time
62 figure(2)
63 plot(Time,Voltage_1,'linewidth',1.5)
64 grid on
65 hold on
66 plot(Time,Voltage_2,'linewidth',1.5)
67 plot(Time,Voltage_3,'linewidth',1.5)
68 title('Voltage over time');
69 xlabel('Time (s)');
70 ylabel('Voltage (V)');
71 legend('Blank Test 1','Blank Test 2','Blank Test 3', 'Location', 'northwest
       ');
72 hold off
73
74 %% Setting negative currents to zero for the blank test
75
76 for i=1:length(Current_1)
77     if Current_1(i)<0
78         Current_1(i)=0;
79     end
80     if Current_2(i)<0
81         Current_2(i)=0;
82     end
83     if Current_3(i)<0
84         Current_3(i)=0;
85     end
86 end
87
88 %% Finding the Peaks of voltage and current
89
90 %finds the peaks in the first blank test
91 figure(3)
92 findpeaks(Voltage_1,Time,'MinPeakProminence',0.05,'MinPeakDistance',20)
93 [pks,locs] = findpeaks(Voltage_1,Time,'MinPeakProminence',0.05,'
       MinPeakDistance',20);
94 [Va] = [pks];                          % Assigning the voltage peaks to a
```

```
    seperate table
[ta] = [locs];                      % Assigning the time of the voltage peak
    to a seperate table
[Ca] = zeros(8,1);                  % Creating a table to store the peaks of
    the current
for j=1:length(ta)                  % finding the current at which the peak
    voltage occurs by using the time
    for i=1:length(Current_1)
        if ta(j)==Time(i)
            Ca(j) = Current_1(i);
        end
    end
end

% Same process for the other 2 blank tests
figure(4)
findpeaks(Voltage_2,Time,'MinPeakProminence',0.05,'MinPeakDistance',20)
[pks,locs] = findpeaks(Voltage_2,Time,'MinPeakProminence',0.05,'
    MinPeakDistance',20);
[Vb] = [pks];
[tb] = [locs];
[Cb] = zeros(8,1);
for j=1:length(tb)
    for i=1:length(Current_2)
        if tb(j)==Time(i)
            Cb(j) = Current_2(i);
        end
    end
end

figure(5)
findpeaks(Voltage_3,Time,'MinPeakProminence',0.05,'MinPeakDistance',20)
[pks,locs] = findpeaks(Voltage_3,Time,'MinPeakProminence',0.05,'
    MinPeakDistance',20);
[Vc] = [pks];
[tc] = [locs];
[Cc] = zeros(8,1);
for j=1:length(tc)
    for i=1:length(Current_3)
        if tc(j)==Time(i)
            Cc(j) = Current_3(i);
        end
    end
end

%% Average of the 3 blank tests
%creates an average value and fills a new column with it
[V] = zeros(8,1);
[C] = zeros(8,1);
for i=1:8
```

```
139     V(i) = (Va(i)+Vb(i)+Vc(i))/3;
140     C(i) = (Ca(i)+Cb(i)+Cc(i))/3;
141 end
142
143 %% Create I-V Curve
144
145 figure(6)
146 hold on
147 plot(V,C);
148 grid on
149 title('I-V Curve');
150 xlabel('Voltage [V]');
151 ylabel('Current [mA]');
152 hold off
153
154
155 %% Create a polynomial function to fit on the curves
156
157 %pfit = polyfit(x,y, number of polynomials)
158 pfit = polyfit([V;0;0;0;0;0;0;0;0;0;0;0;0;0;0;0;0;0;0;0;0], [C
    ;0;0;0;0;0;0;0;0;0;0;0;0;0;0;0;0;0;0;0;0], 1);
159
160 %use polyval([the function], [the x values]) to calculate what the output
161 %of the the function is at certain values.
162
163 %% Create Voltage function to substract from characterization
164
165 V_Charge = (I_Charge-pfit(2))/pfit(1);
166
167 V_Discharge = (-I_Discharge-pfit(2))/pfit(1);
168
169
170 %% Load characterization
171
172 %plot the figure of the cycling test
173 figure(7)
174 hold on
175 plot(Cycling_Time,Cycling_Voltage);
176 grid on
177 grid minor
178 title('Voltage over time');
179 xlabel('Time (s)');
180 ylabel('Voltage [V]');
181 hold off
182
183 %% Identify Charge and Discharge cycles
184 % We substract the voltage of the blank test from the charge and discharge
185 % voltage
186 Final_Voltage = zeros(length(Cycling_Time),1);
187 for i=1:length(Cycling_Time)
```

```
    if Cycling_Current(i)<-0.1
        Final_Voltage(i) = Cycling_Voltage(i)-V_Discharge;
    elseif Cycling_Current(i)>0.1
        Final_Voltage(i) = Cycling_Voltage(i)-V_Charge;
    else
        Final_Voltage(i) = Cycling_Voltage(i);
    end
end

%create a plot with the corrected voltage values for the blank test
figure(8)
hold on
plot(Cycling_Time,Final_Voltage);
grid on
grid minor
title('Voltage over time corrected for the blank test');
xlabel('Time (s)');
ylabel('Voltage [V]');
xlim([0 14000]);
ylim([0 7]);
hold off

%% Setting current fluctuations to zero

%The current tends to fluctuate around 0. This sets those values to 0 to
%make calculations and splitting easier.
for i=1:length(Cycling_Current)
    if Cycling_Current(i)<0.15 && Cycling_Current(i)>-0.15
        Cycling_Current(i)=0;
    end
end



%% Splitting the cycles into seperate colomns for each cycle
Charge_I = zeros(length(Cycling_Time),50);
Charge_V = zeros(length(Cycling_Time),50);
Discharge_I = zeros(length(Cycling_Time),50);
Discharge_V = zeros(length(Cycling_Time),50);
j = 1;

for i=1:length(Cycling_Time)
    if i==length(Cycling_Time)
        break
    end
    if Cycling_Current(i)<0
        Discharge_I(i,j) = Cycling_Current(i);
        Discharge_V(i,j) = Final_Voltage(i);
        if Cycling_Current(i+1) >=0
            j=j+1;
```

```
238             end
239         else
240             Discharge_I(i,j) = 0;
241             Discharge_V(i,j) = 0;
242         end
243     end
244
245     j=1;
246
247     for i=1:length(Cycling_Time)
248         if i==length(Cycling_Time)
249             break
250         end
251         if Cycling_Current(i)>0
252             Charge_I(i,j) = Cycling_Current(i);
253             Charge_V(i,j) = Final_Voltage(i);
254             if Cycling_Current(i+1)<=0
255                 j=j+1;
256             end
257         else
258             Charge_I(i,j) = 0;
259             Charge_V(i,j) = 0;
260         end
261     end
262
263     %% Calculating Efficiencies
264
265
266     j=1;
267     deltat=0.2; %the delta T steps made in the Ivium
268
269     for i=1:length(Cycling_Time)
270         if Discharge_I(i,j)<0
271             Cout(i,j) = Discharge_I(i,j)*deltat;
272             Eout(i,j) = Discharge_I(i,j)*Discharge_V(i,j)*deltat;
273
274             if Discharge_I(i+1,j)>=0
275                 j=j+1;
276             end
277
278         end
279     end
280
281     TotalCount_Discharge_I = sum(Cout,1);
282     TotalCount_Discharge_E = sum(Eout,1);
283
284     j=1;
285     %
286     for i=1:length(Cycling_Time)
287         if i==length(Cycling_Time)
```

```
288             break
289         end
290         if Charge_I(i,j)>0
291             Cin(i,j) = Charge_I(i,j)*deltat;
292             Ein(i,j) = Charge_I(i,j)*Charge_V(i,j)*deltat;
293             if Charge_I(i+1,j)<=0
294                 j=j+1;
295             end
296
297         end
298     end
299
300     %Getting average of voltage for each cycle used for power density
301     Total_V=zeros(1,50);
302     for j=1:50
303         f = 0;
304         for i=1:length(Cycling_Time)
305             if Discharge_V(i,j)~=0
306                 Total_V(j) = Total_V(j)+Discharge_V(i,j);
307                 f=f+1;
308             end
309         end
310         PD(j) = ((I_Discharge/1000)*Total_V(j)/f)/(M*A);
311     end
312
313     %Sum all the charge currents and voltages
314     TotalCount_Charge_I = sum(Cin,1); %in mA
315     TotalCount_Charge_E = sum(Ein,1); %in W*s=J
316
317     %Calculate the efficiencies
318     C_E = (-TotalCount_Discharge_I./TotalCount_Charge_I)*100;
319     RTE = (-TotalCount_Discharge_E./TotalCount_Charge_E)*100;
320     VE = (RTE./C_E)*100;
321     ED = ((-TotalCount_Discharge_E.*2.778e-7)./1000)/V_solution; %/1000 to
        convert mA to A
322
323     %% Calculate energy lost
324
325     E_lost = (TotalCount_Charge_E/1000) - (TotalCount_Discharge_E/1000);
326     E_Ri = (R_i*(TotalCount_Charge_I/1000)) + -(R_i*(TotalCount_Discharge_I
        /1000));
327     E_co = E_lost - E_Ri;
328
329
330
331     %% Plot all efficiencies
332     C_E_Cycles = 1:50;
333     figure(9)
334     hold on
335     grid on
```

```
grid minor
xlim([0 50]);
ylim([0 100]);
plot(C_E_Cycles,C_E);
title('Coulombic Efficiency in [%]');
ylabel('Coulombic Efficiency in [%]');
xlabel('Number of Cycles');
hold off

figure(10)
hold on
grid on
grid minor
xlim([0 50]);
ylim([0 100]);
plot(C_E_Cycles,RTE);
title('Round Trip Efficiency in [%]');
ylabel('Round Trip Efficiency in [%]');
xlabel('Number of Cycles');
hold off

figure(11)
hold on
grid on
grid minor
xlim([0 50]);
ylim([0 100]);
plot(C_E_Cycles,VE);
title('Voltage Efficiency in [%]');
ylabel('Voltage Efficiency in [%]');
xlabel('Number of Cycles');
hold off

figure(12)
hold on
grid on
grid minor
xlim([0 50]);
ylim([0 4]);
plot(C_E_Cycles,ED);
title('Energy Density in [kWh/m^3]');
ylabel('Energy Density in [kWh/m^3]');
xlabel('Number of Cycles');
hold off

figure(13)
hold on
grid on
grid minor
ylim([0 9]);
```

```
386 xlim([0 50]);
387 plot(C_E_Cycles, PD);
388 title('Power Density in [W/m^2]');
389 ylabel('Power Density in [W/m^2]');
390 xlabel('Number of Cycles');
391 hold off
392
393 figure(14)
394 hold on
395 grid on
396 grid minor
397 title('Energy lost by co-ions in [W]');
398 plot(C_E_Cycles, E_co);
399 hold off
```

G Matlab Code for Characterization Experiments

```
clear all; clc; close all;


%All data and constants are set at the start. Remember that the system
%generally works in mA
%% Which BPM?
BPM = ('BPM3');

%% Set constants of the system

I_Charge_IVT = 66/1000; %charge current [A]
I_Discharge_IVT = 66/1000; %discharge current [A]
M = 4; %number of membranes in the triplet
A = 22*10^-4; %Surface area of the membrane [m^2]

%% Loading the Blank Test Data
%xlsread function is slower than table2array, but easier to manipulate

%Blank Test
Excel_Blank = readtable('SGB_L_21012020_BlankTestBPM1.xlsx');
BlankTest = table2array(Excel_Blank);

Time_Blank = xlsread('SGB_L_21012020_BlankTestBPM1.xlsx','A1:A12001');

% First Blank Test
Current_1 = (xlsread('SGB_L_21012020_BlankTestBPM1.xlsx','B1:B12001')/1000)
    ; %[A]
Voltage_1 = xlsread('SGB_L_21012020_BlankTestBPM1.xlsx','C1:C12001'); %[V]

% Second Blank Test
Current_2 = (xlsread('SGB_L_21012020_BlankTestBPM1.xlsx','E1:E12001')/1000)
    ; %[A]
Voltage_2 = xlsread('SGB_L_21012020_BlankTestBPM1.xlsx','F1:F12001'); %[V]

% Third Blank Test
Current_3 = (xlsread('SGB_L_21012020_BlankTestBPM1.xlsx','H1:H12001')/1000)
    ; %[A]
Voltage_3 = xlsread('SGB_L_21012020_BlankTestBPM1.xlsx','I1:I12001'); %[V]



%% Loading the Characterisation Tests

%OCV test
Excel_OCV = readtable('SGB_L_22012020_StandardBPM1_OCV.xlsx');
OCV = table2array(Excel_OCV);

Time_OCV = OCV(:,1);
```

```
Voltage_OCV = OCV(:,3); %[V]
Current_OCV = OCV(:,2)/1000; %[A]

%IVT Test

Excel_IVT = readtable('SGB_L_22012020_StandardBPM1_IVT.xlsx');
IVT = table2array(Excel_IVT);

Time_IVT = IVT(:,1);
Voltage_IVT = IVT(:,3); %[V]
Current_IVT = IVT(:,2)/1000; %[A]

%IV Test
Excel_IV = readtable('SGB_L_22012020_StandardBPM1_IV.xlsx');
IV = table2array(Excel_IV);

Time_IV = IV(:,1);
Voltage_IV = IV(:,3); %[V]
Current_IV = IV(:,2)/1000; %[A]

%Single Discharge
Excel_Single = readtable('SGB_L_22012020_StandardBPM1_SingleDischarge.xlsx'
    );
Single = table2array(Excel_Single);

Time_Single = Single(:,1);
Voltage_Single = Single(:,3); %[V]
Current_Single = Single(:,2)/1000; %[A]



%% Plot OCV Curve

figure(1)
plot(Time_OCV, Voltage_OCV);
hold on
grid on
xlabel('Time [s]');
ylabel('Voltage [V]');
legend('OCV Standard BPM');
title(['OCV ', BPM]);
ylim([0 1]);
hold off

%% Setting negative currents to zero for the blank test
%An extra precaution in order to prevent unwanted data.
for i=1:length(Current_1)
    if Current_1(i)<0
        Current_1(i)=0;
    end
```

```
95      if Current_2(i)<0
96          Current_2(i)=0;
97      end
98      if Current_3(i)<0
99          Current_3(i)=0;
100     end
101 end
102
103 %% Finding the Peaks of voltage and current in blank test
104 figure(3)
105 findpeaks(Voltage_1,Time_Blank,'MinPeakProminence',0.05,'MinPeakDistance'
        ,20)
106 [pks,locs] = findpeaks(Voltage_1,Time_Blank,'MinPeakProminence',0.05,'
        MinPeakDistance',20);
107 xlabel('Current [A]');
108 ylabel('Voltage [V]');
109 [Va] = [pks];                       % Assigning the voltage peaks to a
        seperate table
110 [ta] = [locs];                      % Assigning the time of the voltage peak
         to a seperate table
111 [Ca] = zeros(8,1);                  % Creating a table to store the peaks of
         the current
112 for j=1:length(ta)                  % finding the current at which the peak
        voltage occurs by using the time
113     for i=1:length(Current_1)
114         if ta(j)==Time_Blank(i)
115             Ca(j) = Current_1(i);
116         end
117     end
118 end
119
120 % Same process for the other 2 blank tests
121 figure(4)
122 findpeaks(Voltage_2,Time_Blank,'MinPeakProminence',0.05,'MinPeakDistance'
        ,20)
123 [pks,locs] = findpeaks(Voltage_2,Time_Blank,'MinPeakProminence',0.05,'
        MinPeakDistance',20);
124 xlabel('Current [A]');
125 ylabel('Voltage [V]');
126 [Vb] = [pks];
127 [tb] = [locs];
128 [Cb] = zeros(8,1);
129 for j=1:length(tb)
130     for i=1:length(Current_2)
131         if tb(j)==Time_Blank(i)
132             Cb(j) = Current_2(i);
133         end
134     end
135 end
136
```

```
figure(5)
findpeaks(Voltage_3,Time_Blank,'MinPeakProminence',0.05,'MinPeakDistance'
    ,20)
[pks,locs] = findpeaks(Voltage_3,Time_Blank,'MinPeakProminence',0.05,'
    MinPeakDistance',20);
xlabel('Current [A]');
ylabel('Voltage [V]');
[Vc] = [pks];
[tc] = [locs];
[Cc] = zeros(8,1);
for j=1:length(tc)
    for i=1:length(Current_3)
        if tc(j)==Time_Blank(i)
            Cc(j) = Current_3(i);
        end
    end
end

%% Average of the 3 blank tests
[V] = zeros(8,1);
[C] = zeros(8,1);
for i=1:8
    V(i) = (Va(i)+Vb(i)+Vc(i))/3;
    C(i) = (Ca(i)+Cb(i)+Cc(i))/3;
end

%% Create I-V Curve from the blank

figure(6)
hold on
plot(V,C);
grid on
title('I-V Curve of Blank Test');
xlabel('Voltage [V]');
ylabel('Current [mA]');
hold off


%% Create a polynomial function to fit on the curves of the IV Blank test
%From there we can calculate the Resistance (R) for the cell and
%electrolyte

%pfit = polyfit(x,y, number of polynomials)
pfit = polyfit([V;0;0;0;0;0;0;0;0;0;0;0;0;0;0;0;0;0;0;0;0;0;0;0;0], [C
    ;0;0;0;0;0;0;0;0;0;0;0;0;0;0;0;0;0;0;0;0;0;0;0;0], 1);
R = 1/pfit(1);

%use polyval([the function], [the x values]) to calculate what the output
%of the the function is at certain values.
%The zero's in pfit are added in order to minimize the constant variable
```

```
    pfit(2) in
%pfit=pfit(1)*x+pfit(2)

%It can be assumed that R is practically constant for all values.

%% Create Voltage function to substract from characterization
%V_charge is an x value. Calculates from y=ax+b

% V_Charge = (I_Charge_IVT-pfit(2))/pfit(1);
%
% V_Discharge = (-I_Discharge_IVT-pfit(2))/pfit(1);

%% Identify Charge and Discharge cycles for the IVT
% We substract the voltage of the blank test from the charge and discharge
% voltage
%Should check if this is correct.
% Final_Voltage_IVT = zeros(length(Time_IVT),1);


%substract the blank test from the IVT test
Final_Voltage_IVT = Voltage_IVT-(Current_IVT*R);


% for i=1:length(Time_IVT)
%     if Current_IVT(i)<(-0.5/1000)
%         Final_Voltage_IVT(i) = Voltage_IVT(i)-V_Discharge;
%     elseif Current_IVT(i)>(0.5/1000)
%         Final_Voltage_IVT(i) = Voltage_IVT(i)-V_Charge;
%     else
%         Final_Voltage_IVT(i) = Voltage_IVT(i);
%     end
% end


%% Plot the IVT test

figure(7)
hold on
grid on
plot(Time_IVT,Final_Voltage_IVT);
plot(Time_IVT, Voltage_IVT);
xlabel('Time [s]');
ylabel('Voltage [V]');
ylim([0 1.5]);
legend('Corrected for the Blank Test', 'Without Blank Test');
title(['IVT ', BPM]);

hold off

%% Process IV test
```

```
233
234
235 New_VoltageIV = abs(Voltage_IV-Voltage_IV(1,1));
236
237 figure(8)
238 findpeaks(New_VoltageIV,'MinPeakProminence',0.05,'MinPeakDistance',500)
239 [pks,locs] = findpeaks(New_VoltageIV,'MinPeakProminence',0.05,'
    MinPeakDistance',500);
240 [V_IV] = [pks];                    % Assigning the voltage peaks to a
    seperate table
241 [t_IV] = [locs];                   % Assigning the time of the voltage
    peak to a seperate table
242 for j=1:length(t_IV)
243     Voltage_Peaks_IV(j)=Voltage_IV(locs(j));
244     Current_Peaks_IV(j)=Current_IV(t_IV(j));
245 end
246
247 %Create current density
248 Current_Density_IV = (Current_Peaks_IV/A);
249
250 %Substract blank from IV test
251 Final_Voltage_IV = Voltage_Peaks_IV - (Current_Peaks_IV*R);
252
253 %% Plot IV test
254 figure(9)
255 hold on
256 plot(Current_Density_IV, Final_Voltage_IV,'*');
257 grid on
258 xlim([-120 120]);
259 ylim([0 2]);
260 title(['IV ', BPM]);
261 xlabel('Current Density [A/m^2]');
262 ylabel('Voltage [V]');
263
264
265 %% Process Single Discharge
266
267 %Substract blank from Single Discharge
268
269 Final_Voltage_Single = Voltage_Single - (Current_Single*R);
270
271 %Plot Single Discharge
272
273 figure(10)
274 hold on
275 plot(Time_Single, Final_Voltage_Single);
276 grid on
277 ylim([0 1]);
278 xlabel('Time [s]');
279 ylabel('Voltage [V]');
```

```
280  title(['Single Discharge ', BPM]);
```

H Matlab Code for the OCV Intervals Measurement Experiment

```
close all;clear all;clc;

%% Loading the experimental results
Time = xlsread('SGB_XG_25112019_BlankTest.xlsx','A2:A12001');

% First Blank Test
Current_1 = xlsread('SGB_XG_20112019_BlankTest.xlsx','B2:B12001');
Voltage_1 = xlsread('SGB_XG_20112019_BlankTest.xlsx','C2:C12001');

% Second Blank Test
Current_2 = xlsread('SGB_XG_20112019_BlankTest.xlsx','E2:E12001');
Voltage_2 = xlsread('SGB_XG_20112019_BlankTest.xlsx','F2:F12001');

% Third Blank Test
Current_3 = xlsread('SGB_XG_20112019_BlankTest.xlsx','H2:H12001');
Voltage_3 = xlsread('SGB_XG_20112019_BlankTest.xlsx','I2:I12001');

%% Plotting
% Plot Current over time
figure(1)
plot(Time,Current_1,'linewidth',1.5)
grid on
grid minor
hold on
plot(Time,Current_2,'linewidth',1.5)
plot(Time,Current_3,'linewidth',1.5)
title('Current over time');
xlabel('Time (s)');
ylabel('Current (mA)');
legend('Blank Test 1','Blank Test 2','Blank Test 3');
hold off

% Plot Voltage over time
figure(2)
plot(Time,Voltage_1,'linewidth',1.5)
grid on
grid minor
hold on
plot(Time,Voltage_2,'linewidth',1.5)
plot(Time,Voltage_3,'linewidth',1.5)
title('Voltage over time');
xlabel('Time (s)');
ylabel('Voltage (V)');
legend('Blank Test 1','Blank Test 2','Blank Test 3');
hold off

```

```
%% Setting negative currents to zero for the blank test
for i=1:length(Current_1)
    if Current_1(i)<0
        Current_1(i)=0;
    end
    if Current_2(i)<0
        Current_2(i)=0;
    end
    if Current_3(i)<0
        Current_3(i)=0;
    end

%% Setting voltage fluctuations to zero
    if Voltage_1(i)<0.01
        Voltage_1(i)=0;
    end
    if Voltage_2(i)<0.01
        Voltage_2(i)=0;
    end
    if Voltage_3(i)<0.01
        Voltage_3(i)=0;
    end
end

%% Finding the Peaks of voltage and current
figure(3)
findpeaks(Voltage_1,Time,'MinPeakDistance',50)
[pks,locs] = findpeaks(Voltage_1,Time,'MinPeakDistance',50);
[Va] = [pks];                       % Assigning the voltage peaks to a
   seperate table
[ta] = [locs];                      % Assigning the time of the voltage peak
    to a seperate table
[Ca] = zeros(8,1);                  % Creating a table to store the peaks of
    the current
for j=1:length(ta)                  % finding the current at which the peak
   voltage occurs by using the time
    for i=1:length(Current_1)
        if ta(j)==Time(i)
            Ca(j) = Current_1(i);
        end
    end
end

% Same process for the other 2 blank tests
figure(4)
findpeaks(Voltage_2,Time,'MinPeakDistance',50)
[pks,locs] = findpeaks(Voltage_2,Time,'MinPeakDistance',50);
[Vb] = [pks];
[tb] = [locs];
[Cb] = zeros(8,1);
```

```
for j=1:length(tb)
    for i=1:length(Current_2)
        if tb(j)==Time(i)
            Cb(j) = Current_2(i);
        end
    end
end

figure(5)
findpeaks(Voltage_3,Time,'MinPeakDistance',50)
[pks,locs] = findpeaks(Voltage_3,Time,'MinPeakDistance',50);
[Vc] = [pks];
[tc] = [locs];
[Cc] = zeros(8,1);
for j=1:length(tc)
    for i=1:length(Current_3)
        if tc(j)==Time(i)
            Cc(j) = Current_3(i);
        end
    end
end

%% Average of the 3 blank tests
[V] = zeros(8,1);
[C] = zeros(8,1);
for i=1:8
    V(i) = (Va(i)+Vb(i)+Vc(i))/3;
    C(i) = (Ca(i)+Cb(i)+Cc(i))/3;
end

%% Create I-V Curve

figure(6)
hold on
plot(V,C);
grid on
grid minor
xlabel('Voltage [V]');
ylabel('Current [mA]');
hold off


%% Create a polynomial function to fit on the curves

%pfit = polyfit(x,y, number of polynomials)
pfit = polyfit([V;0;0;0;0;0;0;0;0;0;0;0;0;0;0;0;0;0;0;0;0], [C
    ;0;0;0;0;0;0;0;0;0;0;0;0;0;0;0;0;0;0;0;0], 1);

%use polyval([the function], [the x values]) to calculate what the output
%of the the function is at certain values.
```

```
142
143 %% Create Voltage function to substract from characterization
144 I_Charge = 220;
145 V_Charge = (I_Charge-pfit(2))/pfit(1);
146
147 I_Discharge = 66;
148 V_Discharge = (I_Discharge-pfit(2))/pfit(1);
149
150
151 %% Load characterization
152
153 Excel_Cycling = readtable('SGB_XG_21112019_50cycleInterval.xlsx');
154 Cycling_Test = table2array(Excel_Cycling);
155
156 Cycling_Time = Cycling_Test(:,1);
157 Cycling_Current = Cycling_Test(:,2);
158 Cycling_Voltage = Cycling_Test(:,3);
159
160 figure(7)
161 hold on
162 plot(Cycling_Time,Cycling_Voltage);
163 grid on
164 grid minor
165 title('Voltage over time');
166 xlabel('Time (s)');
167 ylabel('Voltage [V]');
168 hold off
169
170 %% Setting current fluctuations to zero
171 for i=1:length(Cycling_Current)
172     if Cycling_Current(i)<0.1 && Cycling_Current(i)>-0.1
173         Cycling_Current(i)=0;
174     end
175 end
176
177
178
179 %% Identify Charge and Discharge cycles
180 % We substract the voltage of the blank test from the charge and discharge
181 % voltage
182 Final_Voltage = zeros(length(Cycling_Time),1);
183 OCV_Voltage = zeros(length(Cycling_Time),1);
184 for i=1:length(Cycling_Time)
185     if Cycling_Current(i)<-0.1
186         Final_Voltage(i) = Cycling_Voltage(i)-V_Discharge;
187     elseif Cycling_Current(i)>0.1
188         Final_Voltage(i) = Cycling_Voltage(i)-V_Charge;
189     else
190         Final_Voltage(i) = Cycling_Voltage(i);
191         OCV_Voltage(i) = Final_Voltage(i);
```

```
192     end
193 end
194
195 % Plotting the final voltage of the cell over time
196 figure(8)
197 hold on
198 plot(Cycling_Time,Final_Voltage);
199 grid on
200 grid minor
201 title('Voltage over time corrected for the blank test');
202 xlabel('Time (s)');
203 ylabel('Voltage [V]');
204 hold off
205
206 % Plotting the OCV over time
207 figure(9)
208 hold on
209 plot(Cycling_Time,OCV_Voltage);
210 grid on
211 grid minor
212 title('OCV over time');
213 xlabel('Time (s)');
214 ylabel('Voltage [V]');
215 hold off
216
217 %% Finding the max OCV of each open cell cycle
218 OCV = zeros(length(Cycling_Time),1);
219 for i=1:length(Cycling_Time)
220     if Cycling_Current(i)<-0.1
221         if (OCV_Voltage(i-1)-OCV_Voltage(i))>0
222             OCV(i) = OCV_Voltage(i-1);
223         end
224     elseif Cycling_Current(i)>0.1
225         if (OCV_Voltage(i-1)-OCV_Voltage(i))~=0
226             OCV(i) = OCV_Voltage(i-1);
227         end
228     end
229 end
230
231
232
233 % Plotting the max OCV over time in each open cell cycle
234 figure(10)
235 hold on
236 plot(Cycling_Time,OCV,'.');
237 grid on
238 grid minor
239 title('Max OCV over time');
240 xlabel('Time (s)');
241 ylabel('Voltage [V]');
```

```
242 ylim([0  4.5]);
243 hold off
244
245 %%% Discharge
246 %
247 % A = [1.58  1.39  1.272  1.165  1.566  1.434  1.262  1.181  1.571  1.413  1.262
        1.173  1.552  1.428  1.27  1.206];
248 % B = [0.89  0.7399  0.57  0.33  0.8969  0.775  0.55  0.3949  0.8899  0.7429  0.5379
        0.3554  0.875  0.754  0.526  0.3699];
249 %
250 % Delta_Dis = A - B;
251 % R_dis = Delta_Dis/(66/1000);
252 %
253 % test = 1:16;
254 % figure(11)
255 % hold on
256 % plot(test, R_dis);
257 % ylim([0  15]);
258 %
259 %
```

References

[1] IRENA. Global renewables outlook: Energy transformation 2050. *IRENA*, 2020.

[2] T. Schmidt et al. J. Hoppmann, J. Volland. Renewables and electricity storage. *Renewable and Sustainable Energy Reviews*, 39, 2014.

[3] IRENA. Renewables and electricity storage. *IRENA*, 2015.

[4] Ioannis Hadjipaschalis. Overview of current and future energy storage technologies for electric power applications. *Renewable and Sustainable Energy Reviews*, 2008.

[5] I. Knight A. Chatzivasileiadi, E. Ampatzi. Characteristics of electrical energy storage technologies and their applications in buildings. *Renewable and Sustainable Energy Reviews*, 25:814–830, 2013.

[6] Xing Luo. Overview of current development in electrical energy storage technologies and the application potential in power system operation. *Applied Energy*, 2014.

[7] Jiabing Xia. Reverse electrodialysis with bipolar membranes as an energy storage system. 2018.

[8] Jens Burfeind Christian Doetsch. Vanadium redox flow batteries. *Storage Systems*, 2016.

[9] W.J. van Egmond. Concentration gradient flow batteries. 2018.

[10] D Stone P Upham P Taylor, R Bolton. Developing pathways for energy storage in the uk using a coevolutionary framework. 2012.

[11] A Akhil et al. Doe/epri electricity storage handbook in collaboration with nreca. 2015.

[12] Holmström VJM Emrén AT. Energy storage in a fuel cell with bipolar membranes burning acid and hydroxide. *Energy*, 1983.

[13] A. Aldaz A. Sáez, V. Montiel. An acid-base electrochemical flow battery as energy storage system. *International Journal of Hydrogen Energy*, 41, 2016.

[14] Haisheng Chen. Progress in electrical energy storage system: A critical review. *Progress in natural science*, 2009.

[15] Heinrich Strathmann Ulrich Nieken Jiabing Xia, Gerhart Eigenberger. Acid-base flow battery, based on reverse electrodialysis with bi-polar membranes: Stack experiments. 2020.

[16] Faizur Rahman. Vanadium redox battery: Positive half-cell electrolyte studies. *Journal Of Power*, 2008.

[17] W.J. van Egmond. Performance of an enviromentally benign acid base flow battery at high energy density. 2008.

[18] J. González-García et al. C. Ponce de Léon, A. Frías-Ferrer. Redox flow cells for energy conversion. *Journal of Power Sources*, 160:716–732, 2006.

[19] O. Coronell R. Kingsbury, K. Chu. Energy storage by reversible electrodialysis: The concentration battery. *Journal of Membrane Science*, 495:502–516, 2015.

[20] F. Chlanda et al. K. Nagasubramanian. Use of bipolar membranes for generation of acid and base - an engineering and economic analysis. *Journal of Membrane Science*, 2:109–124, 1977.

[21] Yoshinobu Tanaka. Ion exchange membranes: Fundamentals and applications. *Membrane Science and Technology*, 12:383–404, 2007.

[22] N. Van Der Vegt et al. F. Wilhelm, I. Pünt. Optimisation strategies for the preparation of bipolar membranes with reduced salt ion leakage in acid-base electrodialysis. *Journal of Membrane Science*, 182:13–28, 2001.

[23] C. Jiang et al. Q. Wang, B. Wu. Improving the water dissociation efficiency in a bipolar membrane with amino-functionalized mil-101. *Journal of Membrane Science*, 524:370–376, 2017.

[24] P.M. Biesheuvel M. Tedesco, H.V.M Hamelers. Nernst-planck transport theory for (reverse) electrodialysis: I. effect of co-ion transport through the membranes. *Journal of Membrane Science*, 510:370–381, 2016.

[25] Fumasep. Fumasep iem specification sheet.

[26] David A. Vermaas Michel Saakes Kitty Nijmeijer Enver Güler, Rianne Elizen. Performance-determining membrane properties in reverse electrodialysis. *Membrane Science Technology*, 2013.

[27] H. Strathmann. Ion exchange membrane seperation processes. *Membrane Science and Technology*, 9, 2004.

[28] D.A. Vermaas J. Veerman. Reverse electrodialysis: Fundamentals. *Sustainable Energy from Salinity Gradients*, 2016.

[29] M.A. Cohen Stuart P.M. Biesheuvel A.H. Galama, J.W. Post. Validity of the boltzmann equation to describe donnan equilibrium at the membrane-solution interface. *Membrane Science Technology*, 2013.

[30] Yufeng Xue Lichoa Xu Chunbo Zhu Rengui Lu, Aochi Yang. Analysis of the key factors affecting the energy efficiency of batteries in electric vehicle. *World Electric Vehicle Journal*, 4, 2010.

[31] Heinrich Strathmann Ulrich Nieken Jiabing Xia, Gerhart Eigenberger. Flow battery based on reverse electrodialysis with bipolar membranes: Single cell experiments. *Journal of membrane science*, 2018.

[32] J. Veerman M. Saakes H.H.M. Rijnaarts J.W. Post A.H. Galama, D.A. Vermaas. Membrane resistance: The effect of salinity gradients over a cation exchange membrane. *Membrane Science Technology*, 2013.

[33] F. A. Vugt F. G. Wilhelm. Bipolar membrane electrodialysis membrane development and transport characteristics. 2001.

[34] Maurice Maeck Henry D. Hurwitz Claude Gavach Rachid El Moussaoui, Gérald Pourcelly. Co-ion leakage through bipolar membranes. influence on i-v responses and water splitting efficiency. *Journal of Membrane Science*, 90:283–292, 1994.

[35] A. Cipollina G. Micale M. Ciofalo L. Gurreri, A. Tamburini. Cfd prediction of concentration polarization phenomena in spacer-filled channels for reverse electrodialysis. *Journal of Membrane Science*, 468:133–148, 2014.

[36] Kitty Nijmeijer D.A. Vermaas, Michel Saakes. Enhanced mixing in the diffusive boundary layer for energy generation in reverse electrodialysis. *Journal of Membrane Science*, 453:312–319, 2013.

[37] Elena I. Belova Philippe Sistat Patrice Huguet Gérald Pourcelly Christian Larchet Victor V. Nikonenko, Natalia D. Pismenskaya. Intensive current transfer in membrane systems: Modelling, mechanisms and application in electrodialysis. *Advances is Colloid and Interface Science*, 160:101–123, 2010.

[38] Seung-Hyeon Moon Jae-Hwan Choi. Structural change of ion-exchange membrane surfaces under high electric fields and its effects on membrane properties. *Advances is Colloid and Interface Science*, 265:93–100, 2003.

[39] J. Pretzm E. Straude I. Rubinstein. Open circuit voltage in a reverse electrodialysis cell. 2001.

[40] M. Saakes S.J. Metz G.J. Harmsen J. Veerman, J.W. Post. Reducing power losses caused by ionic shortcut currents in reverse electrodialysis stacks by a validated model. *Journal of Membrane Science*, 310:418–430, 2008.

[41] V. Aravindan et al. M. Ulaganathan, A. Jain. Bio-mass derived mesoporous carbon as superior electrode in all vanadium redox flow battery with multicouple reactions. *Journal of Power Sources*, 274:847–850, 2015.

[42] Frank M. White. *Fluid Mechanics, 6th Edition*. McGraw Hill, 2009.

[43] Isidor Buchmann. Coulombic and energy efficiency with the battery.

[44] G. Poon H. Verseema M. Skyllas-Kazacos, G. Kazakos. Recent advances with unsw vanadium-based redox flow batteries. *International Journal of Energy Research*, 34(2):182–189, 2010.